



UNIVERSITY OF GENOA

MASTER'S PROGRAM IN BIOENGINEERING

Thesis submitted in partial fulfillment of the requirements for the title of
Master of Bioengineering

Experimental validation of IMU-based gait measurement system on challenging terrains

Pietro Della Vecchia

March 2023

Thesis advisor: Prof. Francesco Crenna

Thesis co-advisor: Dr. Ing. Diego Torricelli

Contents

| | |
|--|-----------|
| Summary | 7 |
| Chapter 1 - Introduction | 8 |
| 1.1 Motivation..... | 8 |
| 1.2 Research questions | 10 |
| Chapter 2 - State of the art | 12 |
| 2.1 Parkinson Disease..... | 12 |
| 2.2 Gait analysis..... | 14 |
| 2.3 Motion capture systems | 21 |
| 2.3.1 Stereophotogrammetry systems | 22 |
| 2.3.2 Inertial Measurement Units systems | 25 |
| 2.4 Gait events detection | 28 |
| 2.5 Statistical Analysis | 30 |
| Chapter 3 - Materials and Methods | 36 |
| 3.1 Experimental set-up | 36 |
| 3.1.1 Instrumental set-up..... | 37 |
| 3.1.2 Experimental protocol..... | 40 |
| 3.1.3 Subject selection and categories | 49 |
| 3.1.4 Subjects anthropometry | 51 |
| 3.2 Subject set-up..... | 55 |
| 3.2.1 Vicon..... | 55 |
| 3.2.2 Xsens..... | 62 |
| 3.3 Subject calibration..... | 64 |
| 3.3.1 Vicon..... | 64 |

| | |
|--|------------|
| 3.3.2 Xsens | 66 |
| 3.4 Postprocessing phase..... | 67 |
| 3.4.1 Vicon..... | 67 |
| 3.4.2 Xsens..... | 70 |
| 3.5 Gait events detection | 71 |
| 3.5.1 Vicon..... | 71 |
| 3.5.2 Xsens | 75 |
| 3.6 Data processing..... | 83 |
| 3.6.1 Detector qualification | 83 |
| 3.6.2 Error qualification | 86 |
| 3.6.3 Data implementation | 87 |
| Chapter 4 - Results..... | 88 |
| 4.1 Experimental database | 88 |
| 4.1.1 Gold standard..... | 88 |
| 4.1.2 Method 1: Zijlstra | 90 |
| 4.1.3 Method 2: IMU on the foot..... | 91 |
| 4.1.4 Method 3: IMU on the shank..... | 93 |
| 4.2 Detection analysis | 95 |
| 4.2.1 Method 1: Zijlstra | 95 |
| 4.2.2 Method 2: IMU on the foot..... | 98 |
| 4.2.3 Method 3: IMU on the shank..... | 108 |
| 4.3 Statistical analysis on the errors | 117 |
| 4.3.1 Method 1: Zijlstra | 117 |
| 4.3.2 Method 2: IMU on the foot..... | 121 |
| 4.3.3 Method 3: IMU on the shank..... | 125 |
| Chapter 5 - Discussion | 139 |
| Chapter 6 – Conclusion | 145 |
| Bibliography | 146 |

Figure index

| | |
|--|----|
| Figure 2.1: The eight phases of the human gait cycle. (https://www.streifeneder.com/)..... | 15 |
| Figure 2.2: Reference planes for gait analysis. | 19 |
| Figure 2.3: World Reference Frame set-up with the Vicon calibration wand. | 23 |
| Figure 2.4: Xsens 17 sensors, full body configuration. | 27 |
| Figure 2.5: Example of how the ANOVA table is presented in MATLAB..... | 35 |
| Figure 3.1: Configuration set-up. | 37 |
| Figure 3.2: Start recording output configuration on the Xsens software..... | 38 |
| Figure 3.3: Stop recording output configuration on the Xsens software. | 39 |
| Figure 3.4: Flat terrain at 15°. | 41 |
| Figure 3.5: Mat terrain at 0°. | 42 |
| Figure 3.6: Mat terrain at 15°. | 43 |
| Figure 3.7: Terrasensa terrain at 0°. | 44 |
| Figure 3.8: Terrasensa terrain at 15°. | 45 |
| Figure 3.9: M terrain at 0°. | 46 |
| Figure 3.10: M terrain at 15°. | 47 |
| Figure 3.11: Masses and heights histograms. | 49 |
| Figure 3.12: BMIs histogram. | 50 |
| Figure 3.13: Vicon markers name and position on the body, back view. | 55 |
| Figure 3.14: Vicon markers name and position on the body, front view. | 56 |
| Figure 3.15: label and position of the markers of the head. | 56 |
| Figure 3.16: label and position of the markers of the torso. | 57 |
| Figure 3.17: label and position of the markers of the upper limbs. | 58 |
| Figure 3.18: label and position of the markers of the pelvis. | 59 |
| Figure 3.19: label and position of the markers of the lower limbs..... | 60 |
| Figure 3.20: Markers added. | 61 |
| Figure 3.21: IMU Xsens sensors positions on the body. | 62 |
| Figure 3.22: An instrumented subject before starting the experimental trials..... | 63 |
| Figure 3.23: static calibration of Vicon, view on the Nexus software. | 64 |
| Figure 3.24: functional calibration of Vicon, view on the Nexus software..... | 65 |
| Figure 3.25: calibration window on the 'MVN Analyze' software. | 66 |
| Figure 3.26: Filling gaps tool on the Nexus software..... | 68 |
| Figure 3.27: dynamic pipeline on the Nexus software. | 70 |
| Figure 3.28: Example of the frame selected for the IC instants on flat terrain. | 72 |
| Figure 3.29: Example of the frame selected for the EC instants on mat terrain. | 74 |
| Figure 3.30: IC instants identification of the 'Zijlstra' method - MATLAB. | 76 |
| Figure 3.31: EC instants identification of the foot acceleration method - MATLAB..... | 78 |
| Figure 3.32: IC instants identification of the foot acceleration method - MATLAB..... | 80 |
| Figure 3.33: IC & EC instants identification of the shank angular velocity method – MATLAB..... | 82 |
| Figure 3.34: Threshold criterion to select the correct, missed and extra events. | 85 |
| Figure 4.1: Missed events areogram – Zijlstra method. | 95 |
| Figure 4.2: Extra events areogram – Zijlstra method. | 96 |
| Figure 4.3: Missed EC events areogram – method of the IMU on the left foot. | 98 |

| | |
|---|-----|
| Figure 4.4: Extra EC events areogram – method of the IMU on the left foot. | 99 |
| Figure 4.5: Missed IC events areogram – method of the IMU on the left foot. | 100 |
| Figure 4.6: Extra IC events areogram - method of the IMU on the left foot. | 101 |
| Figure 4.7: Missed EC events areogram – method of the IMU on the right foot. | 102 |
| Figure 4.8: Extra EC events areogram – method of the IMU on the right foot. | 103 |
| Figure 4.9: Missed IC events areogram – method of the IMU on the right foot. | 105 |
| Figure 4.10: Extra IC events areogram – method of the IMU on the right foot. | 106 |
| Figure 4.11: Missed EC events areogram – method of the IMU on the left shank. | 108 |
| Figure 4.12: Extra EC events areogram – method of the IMU on the left shank. | 109 |
| Figure 4.13: Missed IC events areogram – method of the IMU on the left shank. | 110 |
| Figure 4.14: Extra IC events areogram – method of the IMU on the left shank. | 111 |
| Figure 4.15: Missed EC events areogram – method of the IMU on the right shank. | 113 |
| Figure 4.16: Extra EC events areogram – method of the IMU on the right shank. | 114 |
| Figure 4.17: Missed IC events areogram – method of the IMU on the right shank. | 115 |
| Figure 4.18: Extra IC events areogram – method of the IMU on the right shank. | 116 |
| Figure 4.19: Zijlstra method boxplot, errors on different terrains. Healthy subjects vs Parkinson disease patients. | 117 |
| Figure 4.20: Zijlstra method boxplot, errors of each healthy subject. | 118 |
| Figure 4.21: Anova on the BMI group – Zijlstra method. | 118 |
| Figure 4.22: Anova on the terrain and inclination groups – Zijlstra method. | 119 |
| Figure 4.23: Boxplot of the errors on the different terrain inclinations - Zijlstra method. | 119 |
| Figure 4.24: error plot of all the subjects - Zijlstra method. | 120 |
| Figure 4.25: foot method boxplot, errors on different terrains. Healthy subjects vs Parkinson disease patients. IC left instants. | 121 |
| Figure 4.26: foot method boxplot, errors of each healthy subject. IC left instants. | 122 |
| Figure 4.27: Anova from MATLAB on the height group of the IC instants – left foot method. | 122 |
| Figure 4.28: Anova from MATLAB on the BMI group of the IC instants – left foot method. | 123 |
| Figure 4.29: foot method boxplot, errors on different terrains. Healthy subjects vs Parkinson disease patients. IC right instants. | 123 |
| Figure 4.30: foot method boxplot, errors of each healthy subject. IC right instants. | 124 |
| Figure 4.31: Anova from MATLAB on the BMI group of the IC instants – right foot method. | 124 |
| Figure 4.32: shank method boxplot, errors on different terrains. Healthy subjects vs Parkinson disease patients. EC left instants. | 125 |
| Figure 4.33: shank method boxplot, errors of the healthy subjects. EC left instants. | 126 |
| Figure 4.34: Anova from MATLAB on the height group of the EC instants – left shank method. | 126 |
| Figure 4.35: Anova from MATLAB on the terrain and inclination groups of the EC instants – left shank method. | 127 |
| Figure 4.36: Boxplot of the errors on the different terrain inclinations of the EC instants - left shank method. | 127 |
| Figure 4.37: error plot of all the subjects of the EC instants - left shank method. | 128 |
| Figure 4.38: shank method boxplot, errors on different terrains. Healthy subjects vs Parkinson disease patients. IC left instants. | 129 |
| Figure 4.39: shank method boxplot, errors of each healthy subject. IC left instants. | 130 |
| Figure 4.40: Anova from MATLAB on the BMI group of the IC instants – left shank method. | 130 |
| Figure 4.41: Anova from MATLAB on the terrain and inclination groups of the IC instants – left shank method. | 131 |

| | |
|--|-----|
| Figure 4.42: boxplot of the errors on the various inclinations of the IC instants – left shank method..... | 131 |
| Figure 4.43: error plot of all subjects of the IC instants – left shank method. | 132 |
| Figure 4.44: shank method boxplot, errors on different terrains. Healthy subjects vs Parkinson disease patients. EC right instants. | 133 |
| Figure 4.45: shank method boxplot, errors of each healthy subject. EC right instants..... | 134 |
| Figure 4.46: Anova from MATLAB on the BMI group of the EC instants – right shank method..... | 134 |
| Figure 4.47: Anova from MATLAB on the terrain and inclination groups of the EC instants – right shank method. | 135 |
| Figure 4.48: boxplot of the errors on the various inclinations of the EC instants – right shank method..... | 135 |
| Figure 4.49: error plot of all subjects of the EC instants – right shank method. | 136 |
| Figure 4.50: shank method boxplot, errors on different terrains. Healthy subjects vs Parkinson disease patients. IC right instants. | 137 |
| Figure 4.51: shank method boxplot, errors of each healthy subject. IC right instants..... | 138 |
| Figure 4.52: Anova from MATLAB on the BMI group of the IC instants – right shank method..... | 138 |
| Figure 5.1: histogram of the errors – Zijlstra method. | 143 |
| Figure 5.2: histogram of the errors – right foot method, IC instants. | 144 |

Table index

| | |
|--|----|
| Table 2-1: List of instrumental measurement systems to evaluate gait. | 17 |
| Table 3-1: Subjects’ anthropometric data. | 50 |
| Table 3-2: required measurements for Vicon..... | 51 |
| Table 3-3: required measurements for Xsens. | 53 |
| Table 4-1: Number of instants for each terrain condition with the gold standard – all the subjects. | 88 |
| Table 4-2: Number of instants for each terrain condition with the gold standard – Parkinson patients. | 89 |
| Table 4-3: Number of instants for each terrain condition with the Zijlstra method. | 90 |
| Table 4-4: Number of instants for each terrain condition with the second method – all the subjects. | 91 |
| Table 4-5: Number of instants for each terrain condition with the second method – Parkinson patients. | 92 |
| Table 4-6: Number of instants for each terrain condition with the third method – all the subjects. | 93 |
| Table 4-7: Number of instants for each terrain condition with the third method – Parkinson patients. | 94 |

Summary

This thesis aims to verify the IMUs effectiveness in identifying the gait cycle phases. This is only partially present in the literature and limited to regular flat terrain. Therefore, the aim here is to investigate the effectiveness of these sensors for this purpose and extend their application to various irregular terrains.

This study performed a comparison between an inertial sensor system and a stereophotogrammetry system, used as gold standard. The comparison is based on experimental data acquired in the Spanish project, called 'Neuromark', using a slightly modified experimental protocol. In this thesis, ten healthy subjects were analyzed in twelve different configurations of walking and, also, two Parkinson's disease patients data of the project were examined. Some codes, that use acceleration and angular velocity data, were analyzed in term of performance to detect events that are comparable with the ones of the gold standard, having defined threshold methods. In addition, with the comparable events, an analysis on the temporal errors was performed, using a statistical test, as it is the analysis of variance. The results can give some indications on the recommended positions of the IMU sensors in every terrain condition and inclination, and also which method can be considered useful for an analysis on the gait events of the Parkinson disease patients.

Chapter 1 - Introduction

1.1 Motivation

The Parkinson disease is the second most relevant neurodegenerative disease in the world. Doctors usually evaluate it with clinical observations, that lack of an objective analysis leads to an incorrect diagnose in the 35% of the cases [C.H. Adler, 2014]. Moreover an early diagnosis is difficult with current methods, and the evolution of the patient following different therapies is complex and affected by large uncertainties. Parkinson severely impairs the quality of life of patients, due to the motor and non-motor underlying alterations that it implies. As already depicted an early diagnosis is difficult, and the current diagnostic procedures depend on the clinical subjective analysis of motor cues in accordance with certain rating scales, one of the most used is the Unified Parkinson's Disorders Rating Scale (UPDRS) or the Hoehn and Yahr (HY) scale [Mirelman A, 2019]. For these reasons there are several studies that aim to build an early diagnose system. For example, the paper from Yuzhe Yang and Katabi uses breathing signals during the night either with a wireless system that sends and receives radio waves or with a system that uses a kind of sensor belt placed over the patient's ribcage that can detect its movements. The paper from Wei Fu and Chen wants to build an artificial intelligence system that functions as an olfactory system, capable of diagnosing Parkinson's disease from the smell of the skin. Clinical studies on the effectiveness of foot stimulation for Parkinson's disease patients [Kleiner and Pandis, 2015]. Design of devices useful for combined forced motor training of the upper limbs in patients with Parkinson's disease, improving movement and posture in 100 percent of patients [Messa and Rossi, 2019]. Again, studies demonstrating the effectiveness of surgical implantation of

electrodes in the subthalamic nucleus [Thenaisie and Moraud, 2022].

At the moment, there is no cure for Parkinson's disease. The most extended treatment are:

- Intake of levodopa. This substance is converted into dopamine into the brain, which improves the motor capabilities of the patient. But, not all parkinsonian gait features are responsive to this treatment [Roemmich and Hass, 2014].
- Deep Brain Stimulation (DBS) is used as a later stage treatment when dopaminergic medication does not control symptoms [A.L. Benabid, 2009].

1.2 Research questions

In the project 'Neuromark', that wants to find the most important features in gait cycle analysis to discriminate if a person is an healthy subject or a Parkinson's disease patient and the illness severity, using machine learning, the Inertial Measurement Units sensors are used because they are convenient and manageable. So, it occurred to me to validate this system and to see if it is now possible to use this special kind of sensors for gait measurements when walking on different terrain conditions. In particular, the research question in this thesis wants to verify if we can reliably obtain spatio-temporal parameters with these sensors. To do this, it is evident in literature the importance to detect correctly and more precise as possible the gait events instants during the walk. If this occurs, it may open up diagnostic opportunities to any doctor's office, even of not equipped with a complex and expensive system to install like an optoelectronic motion capture system, or monitor patients from home in more severe cases to obtain regular data on daily activities or conduct experiments outdoor.

So, can an IMUs system acceptably replace a stereophotogrammetry system? Is it possible to use Inertial Measurement Unit sensors in an experimental protocol like the one used in this thesis? Are there body positions where it is advisable to put the IMUs sensors to have a precise measure? Does it depend on terrains? Or on the configurations of them?

We can expect that this kind of comparison will confirm the possibility to use IMU sensors in the measurement of gait parameters with acceptable errors range when operating on regular terrains such as a flat rigid floor, both horizontal (0 deg) or slightly inclined (15 deg). On the other hand, it is reasonable to encounter some difficulties when irregular terrains are involved as it will be presented later in the 'Experimental protocol' section.

Furthermore, with the statistical analysis we can see if the variabilities of the results depend on the subjects anthropometric characteristics like the weight, the body mass index (BMI), the height, on the pathological conditions of the subjects or only on the terrains characteristics. In order to have a good data base, the latter must not depend on the anthropometric characteristics of the subjects, instead it is possible that depend on the pathological conditions, because, as it will be presented in the 'Parkinson disease' section, the patients involved in this experiments can have balance and stability problems. These issues can lead to particular acceleration and angular velocity signals , that the algorithms may not handle properly.

Chapter 2 - State of the art

2.1 Parkinson Disease

Gait disorders are a common manifestation among patients with Parkinson Disease (PD), and according to their pattern of occurrence they can be classified as: continuous, or episodic [Giladi N, 2013]. Continuous (persistent) alterations in gait pattern are usually consistent from step to step so systematic effects can be observed: walking is slow and characterized by a reduced step length and step width ('shuffling gait'); furthermore, arm swing is decreased or absent, a longer double limb support phase can be observed, and patients present higher step variability with increased left/right asymmetry. These persistent gait abnormalities are usually exacerbated under dual-task conditions [Plotnik M, 2011] [Springer S, 2006]. Episodic alterations on the other hand, are occasional, intermittent, and apparently random. They occur in an inexplicable manner, and include: festination, i.e. a tendency to move forward with increasingly rapid, but ever smaller steps, associated with a forward shift of the center of gravity over the stepping feet, and freezing of gait, i.e. brief, episodic absence or marked reduction of forward progression of the feet despite the intention to walk. Freezing of gait may prevent the patient from starting to walk, turning, passing through narrow spaces, and making for specific destinations. While festination is relatively infrequent, freezing of gait is a common and debilitating phenomenon in PD; although primarily related to progression of the disease and disease duration, it can also occur in the early stages. Although the underlying mechanisms (loss of automaticity, impaired regulation of rhythmicity, failure to release inhibition of the stepping program) are still

uncertain [Nutt JG, 2000], freezing of gait is associated with an increased prevalence of falls and loss of independence [Bloem BR, 2004].

Analyzing the gait is important as some of its characteristics, including the spatio-temporal parameters of interest in this work, are in direct correlation with the disease and its extent. Furthermore, given that the dual task increases and thus highlights the problem, irregular terrains can further engage the subject and make the task more onerous similarly to a dual task. In this sense, it is important to have the spatio-temporal parameters also under these conditions, hopefully as good early indicators of the disease. For these reasons, the activity was focused on the validation of methods for measuring spatio-temporal parameters, with reference instruments (Optoelectronic Motion Capture) and instruments of simpler applicability (Inertial Measurement Units), also outside a laboratory, during walks on different types of terrain.

2.2 Gait analysis

Walking can be defined as a method of locomotion in which through alternating and repeated use of the lower limbs [M. D. J. Perry, 1992] provides for the movement of the body in forward while simultaneously allowing stable support.

Recovery of walking function is one of the main goals of neurorehabilitation. The ultimate goal of the rehabilitation is to reduce the likelihood of disability, by helping patients maximize their independence and increase their interaction with their environment throughout life [Stucki G, 2007].

It is known that gait consists of two main phases (% of gait), generally estimated during a comfortable walk. The swing phase (40%) is defined as the period of time when the reference foot is not in contact with the ground, while the stance phase (60%) corresponds to the time when it is in contact with the ground. The stance phase can be further subdivided into: (a) the double support phase (10%) during which both feet are in contact with the ground; (b) the single limb support phase (40%) of the gait cycle, during which the opposite foot swings. So, the human gait cycle pattern can be segmented from two to eight phases in the literature [J. Taborri, 2016] as it is shown in the Figure 2.1.

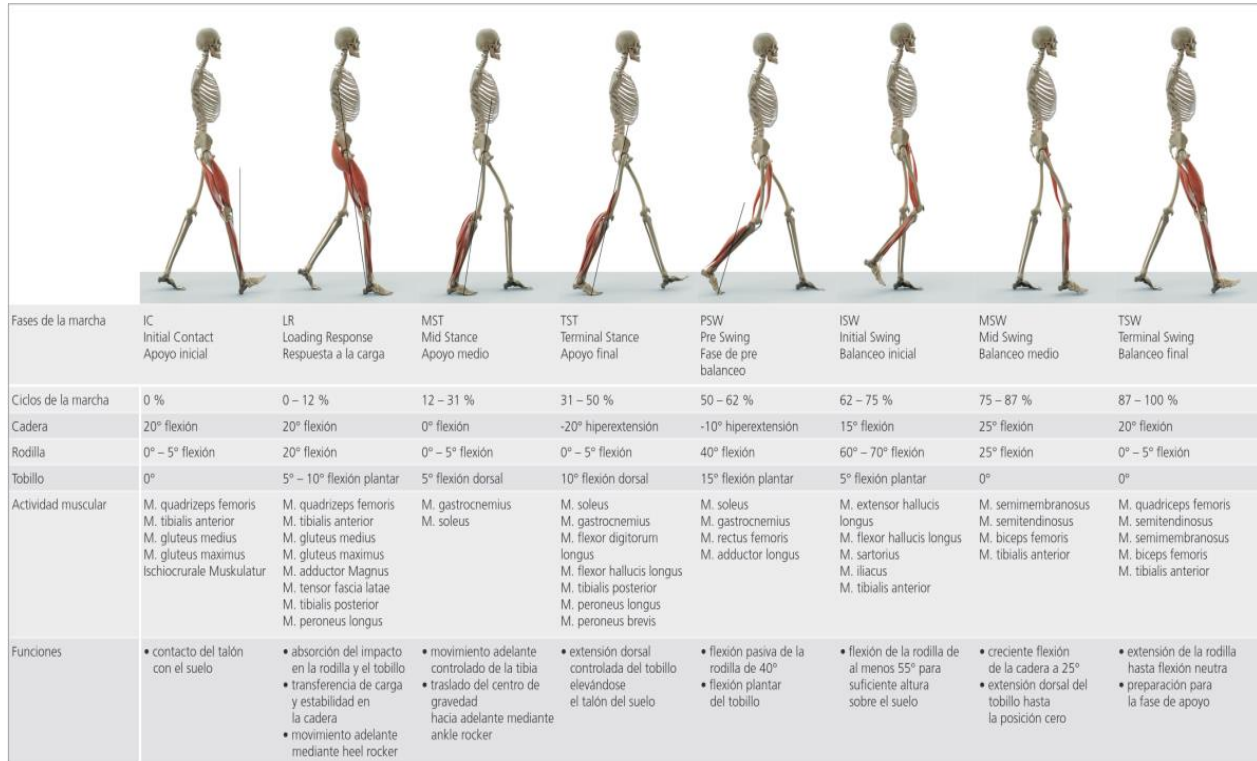


Figure 2.1: The eight phases of the human gait cycle. (<https://www.streifeneder.com/>)

Gait abnormalities can refer to the stance or swing phase of the gait cycle. Stance phase dysfunctions include an abnormality of the support base (equinovarus foot, claw toes, knee hyperextension) and limb or trunk instability (Trendelenburg limping). Swing phase dysfunctions may result in impaired limb advancement [Bensoussan L, 2008].

Gait analysis is used to quantify human motion and it is generally performed in a specialized laboratory. The objectives of gait analysis are to understand the biomechanical features of human gait and to differentiate normal conditions from those defined as pathological. Other important aspects that can be studied are the different biomechanical components of the body (feet, trunk, arms) and their relationship to each other during gait. Finally, gait analysis can help in drawing clinically meaningful inferences about the anatomical and biomechanical functions of the body in patients with different pathologies [Mayich DJ, 2014]. It is to be noted that the clinical course of gait disorders is variable and changes over time in patients with neurological diseases. A better understanding of gait changes related to disease progression or treatment could help clinicians to classify gait disorders. Classifying dysfunctional gait patterns would have important implications from the perspective of improving communication between rehabilitation experts and developing specific interventions based on patients' needs [Kempen JC, 2016] [Mirek E, 2016].

The parameters used in gait analysis can be divided into five types: (a) spatio-temporal parameters; (b) kinematic parameters; (c) kinetic parameters; (d) integrated biomechanics (joint moments and power); and (e) electromyography. Spatio-temporal parameters are the easiest to understand and, with respect to the others, the most applicable in clinical practice. Essentially, the spatio-temporal parameters are gait speed (m/s), stride length (m), cadence (steps/s), step or stride width (m), single limb support time (s), double limb support time (s), and stance time/duration (s). It is important to consider that spatio-temporal parameters are a global expression of gait function and can be directly influenced by several factors (the subjects' sex and age, the measurement method used, the instructions given to the subjects, the type of terrain where the trials are conducted, etc) [Mayich DJ, 2014].

Kinematic parameters are used to study the movement of the body independent of the forces that generate the motion. They are measured as displacements of linear or angular accelerations or velocities, usually recorded with motion tracking devices and/or optical tracking cameras to derive joint angles and limb trajectories. Modern gait analysis laboratories are equipped with optical tracking cameras for either two-dimensional or three-dimensional (3D) gait analysis. A well-equipped movement analysis laboratory has the potential to measure and record the kinematic parameters and many more. The path of movement in three different dimensions and precise quantitative data can be collected simultaneously. Gait analysis devices are generally easy to use and non-invasive for the patient. The table 2-1 shows a list of possible systems that can analyze and evaluate gait.

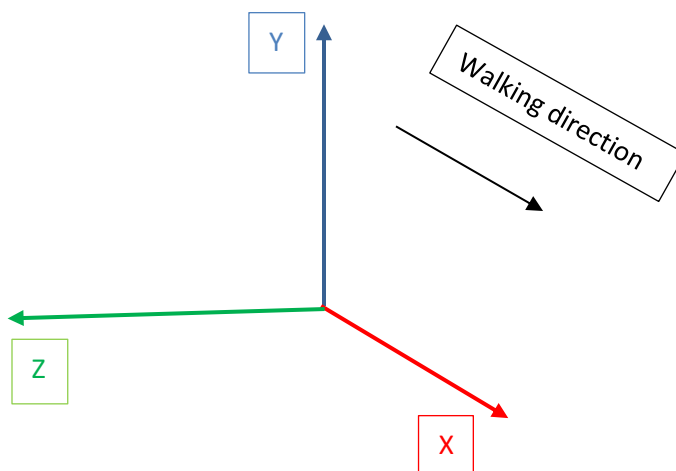
Table 2-1: List of instrumental measurement systems to evaluate gait.

| Devices for gait analysis |
|-------------------------------------|
| Optoelectronics Motion Capture |
| GAITRite system |
| OPTO GAIT photoelectric cell system |
| Electromyography |
| Posturography |
| IMU systems |

Although the assessment of gait disorders is a key area in the field of rehabilitation, there is no agreement on the most appropriate method to select outcome measures, but in the literature the most used system to perform gait analysis is the Optoelectronics Motion Capture. Furthermore, there is no shared consensus between researchers and clinicians on the clinical scales that should be used to assess the treatment effects and gait training [Geroin C, 2013]. Walking independence, velocity, muscle strength, endurance, mobility, and balance are the main aspects of walking with potential implications for rehabilitation. Furthermore, real-time gait analysis techniques often have the goal to be applied in gait rehabilitation [Prasanth, 2021].

So, for all the reasons reported above, it is important to have universal references to analyze the gait cycle. The first step towards a common approach is the definition of the coordinate reference system for gait analysis:

- axis X: direction of the subject motion during walking, it is the antero-posterior direction;
- axis Y: direction perpendicular to the ground and positive from bottom to top, it is the vertical direction;
- axis Z: direction perpendicular to the axis X and to the axis Y following the right hand rule, it is the medio-lateral direction.



In the gait analysis, it is useful and recommended to decompose the motion in planes, the convention comes from the ISB (International Society of Biomechanics), as we can see in the Figure 2.2: the plane being implemented by the two axis X and Y is the sagittal plane, the most important plane in the gait cycle; the plane that the axis X and Z form is the transverse (or horizontal) plane; the plane that is realised by the other two axis, Y and Z, is the frontal (or coronal) plane.

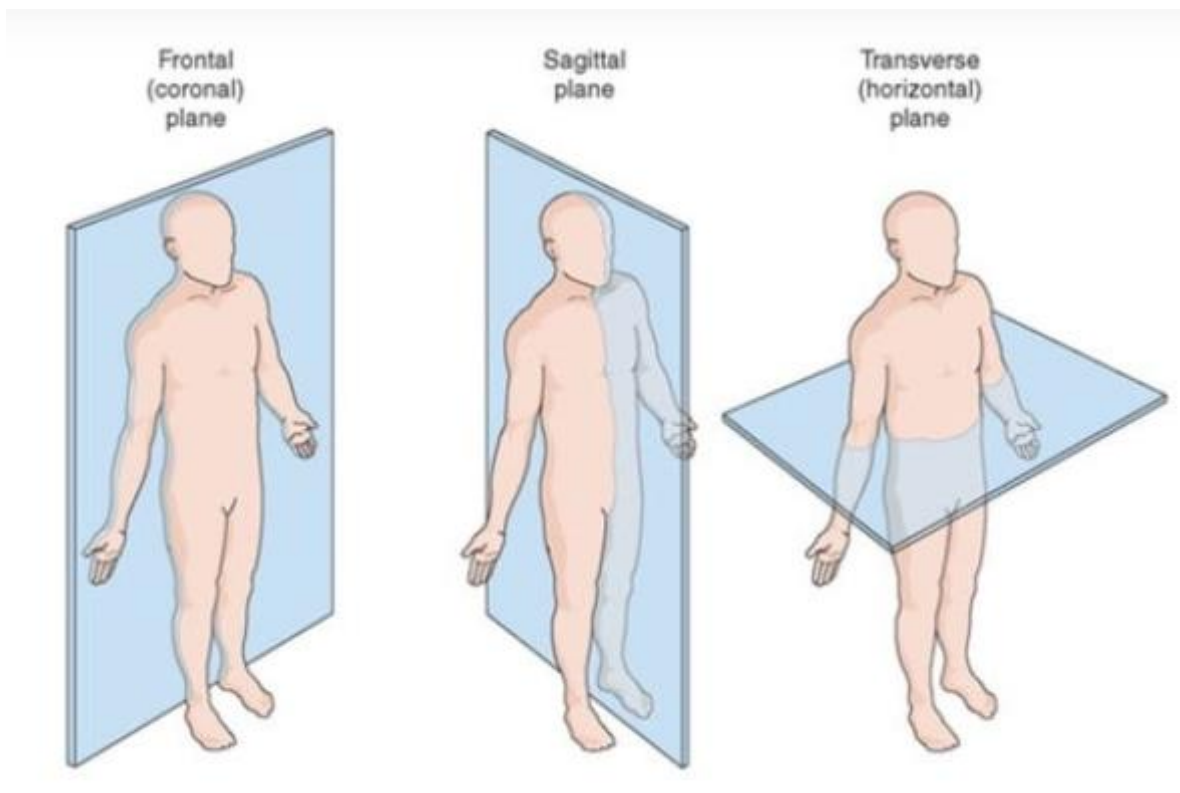


Figure 2.2: Reference planes for gait analysis.

In this thesis, the interest goes to the sagittal plane and on the gait events that determine the most spatio-temporal parameters that exist in gait. The calculation of these parameters comes from the correct identification of the gait events. Gait events correspond to transition between phases, therefore gait segmentation and the detection of gait events are equivalent problems. Most existing approaches to detect gait events include two events: Heel Strike (HS), when the foot first touches the floor, better called Initial Contact (IC), and Toe-Off (TO), when the foot loses contact with the floor, better called End Contact (EC) [R. Caldas, 2017]. In this work, with regard to nominative recruitment, it was decided to call the two events described above, as Initial Contact (IC) and End Contact (EC). The reason lies in the fact that in this thesis we go for an analysis involving challenging terrains where the part of the foot that touches the ground first is not always the heel. Similarly, the last part that touches the ground is not always the toes. The references in literature on irregular terrains are residual and even more rarely there are any specifics on the analysis on this kind of terrains [Torres-Pardo A., 2022].

In conclusion, in order to determine the gait phases, it is necessary to know correctly at which instants the first and last contact (IC and EC) of the foot with the ground occurs, so this thesis' goal focuses on the gait instants determination.

2.3 Motion capture systems

Motion capture is a technology used to record and digitize human movements. It uses sensors placed on the body or cameras that track markers attached to the body to produce a digital representation of motion. There are two main types of motion capture systems: marker-based and markerless. Marker-based systems are based on a biomechanical model to describe the movement under investigation. A proper set of markers identifies landmarks on the subject corresponding to specific points in the model. Cameras can record images of the markers easily detectable since they appear as white dots on a black background. Markers trajectories once labelled, associated to the model, can reproduce the subjects' movement to the level of detail included in the model. Markerless systems use computer vision algorithms to track the movement of the body without the use of markers. In biomechanics, the most accurate state of the art systems in terms of trajectory measurement are marker-based, whereas markerless systems have considerable advantages in terms of subject setup speed even if they are less accurate.

Motion capture systems are widely used in animation, film-making, gaming and biomechanics research [Shubham Sharma, 2019]. The resulting data can be used to animate characters, evaluate physical performance, or study human movement patterns to study a Biomechanical disease or to evaluate a sport performance [Reijne, 2018]. These systems can range from simple setups using just a few cameras to complex setups using multiple cameras and high tech sensors. By studying human motion, researchers can gain a deeper understanding of the mechanics of movement, as well as the factors that influence it. This information can be used to improve the design of medical devices, such as prosthetics, and to develop new treatments for conditions such as Parkinson's disease.

2.3.1 Stereophotogrammetry systems

As already introduced, among the first steps in the biomechanical study of a movement, we have the definition of the biomechanical model of the body segments under analysis. There are some cautions to keep in mind. If the acquisition system is stereophotogrammetric and there is a need to make a three-dimensional model of the body, then one must make sure to place at least three non-aligned markers on each body segment so that its movement can be described in its six degrees of freedom: three coordinates for positions and three possible rotations in the 3D space. If, on the other hand, a two-dimensional analysis is performed, usually, two markers are placed to describe each segment. The stereophotogrammetry systems are measuring instruments that provide markers coordinate. These markers can be active or passive. The active markers have a LED light that has to be received by white light cameras to record markers positions in the global reference frame. The passive markers, instead, reflect infrared wavelengths and they have to be, therefore, the only objects recorded by cameras that are sensitive to infrared wavelengths. The camera set-up is critical to define a proper working volume, and once they are fixed in position and adjusted in their optics, a calibration of the system must be carried out prior to its use in order to refer the images from the different points of view to a common reference frame (world reference system), in the way illustrated in Figure 2.3.



Figure 2.3: World Reference Frame set-up with the Vicon calibration wand.

The coordinates of the markers will be defined according to the origin of the reference system.

To reconstruct the 3D position and consequently the trajectory, each marker has to be recorded at least by two points of view, or considering the hardware used, by at least two cameras. It becomes important to have as many cameras as possible to enable multiple views and to guarantee that during the movement every marker is always seen by at least two cameras [Chiari, 2005].

As already depicted such systems at the state of the art are the most precise and often considered as gold reference standard for movement reconstruction in biomechanics. Nevertheless there are some uncertainty issue. One of these is described in [Cappozzo, 2005], is caused by the skin, where the markers have to be attached. The skin, like all the soft tissues, has a deformability that can introduce some errors while the subject is moving in the experimental trials. So, fixed and stable positioning of the markers is not guaranteed because of the movement of skin and underlying masses (soft tissue or contracting muscles), in general called wobbling masses. This

issue was studied in the past by [K. Gruber, 1998] so current biomechanical models privilege some essential landmarks where such problem is reduced and consider other positions as secondary to complete the information of the segment movement.

Another common problem is the lost in the line of view during the specific trial. In such conditions the marker is seen by less than the minimum number of cameras, so its positions in the 3D space can not be reconstructed. Such problem results in gaps in the marker trajectory, creating discontinuities in the movement. To solve such problem after the experimental session has been completed, the only option is a long and careful process of each trial to try to fill more gaps as possible. On the other hand a careful set-up of the cameras, their appropriate number, and proper marker position selection can help in reducing such a problem during the acquisition phase. So filling appropriately the gaps is important to reconstruct the markers trajectories in the most realistic way. In the current practice, this problem is difficult to avoid because in an experimental trial the subject can interact with several objects and also with his art movements can hide markers to the cameras. Another aspect to be considered is the time required to set both the cameras and the subject with markers. If the former can be done every time and then when setting up a new configuration in the lab the latter is required for every subject considered, healthy or patients. Of course, this point has a great importance in clinical studies.

2.3.2 Inertial Measurement Units systems

The Inertial Measurement Units systems or IMUs are measurement systems based on two inertial sensors and some auxiliary sensor that provides raw measurements of linear accelerations and angular velocities. Main sensors are accelerometers, gyroscopes, while auxiliary sensors are magnetometers, thermometers and pressure sensors. The accelerometers sensors give us acceleration measurements on all the three axis, they have a useful bandwidth from 0 : 1000Hz, they are sensible to the gravity acceleration and the measurement range is over 100m/s^2 , depending on the model. The gyroscopes sensors, instead, give us angular velocity measurements, they are tri-axial sensors and they have a measurement range usually over 2000 deg/s. The magnetometer sensors are useful to measure the earth's magnetic field orientation to define a reference system for the measurement. The auxiliary sensors, when present, are used to compensate the errors that gyroscopes or accelerometers may have due to the environmental conditions. So, for every sensor we have three different kind of data, one for each axis, versus time and it is very important the processing of the raw data after the recording phase. In particular, in motion capture a sensor fusion is operated to obtain finally an orientation measurement. The angular position of the device is then extended to the angular position of the body segment on which the device is fixed, enabling the movement reconstruction. Possible applications of this system are varied, like virtual reality for cinema, ergonomic design for user or biomechanics, where it is possible to reconstruct limbs motion, to develop model of the entire body with minimum invasiveness in field applications.

One of the possible problems that may occur is the distortion of the earth magnetic field. If the magnetometer during the measurement fails, there is still a valid measurement of acceleration and speed, but the sensor fusion to arrive at the orientation in space is no longer reliable. The distortion depends on the distance from the ferro containing metal and thus the construction materials used in the building. The paper written by [W.H.K. de Vries, 2009] gives some advices to not encounter this problem. One of these says to 'map your laboratory on ferromagnetic characteristics before validating' and this can be done with an application that anyone can download on his smartphone. Nowadays the Inertial Measurement Units, called also IMUs, are in the interest of most scientists around the world for their availability, relatively low-cost, portability, lightweight [Ferrari, 2010], but it is not yet clear whether their use can replace systems used for many years until today and of which there are many studies in the literature. So, in the last years, many studies were conducted to evaluate the performances of these systems in a lot of conditions and situations, like in sports [Benjaminse and Otten, 2020], in small movements [S.B. Thies, 2007] and tasks [Robert-Lachaine, 2017], under ambulatory conditions [Karatsidis, 2019], and also military tasks [P. Mavor and Graham, 2020]. In this thesis, for the experiments the IMUs sensors by Xsens (https://base.xsens.com/s/topic/0TO09000000Y06oGAC/mvn-awinda?language=en_US&tabset-acedd=2) was used. It is the leading innovator in 3D motion tracking technology and products for the high quality of its IMU sensors [A. Garcia and Siqueira, 2022]. This system has two possible hardware solutions, one body-wired and one completely wireless, that has been used for this thesis. With this solution, it is necessary the 'MVN Awinda', that uses wireless motion trackers and body straps and receives the data in wireless mode. Called also 'Awinda station', it uses a patented protocol described in [F. Dijkstra and P. J. Slycke, 2009 and 2010] and in [G. Bellusci, 2014 and 2015]. The Xsens company provides also the software where the data collected by the sensors are

combined with the biomechanical models of the human body to obtain segment positions and orientations. It is possible to choose how many sensors to be used in the study. For this work, being experimental trials, it has been chosen to use the full body configuration to have all the possible sensors to investigate after on which sensor can be optimal for the goal of the study. So, 17 sensors were used and they are illustrated in the Figure 2.4.



Figure 2.4: Xsens 17 sensors, full body configuration.

2.4 Gait events detection

A code search in the literature led to the confirmation that IMU and rule-based algorithms are the preferred option among studies, even in those seeking to be validated on subjects with disabilities, like the Parkinson's disease patients [Prasanth, 2021]. Nine papers have been found, but in the end only two were used to write and replicate the code inside them. In the paper of [M. Jasiewicz, 2006], cited more than 280 times in the literature, were reported three methods of gait event detection using angular velocities, linear accelerations, but also the joint angles data to make time windows where the events (Initial Contact and End Contact) have to be searched. These methods were compared with standard pressure-sensitive foot switches. Then, the paper of [Trojaniello and Croce, 2014], cited more than 140 times, was found. The method, not well described, uses two Miniature inertial measurement units (MIMUs) above the ankles and the medio-lateral and sagittal shank angular velocities recorded by these sensors to detect the gait events like the Initial Contact (IC) and End Contact (EC) to, subsequently, estimate the spatio-temporal parameters for both healthy and various pathologic gait patterns. Other two methods were described in a paper recent paper of [Yuzhe Yang and Katabi, 2022], where all the 36 healthy subjects did run trials with different velocities and the IMUs sensors were placed on the ankles. Only the data collected from gyroscope and the accelerometer were used. The results of the algorithms were good, especially, in the trials at the medium speed, where the events detection errors were at their lowest with average errors of 0.0273s and 0.0214s, IC and EC respectively. Another paper, [Milad Nazarahari, 2022], used four IMUs, two on the shanks and two on the feet, to make an algorithm that, afterwards, has been compared with data recorded by two pressure insoles. The events detection was based on the measurement of the foot orientation, in particular on the pitch angle, foot angle, measures in the

sagittal plane. Instead, the trunk acceleration data were used in the paper of [Wiebren Zijlstra, 2003] to analyze their relationships with spatio-temporal gait parameters in healthy subjects. Also algorithms were developed, based on model predictions of the body's center of mass trajectory during walking. This method was tested on subjects that walked on regular ground of 60m with their regular shoes in a public building at three different speed. In the paper, it is explained how the algorithm, that detects the IC events, was developed. It was developed after some observations on the mean trunk acceleration patterns. In every kind of trial, that every kind presents a different speed of the subject, the peak acceleration identifies the foot contact with the ground. Additionally, they observed that in the antero-posterior acceleration pattern, there is always a deceleration phase after the first contact with the floor. Another interesting paper is the one of [A. Garcia and Siqueira, 2022], where they tried to write an algorithm for the IMU that is present in the phone, and this phone located in the thigh pocket. This evaluation was conducted on nine subjects without gait abnormalities and they wanted to see the precision of the algorithm in the detection of four gait events (Heel-Strike, Flat-Foot, Heel-Off and Toe-Off). For this evaluation they used the F1-score metric, often used to evaluate the performances of the algorithm in these conditions [J. D. Farah and Lemaire, 2019], [J. C. Perez-Ibarra and Krebs, 2020]. The paper found that belongs to [G. V. Prateek and Nehorai, 2020] and they tried to write and develop an algorithm to segment the gait cycle with three different events, midstance, toe-off and heel-strike. This algorithm uses the data in the sagittal plane recorded by the gyroscope sensor. This method is presented, but not in details and it is too complicated to replicate. Other algorithms, like the one presented in the paper of [Shuo Jiang, 2017], use the angle signals and their development over time. The paper cited before tried to define a threshold and to use the knee angle signal over time, but its

limitation is that this method was not evaluated sufficiently. Another algorithm of the paper belonging to [A.R. De Asha, 2012] uses the contralateral peak hip extension to detect the IC instants and they showed it using a force platform placed on the ground.

2.5 Statistical Analysis

Statistical analysis starts with a theory and a model and tries to fit the parameters of the model to the data.

We deal with two hypotheses: the null hypothesis, notated H_0 , that is the general accepted one, and its opposite, the alternative hypothesis, notated H_1 . In an ideal world, in order to determine the correct hypothesis, one should test the entire population. This is hardly the case in everyday practice; thus, we can only test a random sample of that population. One thing we must keep in mind: when choosing the random sample, we need to make sure that it matches the features of the entire population, otherwise the drawn conclusion will most definitely be wrong. After determining the correct sample, we can formulate our hypothesis.

To determine the statistical significance of an event three concepts have to be understood: hypothesis testing, the Normal distribution, and p-level. To find out whether we need to accept or reject the null hypothesis based on the evidence at hand we must perform statistical tests. There are two type of tests: parametric and non-parametric. As the name states, the parametric tests use the statistical parameters from the sample data. The statistical parameters are the mean, standard deviation (or dispersion), and the distribution that governs the data. The most used parametric tests are the t-test and ANOVA. Before applying these tests, we need to verify whether the data is governed by the Normal distribution or not.

The p-level is one of the most powerful statistical tools that can be used. It is a number between 0 and 1. Its values can be interpreted as follows: if the p-level is less than or equal to 0.05, then we can reject the null hypothesis, because there is enough

evidence to support the significance of the results; else if the p-level is greater than 0.05, then we accept the null hypothesis, due to the fact that there is not enough evidence to reject it.

In hypothesis testing we need to discuss the Normal (Gaussian) distribution. A random variable X has a Normal distribution with mean μ and dispersion σ^2 , and density and distribution function with the following formula:

$$f_X(x) = \frac{1}{\sigma\sqrt{2\pi}} \cdot e^{-\frac{(x-\mu)^2}{2\sigma^2}}, -\infty < x < \infty \text{ [eq. 3.1]}$$

The Normal distribution graph is the well-known Gaussian Bell.

The Normal distribution plot can point us some helpful information such as the area under the graph that lies between $x = \mu - \sigma$ and $x = \mu + \sigma$ contains 68% of all the observations from the statistical series. If we widen the area between $x = \mu - 2\sigma$ and $x = \mu + 2\sigma$, 95% of all the observations will fall in this region. This interval is also known as the 95% confidence interval. Widening the area all the way from $x = \mu - 3\sigma$ to $x = \mu + 3\sigma$, 99.7% of the data will be found in that interval.

Plotting the distribution graph can help us determine whether the sample data is governed or not by the Normal distribution. Another way is to apply different statistical tests such Kolmogorov–Smirnov Goodness of Fit test, the Lillifors test, and the Shapiro Wilk W test.

So, to conclude, in order to determine whether we accept or reject the null hypothesis, we need to perform specific tests that will give us a level of significance (p-level).

Normality Tests

These tests are useful to determine the data distribution. They are important to apply when it is not clear that the data distribution can be compared to a Gaussian bell. All of the tests that will be presented, being normality tests, have the null hypothesis that refers to the normality of the data. So, the hypotheses are: - H0: the data is governed by the Normal distribution; H1: the data is not governed by the Normal distribution.

The normality test chosen for this work is the Shapiro Wilk W test [H.W. Lilliefors, 1969], that computes the W statistics. Its steps are:

- n observations have to be arranged in ascending order:

$$x_1 \leq x_2 \leq \dots \leq x_n$$

- the statistics that follow must be computed:

$$Z^2 = \sum_{i=1}^n (x_i - \bar{x})^2$$

- differences have to be computed:

$$d_i = x_{n-i+1} - x_i, \quad \text{for } i = 1, 2, \dots, n/2 \text{ or } (n-1)/2, \\ \text{depending if } n \text{ is odd or even.}$$

- to use the Shapiro Wilk a_i coefficients, it has to be computed:

$$b = \sum_{i=1}^k a_i d_i$$

- Then, the W statistics is computed:

$$W = \frac{b^2}{Z^2}$$

- In conclusion, using the Shapiro Wilk table, it can be decided if the null hypothesis has to be accepted or rejected.

The ANOVA and t-test need also a check if the two groups have approximately the same variance. For doing this, there are two test that can be used.

Equality of Variances

These tests have two hypotheses, the null hypothesis is that the variances are the same and the alternative hypothesis that the variances are not equal to each other.

The first one is the Levene's test that has to be used when the data set does not have a normal distribution. The other one is the Barlett's test, that has to be used in the other case.

The Levene's test was developed by Levene in 1960 [H. Levene, 1960]. This test uses the W statistics:

$$W = \frac{(N-k)}{(k-1)} \cdot \frac{\sum_{i=1}^k N_i (Z_i - Z_{..})^2}{\sum_{i=1}^k \sum_{j=1}^{N_i} (Z_{ij} - Z_i)^2} \text{ [eq. 3.2]}$$

With: k number of data samples, N_i the i-th group's number of samples, N the total number of samples, from all the groups, $Z_{ij} = |Y_{ij} - \bar{Y}_i|$ with Y_{ij} being the value of variable j, from the i-th group, and $\bar{Y}_i, Z_i = \frac{1}{N_i} \sum_{j=1}^{N_i} Z_{ij}, Z_{..} = \frac{1}{N} \sum_{i=1}^k \sum_{j=1}^{N_i} Z_{ij}$.

The W statistics is governed approximately F-distributed with k-1 and N-k degrees of freedom.

The Barlett's test was developed by Barlett in 1937 [M. S. Barlett, 1937]. This test computes the statistics that follow:

$$\chi^2 = \frac{(N-k) \ln(S_p^2) - \sum_{i=1}^k (n_i - 1) \ln(S_i^2)}{1 + \frac{1}{3(k-1)} \left(\sum_{i=1}^k \frac{1}{n_i - 1} - \frac{1}{N-k} \right)} \text{ [eq. 3.3]}$$

Where $N = \sum_{i=1}^k n_i$, S_i variances, $S_p^2 = \frac{1}{N-k} \sum_i (n_i - 1) S_i^2$ the pooled estimate of the variance.

Both tests accept the null hypothesis if the p-level > 0.05.

ANOVA

This test, in particular the one-way ANOVA, uses the variance to compare the groups and its model is

$$y_{ij} = \mu + \tau_i + \epsilon_{ij} \begin{cases} i = 1, 2, \dots, a \\ j = 1, 2, \dots, n \end{cases} \text{ [eq. 3.4]}$$

The experimental design has to be completely randomized. ANOVA studies the variances of the residuals. The residuals are computed as the difference between the mean of each group and each object in that group. The following steps are employed: 1. The mean of each group is computed.

2. The overall mean is computed as the mean of all observations. 3. The within group variation is computed as the total deviation of each object from each sample. 4. The deviation of each group from the overall mean is computed. 5. The F statistics is computed as the ratio between the variation of the group and the variation within the group.

Figure 2.25 presents one-way ANOVA's results in terms of Sum Sq. (sum of squares), degrees of freedom (d. f.), Mean Sq. (mean squares), F-value, and Prob > F.

| Analysis of Variance | | | | | |
|----------------------|---------|-------|----------|-------|------------|
| Source | Sum Sq. | d. f. | Mean Sq. | F | Prob>F |
| bmi | 1.082 | 2 | 0.54102 | 13.74 | 1.2866e-06 |
| Error | 40.7055 | 1034 | 0.03937 | | |
| Total | 41.7876 | 1036 | | | |

Sequential (Type I) sums of squares.

Figure 2.5: Example of how the ANOVA table is presented in MATLAB.

Chapter 3 - Materials and Methods

3.1 Experimental set-up

The data for this study were collected in the Eurobench facility at the Hospital 'Los Madroños' in Brunete, Madrid, Spain. This facility, created under the EU project (<https://eurobench2020.eu/>), offer a common instrumental set up (see par 3.1.1) and a set of test beds, useful for testing several gestures in particular gait, with and without exoskeletons, and in different conditions.

3.1.1 Instrumental set-up

The experiments followed an ordered list of instrumental configurations. For the synchronization set-up of the systems used, the RCA-BNC wire has to be connected from the lock of the Vicon System to the Awinda Station (see Figure 3.1), then the output setup on the VICON system has to be selected.

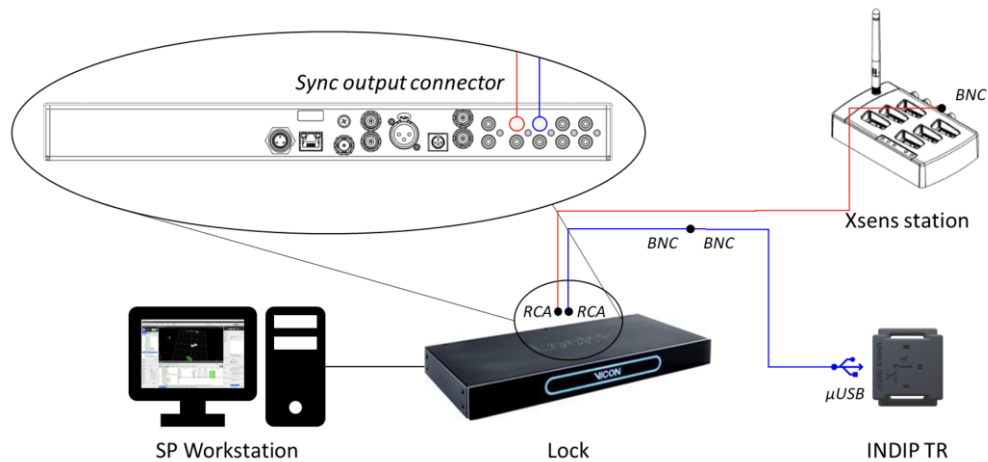


Figure 3.1: Configuration set-up.

On the Xsens software, instead, in the 'Sync Station' menu, the Sync configuration has to be set like in the Figure 3.2 and 3.3.

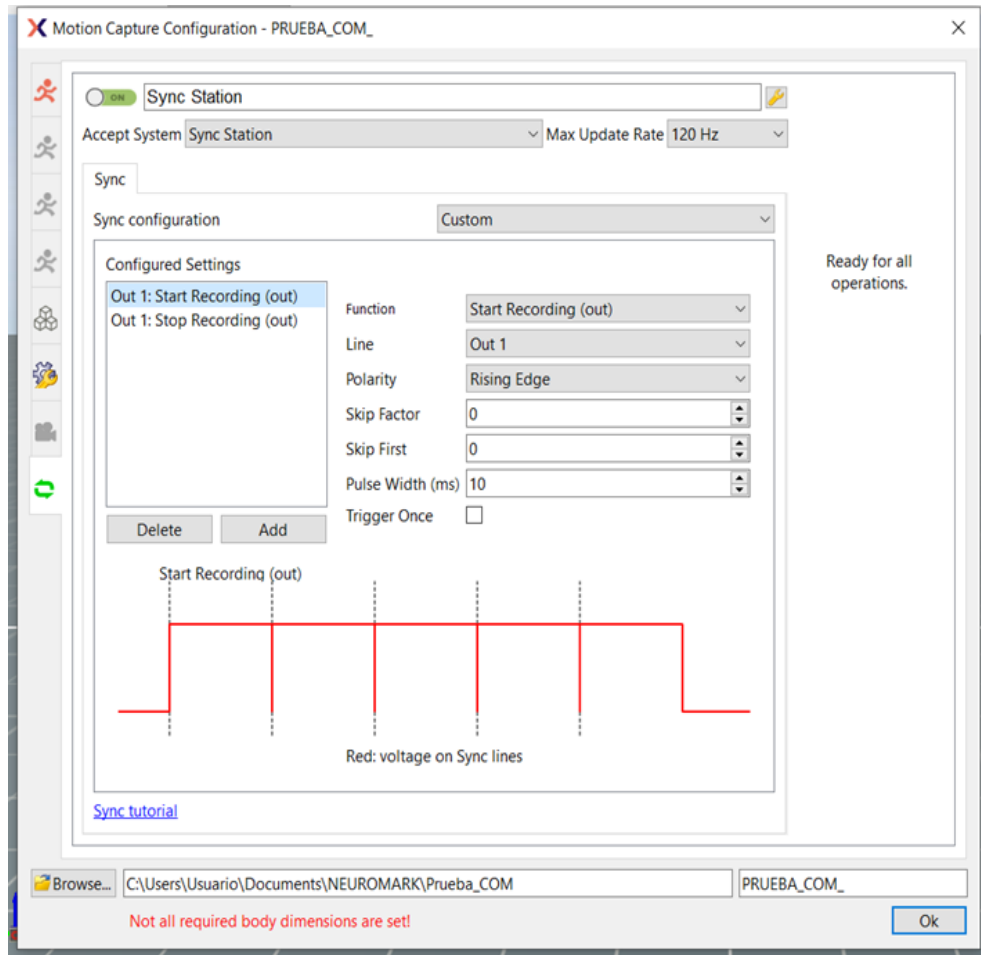


Figure 3.2: Start recording output configuration on the Xsens software.

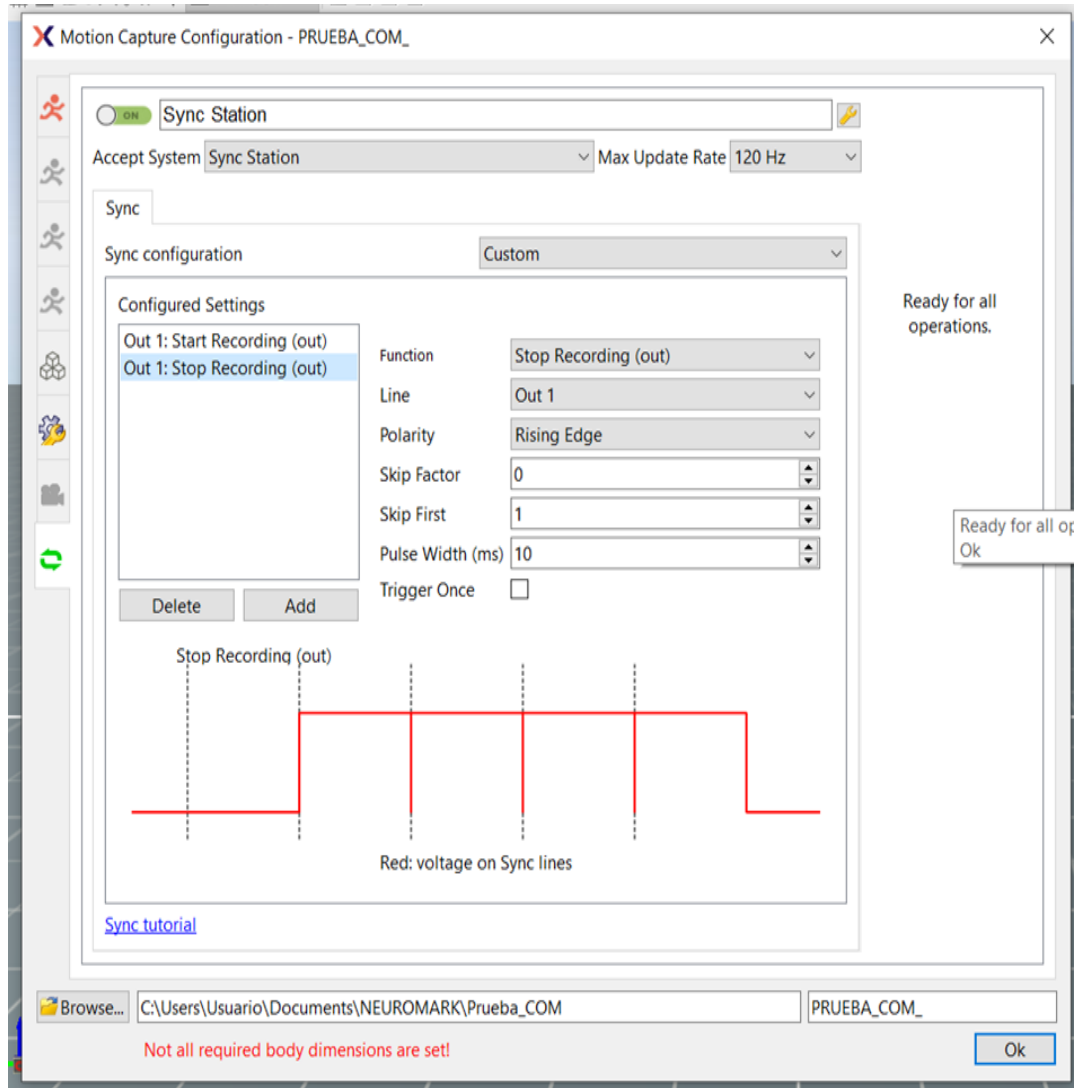


Figure 3.3: Stop recording output configuration on the Xsens software.

Then, it is necessary to perform a check to see if the trigger functions properly. For the motion capture system, the stereophotogrammetric system Vicon, it is necessary a calibration of the cameras before starting the trials and to set the origin of the system with the Vicon calibration wand (see Figure 2.3). In the end all the required measurements of the body segments of the subjects were performed.

3.1.2 Experimental protocol

To the subjects was asked to walk on every terrain at their comfortable walking speed.

Tests were designed to create difficult situations for the gait in order to create critical and sensible conditions to detect Parkinson's disease in the early phases. In this sense we have conceived a protocol based on two main factors: floor inclination and floor or terrain type.

Floor inclination is obtain using the test bed at Eurobench, that can be positioned in flat or inclined up to 15°. By walking on the two directions uphill and downhill gait can be investigated.

The set of possible terrains is really wide, in this study we have selected four of them, based on these criteria: being able to create a long corridor with the same terrain characteristics; having a rigid and compliant terrain; having regular and irregular characteristics.

1. Flat terrain: it is the rigid support of the corridor at Eurobench facility. The rigidity is very similar to a concrete floor.
2. 'M' terrain: it is constitute by rigid wood surfaces (dimension: 50 x 50 cm) inclined alternatively upward and downward of about 10° when they are placed in horizontal position.
3. Mattress (Mat) terrain : it is constitute by three mats arranged one after the other to cover the entire ground. Each mat has a density of 100 Kg/m³.
4. Terrasensa terrain: consisting of elements each 80 x 500 x 500 mm (<http://www.terrasensa-original.de/>) one after the other to cover the entire ground.

All the four terrains were investigated in the three inclination conditions flat, uphill (+ 15°) and downhill (- 15°). The length of the corridor is different for each condition and material due to realization problems. In the following the several conditions are illustrated.

1. Flat terrain:

- 0°: the subject has to walk 10 meters in a flat condition with the platform at 0 degrees.
- 15°: the subject has to walk 4 meters on a regular terrain, but with the platform at 15°, first from down to up and then from up to down (Figure 3.4).



Figure 3.4: Flat terrain at 15°.

2. Irregular terrains:

(a) Mat terrain:

- 0°: the subject has to walk 10 meters in a flat condition with the platform at 0° and with three mats on the platform (Figure 3.5).



Figure 3.5: Mat terrain at 0°.

- 15°: the subject has to walk 4 meters on a regular terrain, but with the platform at 15° and with a mat on the platform, first from down to up and then from up to down (Figure 3.6).



Figure 3.6: Mat terrain at 15°.

(b) 'Terrasensa' terrain:

- 0°: the subject has to walk 10 meters in a flat condition with the platform at 0° and with modules on the all platform (Figure 3.7).



Figure 3.7: Terrasensa terrain at 0°.

- 15°: the subject has to walk 4 meters on a regular terrain, but with the platform at 15° and with modules on the all platform, first from down to up and then from up to down (Figure 3.8).

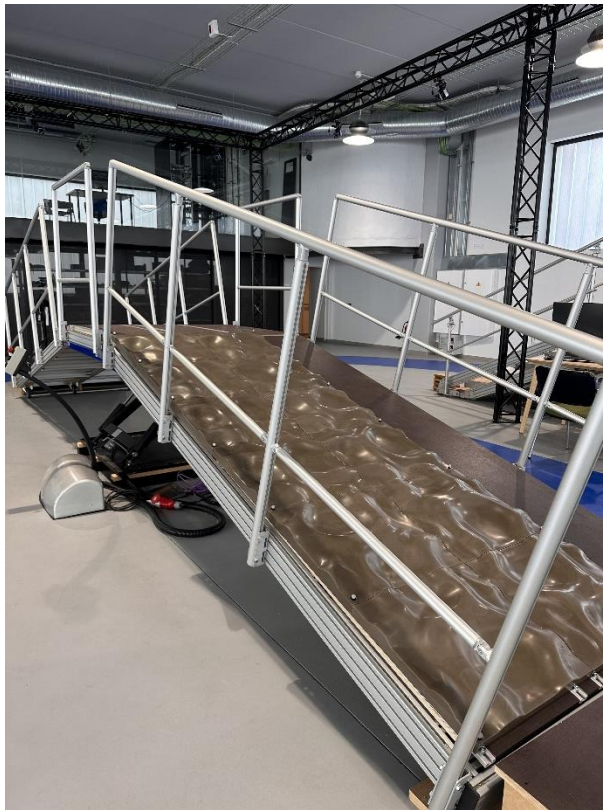


Figure 3.8: Terrasensa terrain at 15°.

(c) M terrain:

- 0°: the subject has to walk 10 meters in a flat condition with the platform at 0° and with the modules that cover all the length of the terrain (Figure 3.9).



Figure 3.9: M terrain at 0°.

- 15°: the subject has to walk 4 meters with the plat-form at 15° and with the modules placed until the end of the inclined terrain, first from down to up and then from up to down (Figure 3.10).



Figure 3.10: M terrain at 15°.

The experimental protocol required the subject to afford the terrains in a random sequence. Between each run, when it is necessary to change conditions, subjects rest on a chair while in about 10 minutes the terrain is prepared for the next trial. Unfortunately, it was not possible to operate in continuity since the corridor enables the testing of only one material at a time.

After every terrain change a new calibration of the Xsens system was performed to ensure correct operation of the collecting data by the IMU sensors and the 'Awinda Station'. Also a check on Nexus for the correct use of the Vicon system was performed every time. For what concern the Parkinson disease patients, the terrain trials were performed only at zero degrees for security reasons.

3.1.3 Subject selection and categories

Subjects included in this study are, from number 1 to 10, healthy, without relevant and known problems to walk in different conditions and terrains, only the subject number 5 has a knee problem: chondromalacia patella, also known as 'runner's knee', is a condition in which the cartilage on the inner surface of the kneecap deteriorates and softens, it starts to hurt when the knee bends 30 degrees, so it hurts only in descending M slope terrain; the other two subjects, number 11 and 12, are Parkinson's disease patients. Specific data are reported in the table 3-1. The Body Mass Index (BMI) was calculated also for each subject, the formula is $BMI = \frac{Weight [Kg]}{Height^2 [m^2]}$.

To have more than one degree of freedom for the statistical analysis that will be conducted later, the values of mass, height and BMI were grouped in more categories. The categories were determined to have the same number of subjects in each category, where it is possible, see Figure 3.11 and 3.12.

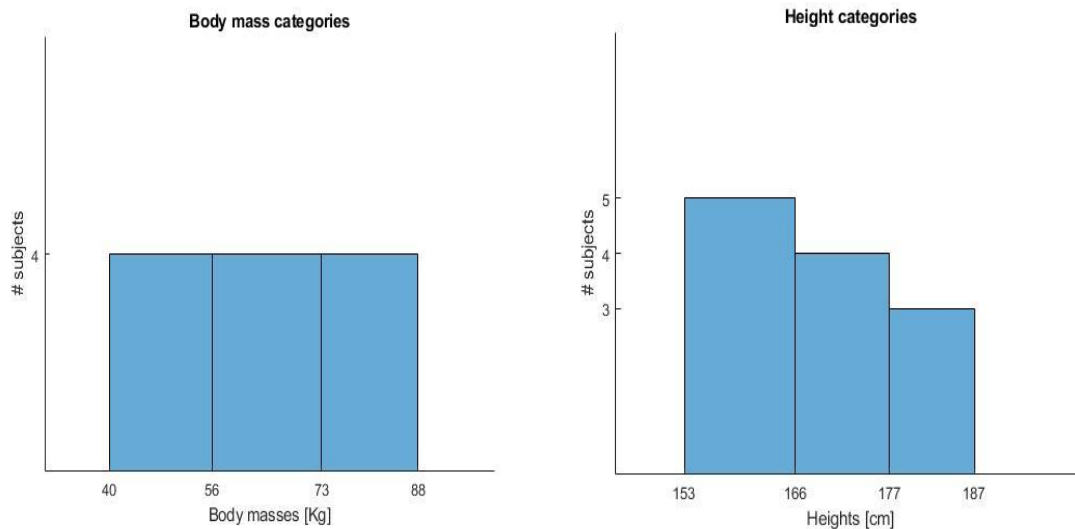


Figure 3.11: Masses and heights histograms.

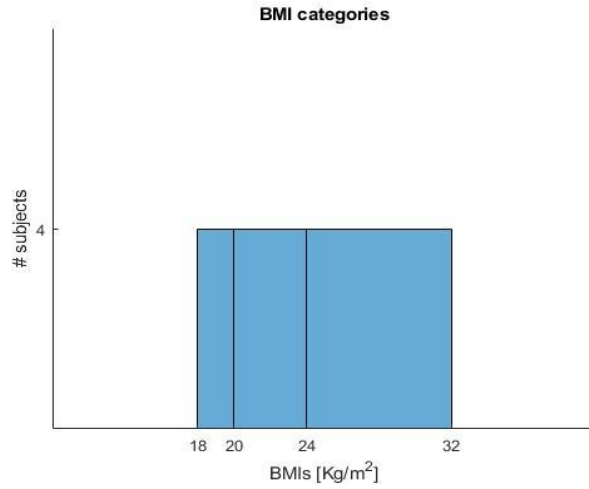


Figure 3.12: BMIs histogram.

Table 3-1: Subjects' anthropometric data.

| Subject number | Sex | Age | Mass[Kg] (Category) | Height[cm] (Category) | BMI[Kg/m ²] (Category) |
|----------------|-----|------|------------------------|--------------------------|---------------------------------------|
| 1 | F | 23 | 61.1 (2) | 174.0 (2) | 20.2 (2) |
| 2 | F | 23 | 51.0 (1) | 166.5 (2) | 18.4 (1) |
| 3 | F | 24 | 52.0 (1) | 167.5 (2) | 18.5 (1) |
| 4 | M | 23 | 87.4 (3) | 187.0 (3) | 25.0 (3) |
| 5 | F | 32 | 72.0 (2) | 176.0 (2) | 23.2 (2) |
| 6 | F | 24 | 54.1 (1) | 166.0 (1) | 19.6 (1) |
| 7 | F | 24 | 57.9 (2) | 166.0 (1) | 21.0 (2) |
| 8 | M | 24 | 85.2 (3) | 185.0 (3) | 24.9 (3) |
| 9 | F | 23 | 49.2 (1) | 162.0 (1) | 18.7 (1) |
| 10 | M | 24 | 64.4 (2) | 179.0 (3) | 20.1 (2) |
| Mean | | 24.4 | 63.4 | 172.9 | 20.9 |
| Standard dev. | | 2.72 | 13.9 | 8.7 | 2.5 |
| 11 | F | 55 | 80.0 (3) | 162.0 (1) | 30.5 (3) |
| 12 | F | 72 | 78.0 (3) | 158.0 (1) | 31.2 (3) |

3.1.4 Subjects anthropometry

According to the measurement systems guides it is necessary to measure some anthropometric characteristic of each subject to set up the proper biomechanical model.

For the Plug-in Gait model of the Vicon system the required measurements are listed in the table 3-2 and explained here:

- Body mass: the mass of the subject [Kg];
- Height: the height of the subject [mm];
- Leg length: distance from the anterior superior iliac spine to the medial malleolus of the ankle [mm]. Measured while standing, if possible. This data is required for the left and right sides;

Table 3-2: required measurements for Vicon.

| Measurements | Units |
|-----------------|-------|
| Body mass | [Kg] |
| Height | [mm] |
| Leg length | [mm] |
| Knee width | [mm] |
| Ankle width | [mm] |
| Shoulder offset | [mm] |
| Elbow width | [mm] |
| Wrist width | [mm] |
| Hand thickness | [mm] |

- Knee width: medial-lateral width of the knee through the flexion axis in millimeters, one for the right side and one for the left side. To be measured while standing, if possible;
- Ankle width: mid-lateral distance between the malleoli of the ankle in millimeters, one for the right side and one for the left side. To be measured standing, if possible;
- Shoulder offset: vertical distance from the center of the glenohumeral joint to the acromion in millimeters, one for the right side and one for the left side;
- Elbow width: distance between the medial and the lateral epicondyles of the humerus in millimeters, one for the right side and one for the left side;
- Wrist width: the anterior-posterior distance of the wrist in millimeters at the position where our wrist marker bar is attached, one for the right side and one for the left side. If the wrist markers are attached directly to the skin, this value should be set to zero and this one was my case, so I put zero for this parameter;
- Hand thickness: the interior posterior thickness between the dorsal and palmar surfaces of the hand in millimeters, one for the right side and one for the left side.

For the Xsens inertial system (see table 3-3), the required measurements are different:

- Body height: if the subject in the experiment has to have the shoes, this measure, like the others, has to be taken with the same shoes that will be used by the person;
- Foot length: distance from the heel to the toe in centimeters;
- Shoulder height: distance from C7 vertebra to the floor in centimeters;
- Shoulder width: from the left acromioclavicular joint to the right acromioclavicular joint in centimeters.
- Elbow span: from the left elbow to the right elbow in centimeters with the subject in T-pose;

Table 3-3: required measurements for Xsens.

| Measurements | Units |
|-----------------|-------|
| Body height | [cm] |
| Foot length | [cm] |
| Shoulder height | [cm] |
| Shoulder width | [cm] |
| Elbow span | [cm] |
| Wrist span | [cm] |
| Arm span | [cm] |
| Hip height | [cm] |
| Hip width | [cm] |
| Knee height | [cm] |
| Ankle height | [cm] |

- Wrist span: from the left wrist to the right wrist in centimeters with the subject in T-pose;
- Arm span: from the end of the left hand to the end of the right hand in centimeters, always with the subject in T-pose;
- Hip Height: measured from the greater trochanter to the ground in centimeters;
- Hip Width: distance between the iliac spines in centimeters;
- Knee height: from the knee to the floor in centimeters;
- Ankle height: from the ankle to the ground in centimeters.

3.2 Subject set-up

3.2.1 Vicon

In the Figure 3.13 and 3.14, the position and the label of the markers that have to be placed on the subjects' body:

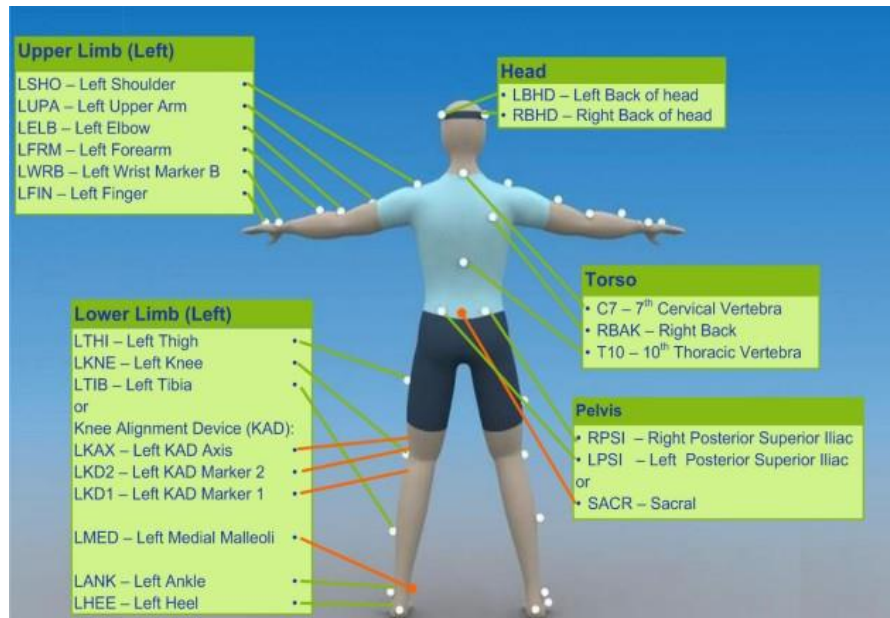


Figure 3.13: Vicon markers name and position on the body, back view.

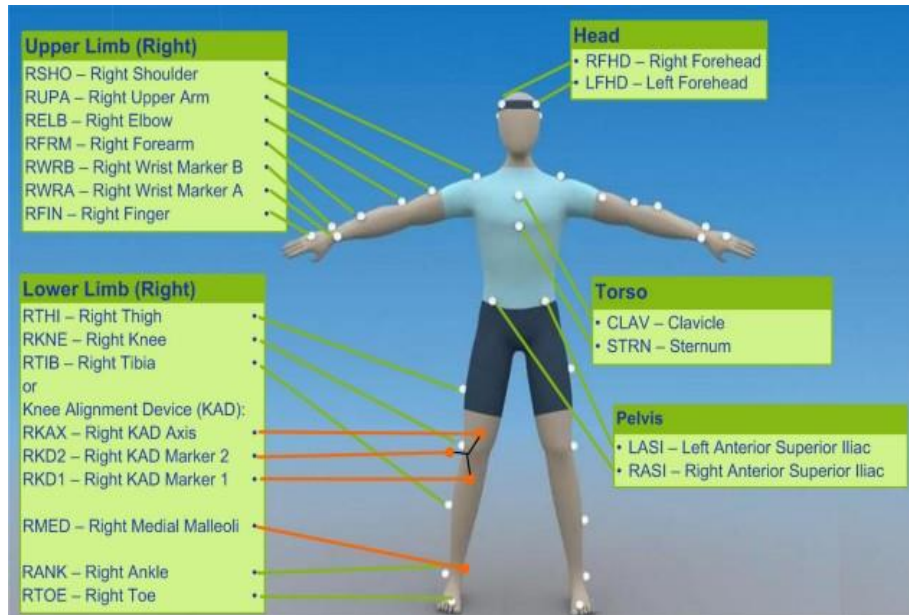


Figure 3.14: Vicon markers name and position on the body, front view.

o Head (Figure 3.15)

| Marker label | Definition | Position on patient |
|--------------|------------------|--|
| LFHD | Left front head | Left temple |
| RFHD | Right front head | Right temple |
| LBHD | Left back head | Left back of head (defines the transverse plane of the head, together with the frontal markers) |
| RBHD | Right back head | Right back of head (defines the transverse plane of the head, together with the frontal markers) |

Figure 3.15: label and position of the markers of the head.

- Torso (Figure 3.16)

| Marker label | Definition | Position on patient |
|--------------|------------------------|---|
| C7 | 7th cervical vertebra | On the spinous process of the 7th cervical vertebra |
| T10 | 10th thoracic vertebra | On the spinous process of the 10th thoracic vertebra |
| CLAV | Clavicle | On the jugular notch where the clavicles meet the sternum |
| STRN | Sternum | On the xiphoid process of the sternum |
| RBAK | Right back | Anywhere over the right scapula (This marker has no equivalent marker on the left side. This asymmetry helps the autolabeling routine determine right from left on the subject. Placement is not critical as it is not included in the Plug-in Gait model calculations.) |

Figure 3.16: label and position of the markers of the torso.

○ Upper limbs (Figure 3.17)

| Marker label | Definition | Position on patient |
|---------------------------------|----------------------|--|
| Left upper limb markers | | |
| LSHO | Left shoulder | On the acromio-clavicular joint |
| *LUPA | Left upper arm | On the upper lateral 1/3 surface of the left arm (Place asymmetrically with RUPA) |
| LELB | Left elbow | On the lateral epicondyle |
| *LFRM | Left forearm | On the lower lateral 1/3 surface of the left forearm (Place asymmetrically with RFRM) |
| LWRA | Left wrist marker A | At the thumb side of a bar attached to a wristband on the posterior of the left wrist, as close to the wrist joint center as possible. Loose markers can be used but for better tracking of the axial rotations, a bar is recommended. |
| LWRB | Left wrist marker B | At the little finger side of a bar attached to a wristband on the posterior of the left wrist, as close to the wrist joint center as possible. Loose markers can be used but for better tracking of the axial rotations, a bar is recommended. |
| LFIN | Left finger | Just proximal to the middle knuckle on the left hand |
| Right upper limb markers | | |
| RSHO | Right shoulder | On the acromio-clavicular joint |
| *RUPA | Right upper arm | On the lower lateral 1/3 surface of the right arm (Place asymmetrically with LUPA) |
| RELB | Right elbow | On the lateral epicondyle approximating the elbow joint axis |
| *RFRM | Right forearm | On the lower lateral 1/3 surface of the right forearm (Place asymmetrically with LFRM) |
| RWRA | Right wrist marker A | At the thumb side of a bar attached symmetrically with a wristband on the posterior of the right wrist, as close to the wrist joint center as possible |
| RWRB | Right wrist marker B | At the little finger side of a bar attached symmetrically with a wristband on the posterior of the right wrist, as close to the wrist joint center as possible |
| RFIN | Right finger | Just below the middle knuckle on the right hand |

Figure 3.17: label and position of the markers of the upper limbs.

- Pelvis (Figure 3.18)

| Marker label | Definition | Position on patient |
|--------------|------------|---|
| SACR | Sacral | On the skin mid-way between the posterior superior iliac spines (PSIS) and positioned to lie in the plane formed by the ASIS and PSIS points. |
| LASI | Left ASIS | Left anterior superior iliac spine |
| RASI | Right ASIS | Right anterior superior iliac spine |
| LPSI | Left PSIS | Left posterior superior iliac spine (immediately below the sacro-iliac joints, at the point where the spine joins the pelvis) This marker is used with the RPSI marker as an alternative to the single SACR marker. |
| RPSI | Right PSIS | Right posterior superior iliac spine (immediately below the sacro-iliac joints, at the point where the spine joins the pelvis) This marker is used with the LPSI marker as an alternative to the single SACR marker. |

Figure 3.18: label and position of the markers of the pelvis.

- Lower limb (Figure 3.19)

| Marker label | Definition | Position on patient |
|---------------------------------|-------------|---|
| Left lower limb markers | | |
| LTHI | Left thigh | Over the lower lateral 1/3 surface of the left thigh |
| LKNE | Left knee | On the flexion-extension axis of the left knee |
| LTIB | Left tibia | Over the lower 1/3 surface of the left shank |
| LANK | Left ankle | On the lateral malleolus along an imaginary line that passes through the transmalleolar axis |
| LHEE | Left heel | On the calcaneus at the same height above the plantar surface of the foot as the toe marker |
| LTOE | Left toe | Over the second metatarsal head, on the mid-foot side of the equinus break between fore-foot and mid-foot |
| Right lower limb markers | | |
| RTHI | Right thigh | Over the upper lateral 1/3 surface of the right thigh |
| RKNE | Right knee | On the flexion-extension axis of the right knee. |
| RTIB | Right tibia | Over the upper 1/3 surface of the right shank |
| RANK | Right ankle | On the lateral malleolus along an imaginary line that passes through the transmalleolar axis |
| RHEE | Right heel | On the calcaneus at the same height above the plantar surface of the foot as the toe marker |
| RTOE | Right toe | Over the second metatarsal head, on the mid-foot side of the equinus break between fore-foot and mid-foot |

Figure 3.19: label and position of the markers of the lower limbs.

Other two markers on each foot were added (red circled in Figure 3.20) to reconstruct the relative positions of the toe marker and heel marker if needed during the processing of the trials on Nexus.

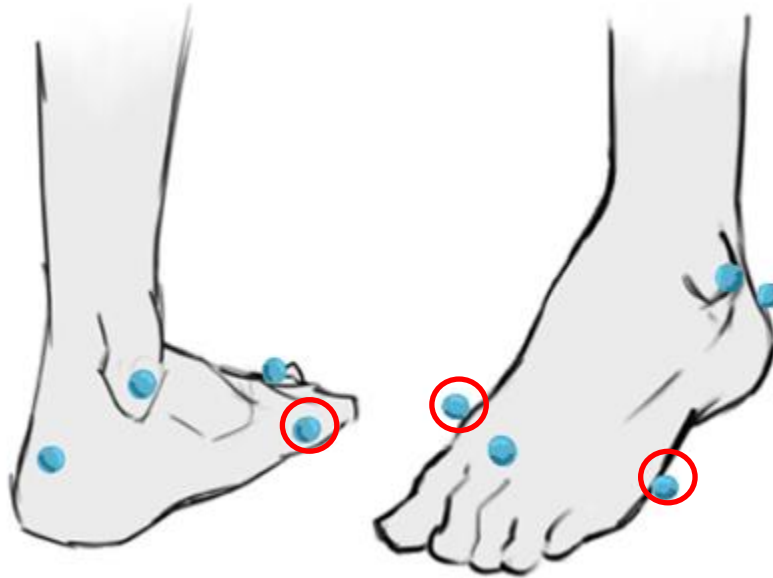


Figure 3.20: Markers added.

3.2.2 Xsens

The IMU sensors positioned on the subjects' body were 17, using the 'MVN Awinda Straps' of Xsens. The online instructions on tutorial.xsens.com/mvn for the full body configuration were followed. The label on the side of the tracker indicates the position on the body, as we can see in the Figure 2.4. The position of the sensors are shown in the Figure 3.21.

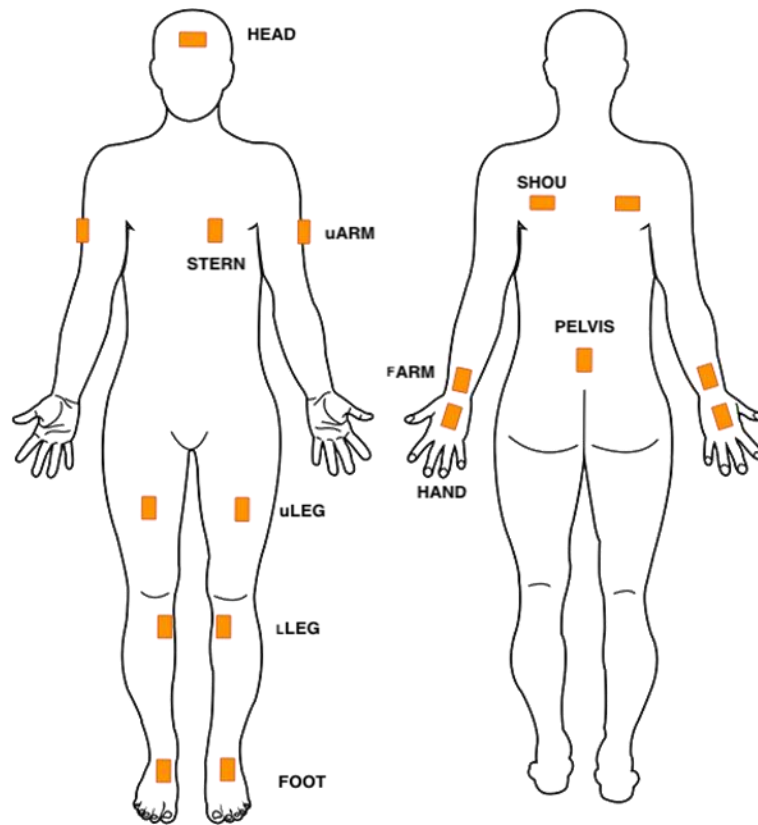


Figure 3.21: IMU Xsens sensors positions on the body.

An example of a subject with all markers and sensor is shown in the Figure 3.22.



Figure 3.22: An instrumented subject before starting the experimental trials.

3.3 Subject calibration

3.3.1 Vicon

Before the dynamic trials, a calibration of the subject has to be performed on the Nexus software. The calibration phase was done, dividing it in two trials, one the classic static trial where the subject has to be in the position shown in the Figure 3.23, with the arms parallel to the ground and the body in the stand position.

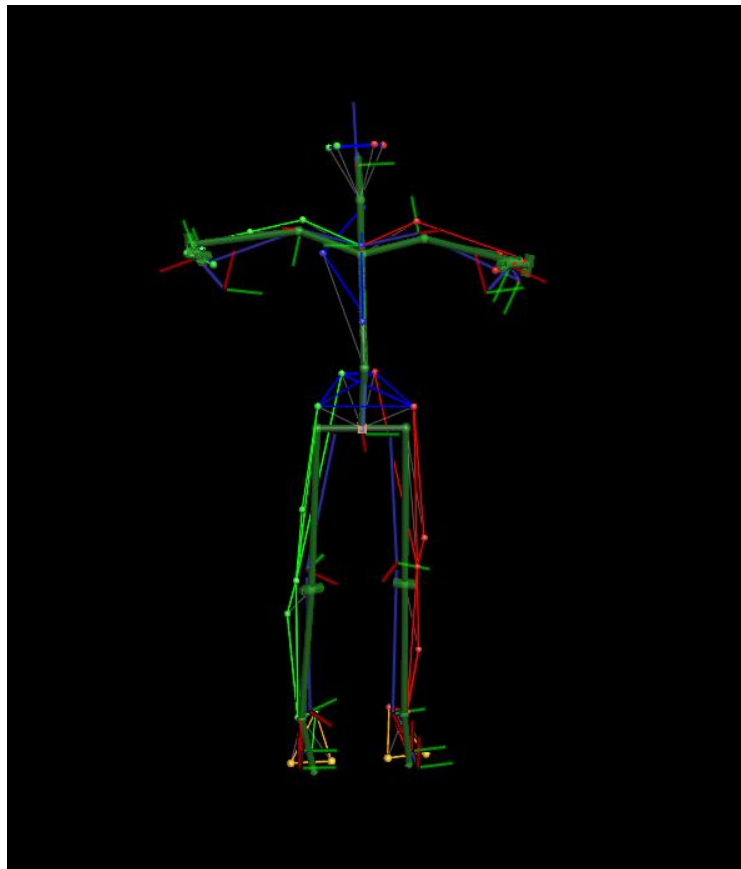


Figure 3.23: static calibration of Vicon, view on the Nexus software.

After this trial, a 'functional calibration' was performed. The subject has to stand in a fixed position and to move alternatively and slowly all the body segments, as it is intuitive from the image of the Nexus software shown in the Figure 3.24.

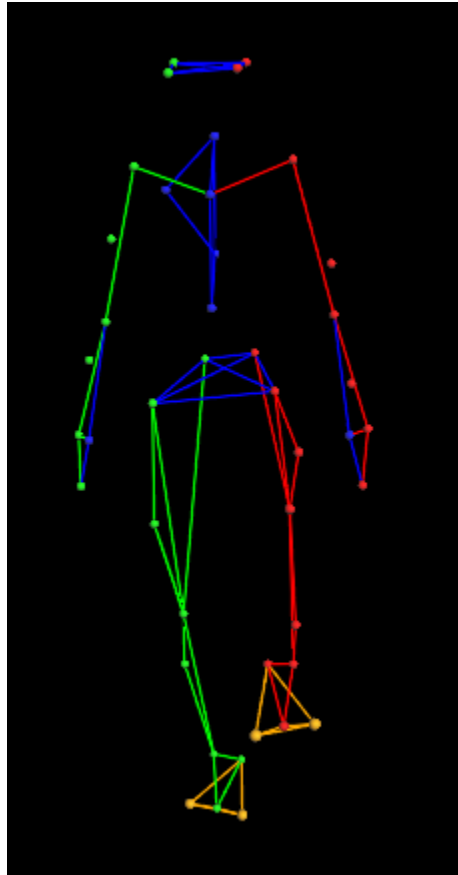


Figure 3.24: functional calibration of Vicon, view on the Nexus software.

3.3.2 Xsens

The Xsens calibration was performed after every change of the terrain. This calibration, that compares as in the Figure 3.25 in the software, asks to the subject to stay in N-pose for few seconds, then to move around the space of the future data acquisition and in the end to stand in the N-pose in the same point where the subject started the calibration. All these commands are explained in live mode by the software 'MVN Analyze'. At the end of the calibration, the software has to say 'calibration was good', if not the calibration has to be repeated until the message above compares on the software window.

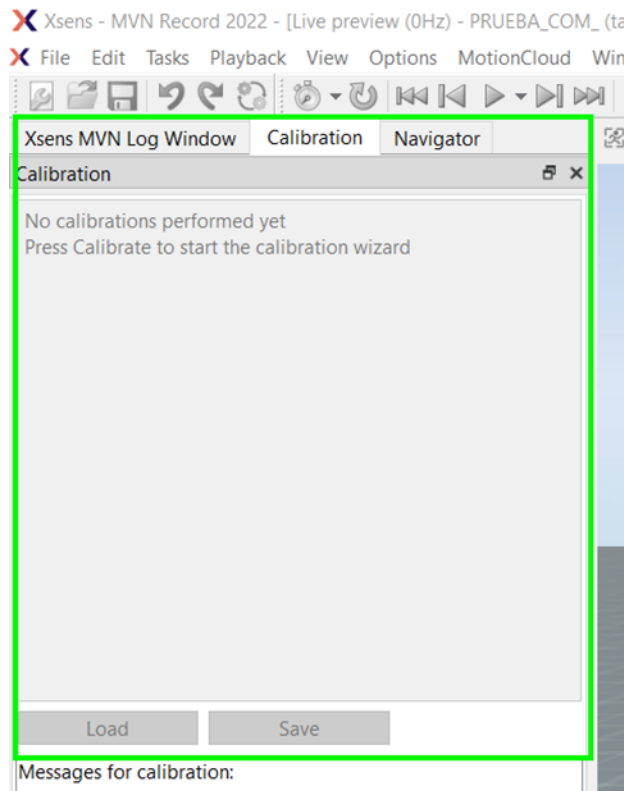


Figure 3.25: calibration window on the 'MVN Analyze' software.

3.4 Postprocessing phase

3.4.1 Vicon

Postprocessing of a Optoelectronics Motion capture test, consist in:

- reconstruction of markers positions – in practice completely automated in Nexus software;
- labelling: almost automatic in nexus software after the subject calibration;
- gap filling.

After this preprocessing the data is ready to be analyzed as regards the gait phases that are the main focus in this thesis. We now introduce some details for the gap filling phase.

Even if the experimental procedure takes into account all possible precautions, gaps in the markers trajectories are almost the gaps are always present. They may be due to particular subject movements such as an hand moving on a marker on the pelvis, or to specific problems for example regarding camera positions with respect to subject movement. The first step to be carried out. A gap is defined as a time instant in which a marker that was previously present in the test now is missing and in the next frames it will be visible again.

There are different methods to fill gaps available in Nexus, that we can see in the Figure 3.26. In this thesis processing the methods mainly used are the following ones.

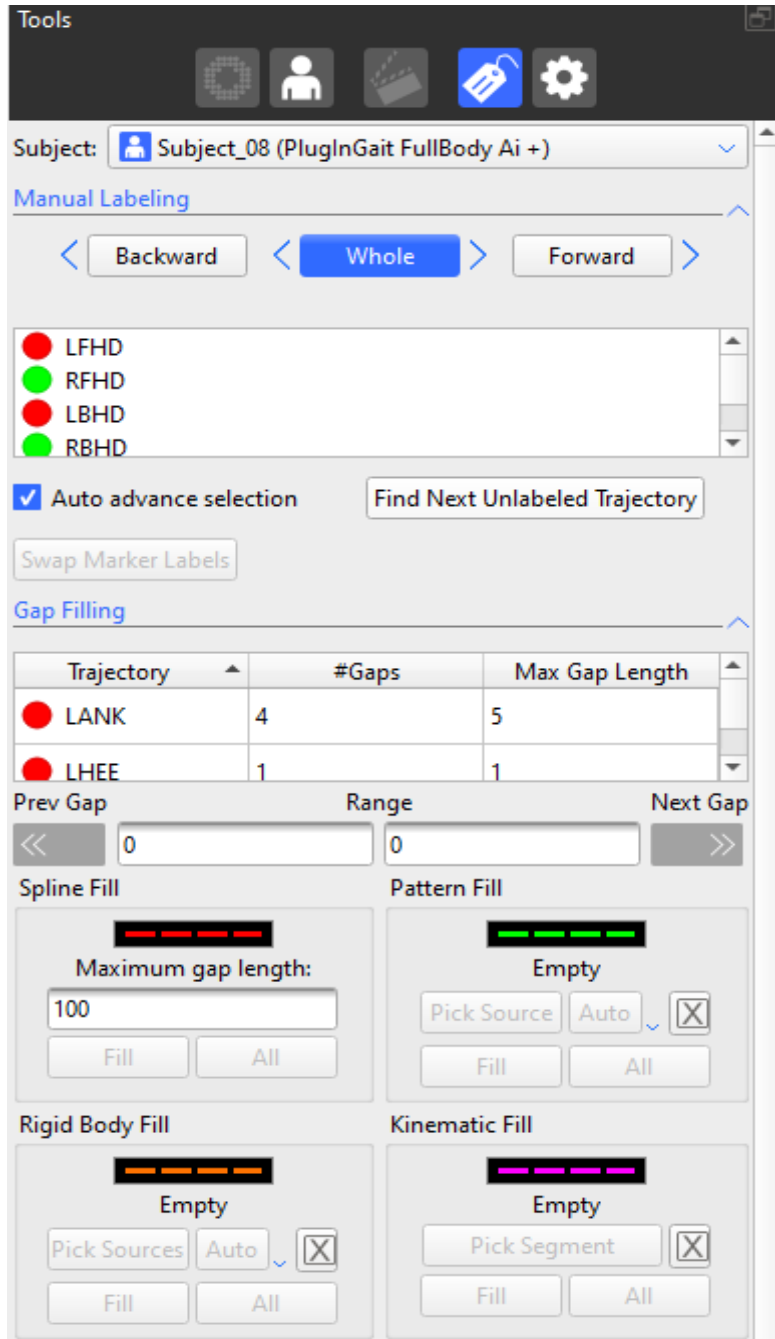


Figure 3.26: Filling gaps tool on the Nexus software.

'Pattern fill' uses the shape of another trajectory without a gap to fill the selected gap. This tool has to be used only if there is a suitable marker with a trajectory similar to the one whose gap you wish to fill. This is typically the case when the trajectories originated from markers attached to the same segment.

'Rigid Body Fill' has to be used when a rigid or semi-rigid relationship exists between markers. As example we can consider: Pelvis (LASI, RASI, LPSI, RPSI markers), Head (LFHD, RFHD, LBHD, RBHD markers) and also Trunk (C7, T10, CLAV, STRN markers), if its flexion is discarded.

Moreover a new method has been used based on extra markers.

This method enables the reconstruction of the right and left ankle and heel markers, using the relative positions of the two added markers on each foot and of the toe marker. Before, it is necessary to save the relative position of them in the static trial, thanks to the 'Run Static Body Language Model' command and to the file.mod created.

Then, in the dynamic trials, if the markers of ankle or heel are not present in one or more frames, it is necessary to run the highlighted command on the Figure 3.27 to fill the gaps of these markers with a reconstructed marker that uses the relative positions saved before. In some frames the capture can lose some markers for multiple reasons, something can cover the marker during the subject movements, or only one camera sees the marker so the position in the 3D space cannot be reconstructed, or the light reflection problems were not avoided correctly during the calibration.

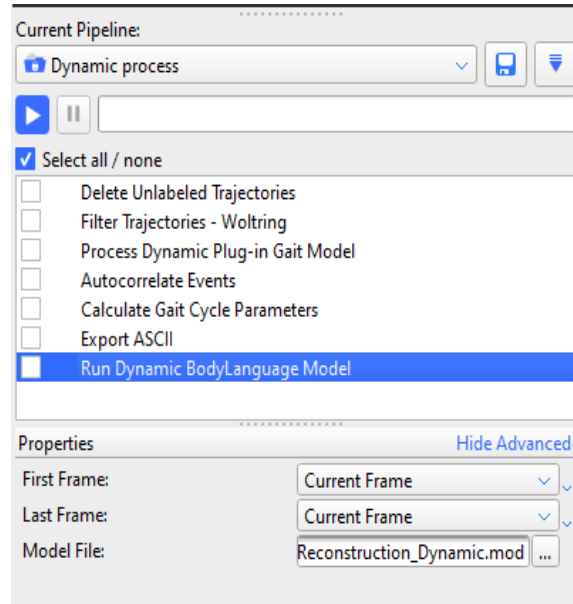


Figure 3.27: dynamic pipeline on the Nexus software.

3.4.2 Xsens

For the Xsens system, there is a software that processes the data, 'MVN Analyze', and can give in output acceleration data, angular velocities data, magnetometer data, joint angles data, the trajectories of constructed markers on the body. This software can give in output these data because it uses biomechanical models of the human body [Schepers].

This software has different scenarios to process the collected data.

For the trials on the flat terrain, the 'Single Level' option has to be selected; for the trials on the M terrain and on the Terrasensa terrain, the 'Multi Level' option has to be selected; for the Mat terrain, there is the option 'Soft Floor'.

For the trials conditions where the terrains are in slope at 15 deg, the option 'Multi Level' has to be selected for every terrain. After this process, the data are saved in file.xlsx and a code to read only the parts where the acceleration, angular velocity and joint angles data was implemented.

3.5 Gait events detection

3.5.1 Vicon

The last processing part done in this software is the most important one, the event selection part, that represents our gold standard.

The concept behind this task lies in the fact that the trajectory is the principal output of this system, so the most accurate one, that not expect calculations inside the software, like derivation to have the velocity or the acceleration data. So, a method that went to see and analyze the trajectory of the foot markers was thought. In general, the point of the heel marker trajectory that has the lowest vertical coordinate is the interested point for the IC instant. It is like that for the flat terrain at 0 deg, but for the other terrains it is not always like that. For this reason, positioning markers every 50 cm on both sides on the irregular terrains was thought and then a template for irregular terrains was created on the Nexus software to help the visualization of the IC event, because on the Mat terrain, for example, the IC instant is the instant when one part of the foot touches the Mat and this one is not the lowest trajectory point, but the point of the trajectory that crosses the lines that reconstruct the Mat terrain on the Nexus software. Also, it was helpful to record the trials with GoPro cameras because in some cases, like the trials on the Terrasensa terrain, the identification of the IC or EC events is very difficult because of the shape of the terrain. For the EC event, the lowest trajectory point of the toe marker before the start of the swing phase is our EC event. In the irregular terrains trials, this fact is not always the same and the reconstruction of the terrains on the software helps another time as it is possible to see in the Figure 3.29.

Practical instructions

Flat terrain:

- Initial Contact: Select the heel marker, look to the lowest trajectory part and see if the marker is aligned with the reconstructed terrain on the software. Select the frame where the cone parts attached to the marker change directions (see Figure 3.28).

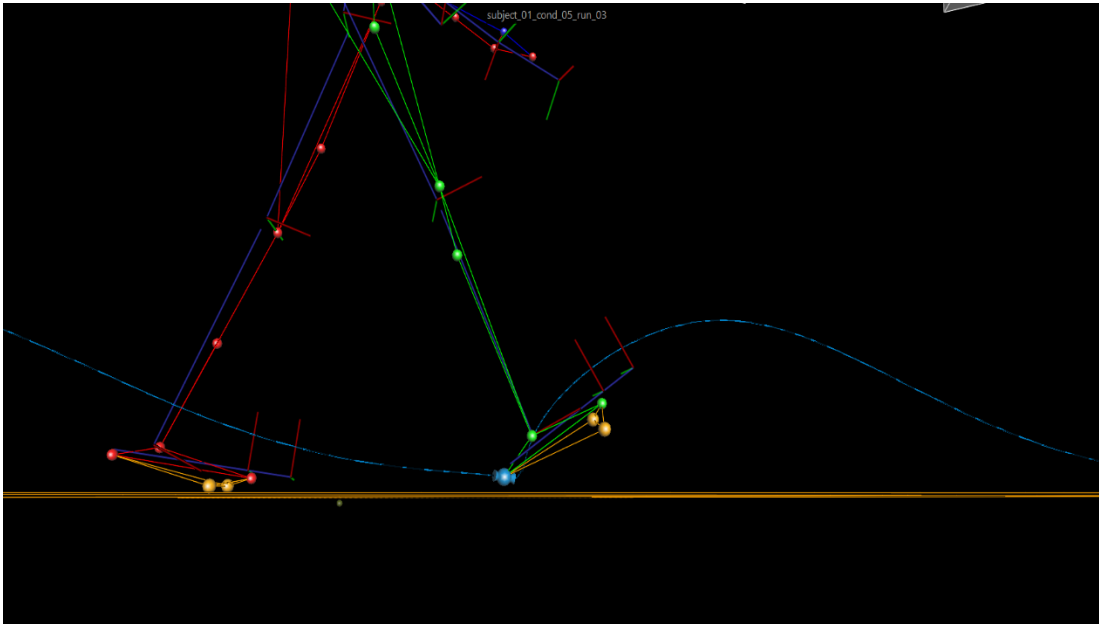


Figure 3.28: Example of the frame selected for the IC instants on flat terrain.

- End Contact: Select the toe marker. Go to the lowest point of the trajectory before the start of the swing phase. Select the second frame in which the cones pointing at the marker have been aligned with the trajectory it will follow.

M terrain:

- Initial Contact: Select the heel marker, look at where the trajectory is at the lowest point and where the marker is aligned with the

reconstructed terrain on the software. Select the frame in which the cone parts attached to the marker change direction.

- End Contact: Select the toe marker. Go to the lowest point of the trajectory before the start of the swing phase. Select the frame in which the cones that point to the marker have been aligned with the trajectory it will follow.

Mat terrain:

- Initial Contact: Select the heel marker. Select the frame where the marker intersects the reconstructed plane of the terrain in its lowest trajectory part. Note that this is not the minimum value of the heel elevation, since the loaded heel will sink a bit in the Mattress.
- End Contact: Select the toe marker. Select the third frame after the alignment of the cone parts attached on the marker in the initial part of the swing phase, where the marker starts to go up.

Terrasensa terrain:

- Initial Contact: Select the heel marker. When the marker is in its lowest point, combine the view of the trials on the video recorded by the camera with the visualization on Nexus, because this terrain has too particular irregularities to try to find a systematic and precise way to define the IC instant.
- End Contact: Select the toe marker. Do the same procedure explained for the IC instant.

This procedure , carried out manually with the best motion capture system at the state of the art, produces result that can be considered as gold standard events for our comparison. Nevertheless the instants are identified manually, so maybe they are affected by some subjectivity,. To

understand the subjectivity level, three engineers of the Cajal Institute in Madrid applied exactly the same procedure to the same data set. In total we can consider 4 operators including myself. The Mean Absolute Errors (MAE) between the data collected by the 4 operators on each terrain does not exceed four hundredths of a second, or 4 frames in motion capture system, so it seems to be a very good method.

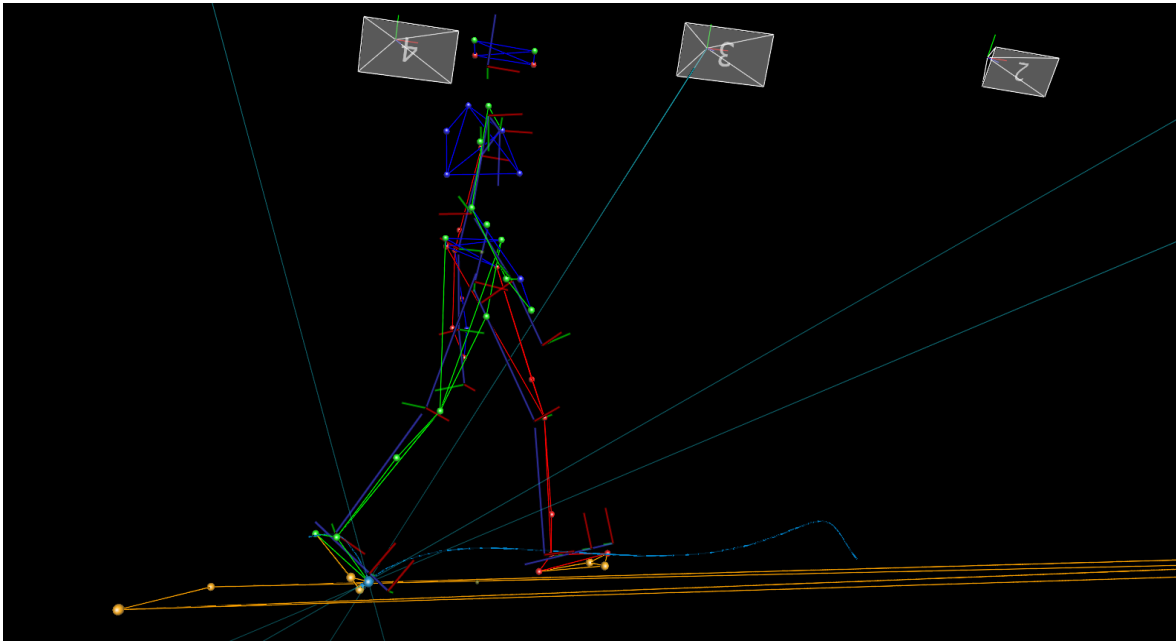


Figure 3.29: Example of the frame selected for the EC instants on mat terrain.

3.5.2 Xsens

For the IMU data, the criteria to select the methods were: use angular velocities or linear acceleration data, principal output data from the IMU sensors, use data that come from the preferred IMU placements, that are the shank and the foot [Prasanth, 2021], algorithms with most citations and the easiest to replicate.

Method 1

The first one chosen method was that of [Wiebren Zijlstra, 2003]. This algorithm takes the antero-posterior acceleration of the IMU on the pelvis. First, it has to be made a removal of low-frequency noise with an high-pass filter of Butterworth of the fourth order and cutoff frequency at 0.1Hz. Then, must be carried out other two filtering operations, both with the low-pass fourth order Butterworth filter and the signal already filtered before, but one at a cut-off frequency of 20Hz and the other at a cut-off frequency of 2Hz. So, in MATLAB the functions 'butter()' and 'filtfilt()' were used. On the signal filtered at the cut-off frequency of 2Hz must be identified the zero-crossing points, so the points where the accelerometer signal goes from being positive to being negative and this operation was made in MATLAB using a for loop where the rows of the acceleration positive values positioned immediately before the first acceleration negative values were saved in a vector called 'zero'. Instead, on the signal filtered at the cut-off frequency of 20Hz must be detected the peaks of the acceleration signal, using the MATLAB function 'findpeaks' that provides the value and the row inside the vector of every identified peak. Analyzing the plots in more trials the best values for the 'MinPeakDistance' and 'MinPeakHeight' parameters of the function were 0 seconds and 0.9m/s^2 , respectively. The next and last step was to define

the peak before the zero-crossing point like the IC instant. It was possible thanks to the implementation of a for loop that saves the position of the peak that presents the smallest difference in frames between the zero-crossing point and the peaks before it. In the Figure 3.30 we can see the visualization of the acceleration signal filtered at 20Hz and 2Hz, the zero-crossing points in red, the peaks in green and the IC instants in black. Then, the values in frame were converted in seconds using the sample frequency of Xsens: 60Hz.

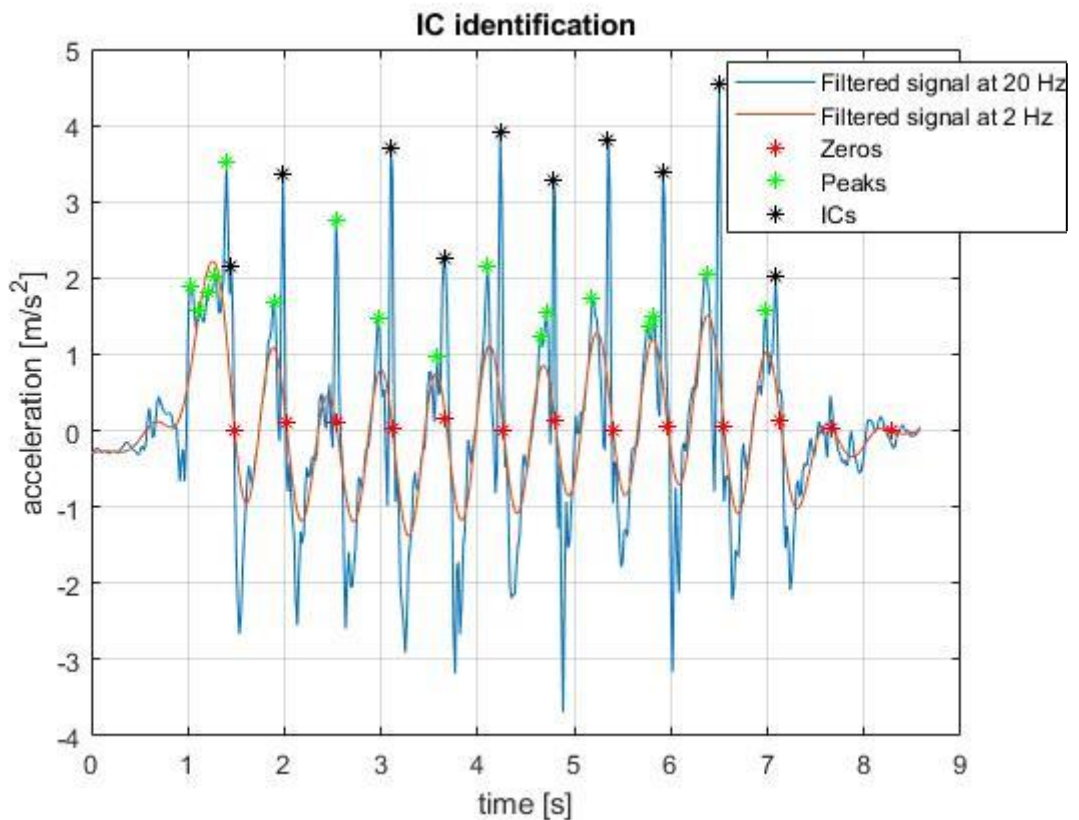


Figure 3.30: IC instants identification of the 'Zijlstra' method - MATLAB.

At the end the IC instants were saved in a file.csv where in a second step were used to create a matrix that describes who was the subject, which was the terrain, the condition and the repetition of the trial.

Method 2

The first algorithm of the paper of [M. Jasiewicz, 2006] was used as our second method, it uses the linear x-directed acceleration of the foot and, in particular, tries to find the peaks located in the EC search windows, located 250ms before and 50ms after each peak of ankle plantar flexion. To do this, a code in MATLAB was implemented. First, the acceleration was filtered with an high-pass filter of Butterworth of the fourth order and cutoff frequency at 0.1Hz to remove the noise from the signal, using the functions 'butter()' and 'filtfilt()'. Other parameters for the filter were analyzed, but the cut-off frequency at 8 or 10 Hz for walking recommended by [Emily J. Miller, 2022] and [Daniel W.T. Wundersitz, 2014] seemed to change too much the signal values. So, the peaks of the acceleration have to be found, the function used was 'islocalmax()' with 'MinProminence' set to 10 m/s², then the function 'find()' to find the frames where these peaks were located in the acceleration signal. Now, it is necessary to create the EC search windows. In the code, the same functions used for the acceleration signal were implemented, also with the same value of the parameter of the function 'islocalmax'. Then, the two extremes said before of the search window were converted in frame values to manage better the rows of the vectors that contain the ankle angle values. In the code, a number of cells in a cell array was set. This number corresponds to the number of peaks found by the 'islocalmax()' function. These cells were fill with the frames that go from the first extreme to the last extreme of the window calculated thanks to the frames where are located the ankle angle peaks found, in the code with a for loop that fills each cell with the described frames. The last step was to write a for loop with an if condition to find the frame of the acceleration peak found before that corresponds to the all possible frames of the window defined above in the cells of the cell array. The same code was used for the left and for the right acceleration signals. An example of the final result is shown in the Figure

3.31 below.

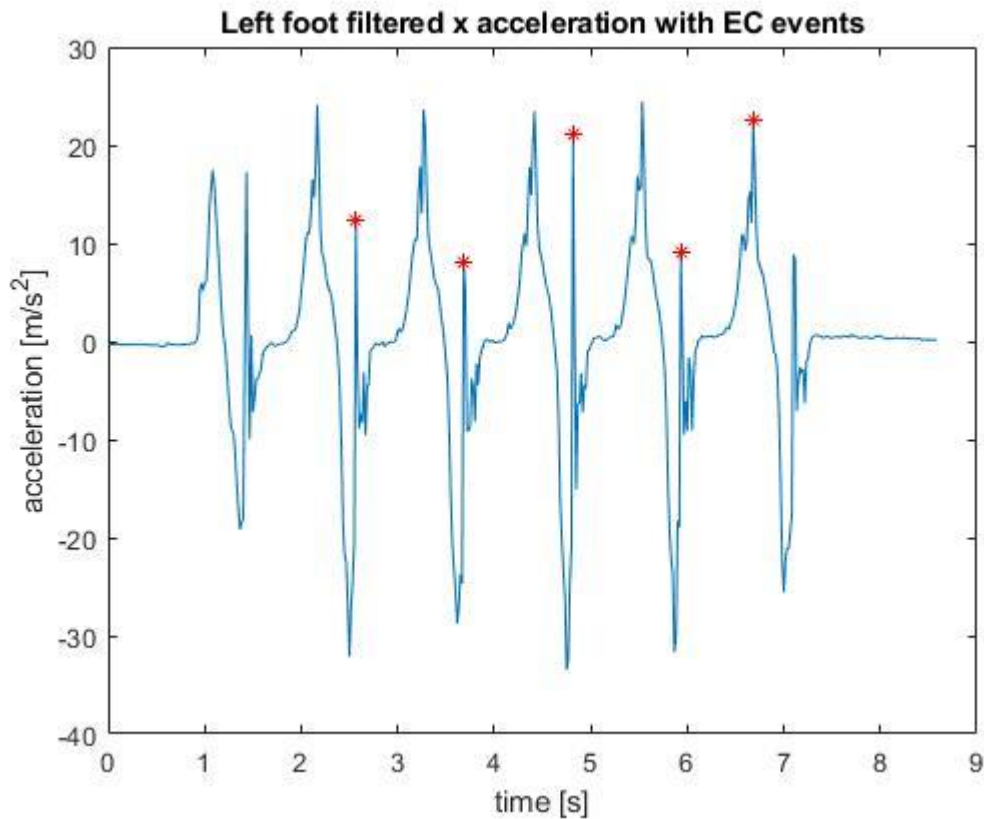


Figure 3.31: EC instants identification of the foot acceleration method - MATLAB.

As the previous method, the EC instants were saved in a file.csv to be used later for the analysis.

Another algorithm, always classified as second method because it uses the linear z-directed acceleration of the foot and it is very similar to the previous algorithm explained. It tries to find the peaks located in the IC search windows, located 100ms before and 100ms after each peak of ankle dorsi flexion. To do this, a code in MATLAB was implemented. First, the acceleration was filtered with an high-pass filter of Butterworth of the fourth order and cutoff frequency at 0.1Hz to remove the noise from the signal, using the functions 'butter()' and 'filtfilt()'. So, the peaks of the acceleration have to be found, the function used

was 'islocalmax()' with 'MinProminence' set to 10 m/s², then the function 'find()' to find the frames where these peaks were located in the acceleration signal. Now, it is necessary to create the IC search windows. In the code, the function 'islocalmin()' was used because the dorsi flexion peaks in the ankle flexion signal are the minimums. The parameter 'MinProminence' was set to the absolute value of the first ankle value in the interested signal, because the subject starts from a standstill pose. Then, the twoextremes said before of the search window were converted in frame values to manage better the rows of the vectors that contain the ankle angle values. Inthe code, a number of cells in a cell array was set. This number corresponds to the number of peaks found by the 'islocalmin()' function. These cells were fill with the frames that go from the first extreme to the last extreme of the window calculated thanks to the frames where are located the ankle angle minimums found, in the code with a for loop that fills each cell with the described frames. The last step was to write a for loop with an if condition to find the frame of the acceleration peak found before that corresponds to the all possible frames of the window defined above in the cells of the cell array. The same code was used for the left and for the right acceleration signals. An example of the final result is shown in the Figure 3.32.

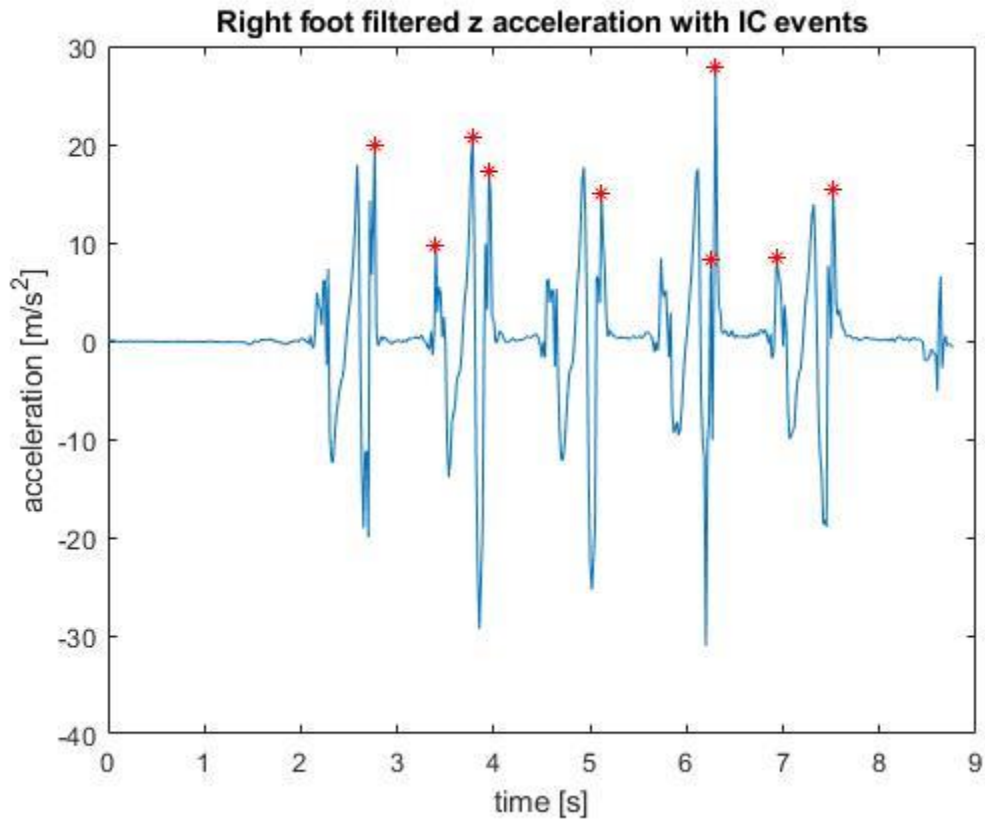


Figure 3.32: IC instants identification of the foot acceleration method - MATLAB.

Then, the IC instants were saved in csv files, ready to use after for the analysis of the data.

Method 3

The last used algorithm uses the sagittal angular velocity of the shank. This code has to search peaks of the velocity and the minimums before each peak have to be associated with EC and the minimums after each peak have to be associated with IC. To do this, the algorithm was implemented in MATLAB. First, the angular velocity signal was filtered with a Savitzky-golay filter, using the 'smoothdata()' function. So, the peaks of the angular velocity have to be found, the function used was 'islocalmax()' with 'MinProminence' set to 1 deg/s, then the function 'find()' to find the frames where these peaks were located in the angular velocity signal. Then, it is necessary to find all the minimum values in the same signal. In the code, the function 'islocalmin()' with 'MinProminence' set to 0 deg/s, then the function 'find()' to find the frames where these minimums were located in the angular velocity signal. Now, the problem is to select only the minimums before and after each angular velocity peak. After trying several solutions, the best way to solve this issue was to implement a solution where the user can select the interested minimum points on the plots of the angular velocity signals. So, in the code a function called 'ginput' was used. This function allows users to select points of interest with a cursor. The value that had to be saved was only the value on the x-coordinate, because the interest is to analyze the instant time found. After having selected all the points in the signal, the enter key on keyboard had to be selected to let the code to save the selected instants. Then, to have an orderly and precise data structure, the selected instants were saved in two different matrices, one for IC and the other for EC, using a for loop and an if condition with the 'mod()' function to take all the impair row values and to assign them to the EC vector, the others to the IC vector. The same code was used for both the right and the left angular velocity signals of the shank.

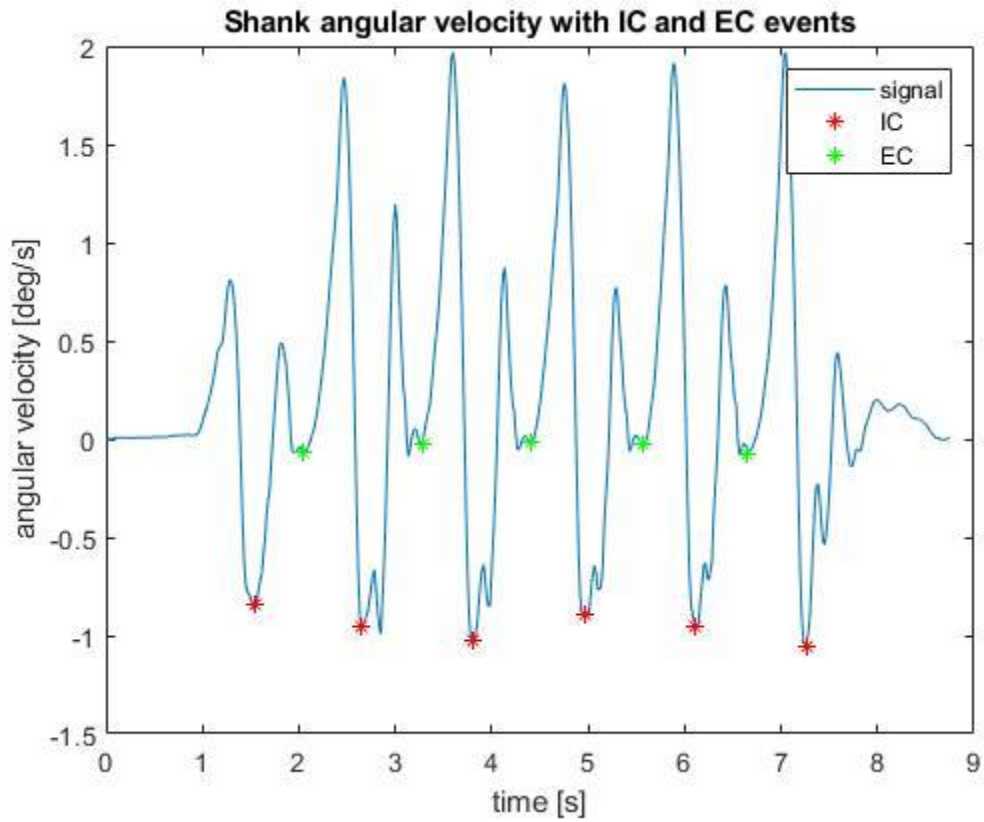


Figure 3.33: IC & EC instants identification of the shank angular velocity method – MATLAB.

An example of the final result is shown in the Figure 3.33 above. In the end, all these values were saved in csv files.

3.6 Data processing

To compare the gait events identified by the selected methods with the gold standard identification carried out by hand on the marker based motion capture data, some data processing is required.

First of all we will analyze the efficiency of the methods as event detector, in other words we will validate their capability to positively identify events or to create false events in the same data set. In the following, it will be presented the procedure used and the rule to consider an event positively identified.

Secondly, only the events positively identified will be considered to evaluate the measurement errors as compared with the gold standard method, it was decided to consider the error between the instants of the IMU codes and the instants of the gold standard. This second part will consider also a statistical analysis of the errors to understand if they depend on subjects anthropometrics characteristics, or on terrain type or inclination.

3.6.1 Detector qualification

After having used the codes that were implemented for the data recorded by the IMU sensors, three files with IC instants and two files with EC instants were present (IC_M, EC_M). These instants had to be compared with the IC and EC instants detected with the gold standard (IC_GD, EC_GD). A big matrix for each IMU method was constructed and also for the gold standard. In this matrix, the first column is a vector with IC/EC instants, the second column a vector with the subject number (from 1 to 12), the third column with the subjects' health to tell if the subject is healthy (1) or a Parkinson's disease patient (0), the fourth column a vector with the same mass category for each subject (a number from 1 to 3), the fifth column a vector with the same height category for each subject (a number from 1 to 3), the sixth column a vector with the

same BMI category for each subject (a number from 1 to 3), the seventh column a vector with the terrain conditions (1 for flat, 3 for M, 9 for Mat and 11 for Terrasensa), the eighth column a vector with the number of the repetition and the ninth column with the vector of the terrain inclinations (-15, 0, 15).

The problem was to have the same number of rows for the gold standard matrix and for the other method matrices, because the methods had not detected the same number of instants in comparison with the gold standard. To solve this issue, a threshold to select the correct events and the correct matrix rows to make the error matrix for each method was implemented. Therefore, if an instant IC_GD has not a corresponding IC_M, which would have to be present in the defined surroundings, we are in presence of a Missed Event. Instead, if there are more IC_Ms in the corresponding IC_GD threshold timeline, one IC_M is saved to be used after for the comparison and the other ones are classified like Extra event. For the method called 'Zijlstra', that detects only the IC instants of gait in sequence, the threshold was defined like this:

$TH_{(i)} = (IC_GD_{(i+1)} - IC_GD_{(i)})/2$, so half the distance between two successive IC_GD events. So, for each IC_GD, an IC_M has to be found in the time line defined by the threshold TH, after, but also before, the corresponding IC_GD.

For the second method, the first one of the paper of [M. Jasiewicz, 2006], the threshold was calculated, calculating first the time of every gait cycle, that is defined as the successive EC_GD instant less the actual EC_GD instant. So, this time of gait cycle was multiplied for 0.4, because an EC instant has not to be confused with the successive IC instant present in the gait cycle that comes 40% of the gait cycle time after the EC instant (swing phase). To this value were added other two values, one was the

mean absolute error (MAE), different for each terrain, that comes from the validation of the Vicon processing method used and the other one is the intrinsic error that is present in the IMU sensors. This intrinsic error is the result of the different sample frequencies that the Vicon system and the Xsens system have.

For the third method, the threshold was calculated like in the second method, but the instants were Initial Contacts. So, the gait cycle time was calculated as the difference between the successive IC_GD instant and the actual IC_GD instant. And, this time, the gait cycle time was multiplied for 0.6, because an IC instant has not to be confused with the successive EC instant present in the gait cycle that comes 60% of the gait cycle time after the IC instant (stance phase).

The same last two principals were used to calculate the thresholds for the last method used. A representative figure is shown in Figure 3.34.

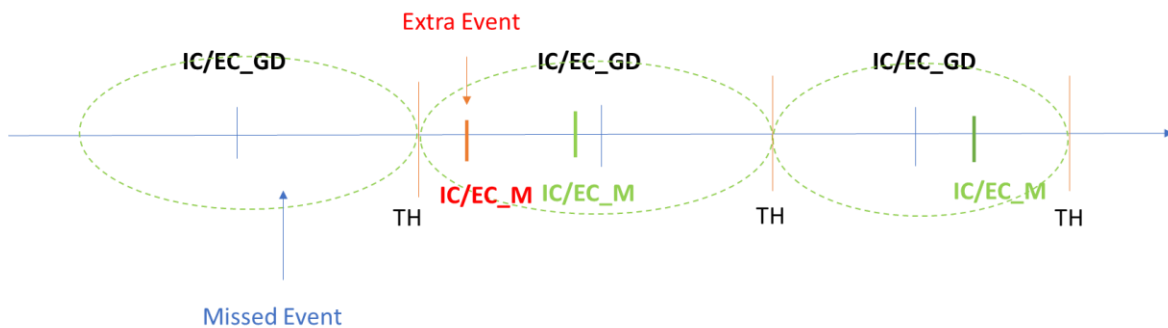


Figure 3.34: Threshold criterion to select the correct, missed and extra events.

3.6.2 Error qualification

The error was calculated only with the correct events selected by the threshold rules explained before. Also the missed and extra events have to be found.

The algorithms that do it were implemented in MATLAB. The outputs of these algorithms are:

1. the Error matrix with in the first column the error vector calculated as $IC/EC_M - IC/EC_GD$ with the comparable instants selected with the threshold methods and in the other columns the corresponding values of subject, health, category of mass, category of height, category of BMI, terrain condition, repetition and terrain inclination.
2. the matrix of the Missed Events with two columns, one where there are the numbers of the terrain conditions, one with the corresponding inclination of the terrains;
3. the matrix of the Extra Events with the same structure of the Missed Events matrix;
4. the Missed Events rate, calculated as $\frac{\# \text{ MISSED EVENTS}}{\# \text{ TOTAL GD EVENTS}} \cdot 100$;
5. the Extra Events rate, calculated as $\frac{\# \text{ EXTRA EVENTS}}{\# \text{ TOTAL GD EVENTS}} \cdot 100$;
6. the Correct Events rate, calculated as $\frac{\# \text{ CORRECT EVENTS}}{\# \text{ TOTAL GD EVENTS}} \cdot 100$.

3.6.3 Data implementation

For the statistical analysis, the Error matrix were used. In particular, the column of the terrain and the inclination were used to make the Analysis of Variance to see which group affect more the variability of the total error in the detection of the gait events. Before another control on the anthropometric groups, columns of the category of mass, height and BMI in the matrix, was performed to verify if the method depends or not on the anthropometric characteristics of the subjects. The function used in MATLAB was the 'anovan()' function.

Chapter 4 - Results

4.1 Experimental database

First of all, in this section we present number of events in each condition available for further processing, considering the gold standard 4.1.1 and the other detection methods (4.1.2, 4.1.3, 4.1.4) used for this work. Moreover the tables distinguish between healthy subjects and Parkinson patients.

4.1.1 Gold standard

The number of instants in each terrain that was detected are presented in the table 4-1 and in the table 4-2, only for the Parkinson patients, that follow.

Table 4-1: Number of instants for each terrain condition with the gold standard – all the subjects.

| Terrain | Inclination [deg] | EC left | EC right | IC left | IC right |
|----------------|--------------------------|----------------|-----------------|----------------|-----------------|
| Flat | -15 | 49 | 50 | 49 | 50 |
| | 0 | 251 | 251 | 251 | 251 |
| | 15 | 41 | 38 | 41 | 38 |
| M | -15 | 62 | 63 | 62 | 63 |
| | 0 | 240 | 246 | 240 | 246 |
| | 15 | 52 | 49 | 52 | 49 |
| Mat | -15 | 42 | 43 | 42 | 43 |
| | 0 | 207 | 206 | 207 | 206 |
| | 15 | 39 | 39 | 37 | 41 |
| Terrasensa | -15 | 57 | 60 | 57 | 60 |
| | 0 | 247 | 242 | 247 | 242 |
| | 15 | 56 | 54 | 56 | 54 |
| Total | | 1343 | 1341 | 1341 | 1343 |

Table 4-2: Number of instants for each terrain condition with the gold standard – Parkinson patients.

| Terrain | Inclination [deg] | EC | IC |
|----------------|------------------------------|-----------|-----------|
| Flat | -15 | 0 | 0 |
| | 0 | 68 | 68 |
| | 15 | 0 | 0 |
| M | -15 | 0 | 0 |
| | 0 | 64 | 64 |
| | 15 | 0 | 0 |
| Mat | -15 | 0 | 0 |
| | 0 | 69 | 69 |
| | 15 | 0 | 0 |
| Terrasensa | -15 | 0 | 0 |
| | 0 | 73 | 73 |
| | 15 | 0 | 0 |
| Total | | 274 | 274 |

4.1.2 Method 1: Zijlstra

The number of instants detected by the method on every terrain and inclination is presented in table 4-3.

Table 4-3: Number of instants for each terrain condition with the Zijlstra method.

| Terrain | Inclination [deg] | IC healthy subjects | IC Parkinson patients |
|-------------------|--------------------------|----------------------------|------------------------------|
| Flat | -15 | 82 | 0 |
| | 0 | 406 | 58 |
| | 15 | 73 | 0 |
| M | -15 | 92 | 0 |
| | 0 | 394 | 61 |
| | 15 | 97 | 0 |
| Mat | -15 | 86 | 0 |
| | 0 | 348 | 67 |
| | 15 | 74 | 0 |
| Terrasensa | -15 | 113 | 0 |
| | 0 | 411 | 70 |
| | 15 | 109 | 0 |
| Total | | 2285 | 256 |
| Sum Totals | | 2541 | |

4.1.3 Method 2: IMU on the foot

The number of instants detected by the method on every terrain and inclination for all the subjects is presented in table 4-4 and for Parkinson patients in table 4-5.

Table 4-4: Number of instants for each terrain condition with the second method – all the subjects.

| Terrain | Inclination [deg] | EC left | EC right | IC left | IC right |
|----------------|--------------------------|----------------|-----------------|----------------|-----------------|
| Flat | -15 | 35 | 39 | 118 | 128 |
| | 0 | 160 | 149 | 704 | 700 |
| | 15 | 27 | 23 | 97 | 71 |
| M | -15 | 47 | 42 | 162 | 167 |
| | 0 | 131 | 142 | 558 | 540 |
| | 15 | 28 | 20 | 101 | 123 |
| Mat | -15 | 42 | 24 | 82 | 80 |
| | 0 | 116 | 118 | 472 | 506 |
| | 15 | 32 | 29 | 82 | 89 |
| Terrasensa | -15 | 47 | 34 | 139 | 151 |
| | 0 | 132 | 116 | 753 | 691 |
| | 15 | 38 | 39 | 116 | 129 |
| Total | | 835 | 775 | 3384 | 3375 |

Table 4-5: Number of instants for each terrain condition with the second method – Parkinson patients.

| Terrain | Inclination [deg] | EC | IC |
|----------------|------------------------------|-----------|-----------|
| Flat | -15 | 0 | 0 |
| | 0 | 19 | 125 |
| | 15 | 0 | 0 |
| M | -15 | 0 | 0 |
| | 0 | 27 | 124 |
| | 15 | 0 | 0 |
| Mat | -15 | 0 | 0 |
| | 0 | 16 | 113 |
| | 15 | 0 | 0 |
| Terrasensa | -15 | 0 | 0 |
| | 0 | 16 | 107 |
| | 15 | 0 | 0 |
| Total | | 78 | 469 |

4.1.4 Method 3: IMU on the shank

The number of instants detected by the method on every terrain and inclination for all the subjects is presented in table 4-6 and for Parkinson patients in table 4-7.

Table 4-6: Number of instants for each terrain condition with the third method – all the subjects.

| Terrain | Inclination [deg] | EC left | EC right | IC left | IC right |
|----------------|--------------------------|----------------|-----------------|----------------|-----------------|
| Flat | -15 | 52 | 52 | 52 | 54 |
| | 0 | 237 | 251 | 243 | 259 |
| | 15 | 38 | 43 | 39 | 45 |
| M | -15 | 67 | 72 | 69 | 74 |
| | 0 | 222 | 250 | 230 | 258 |
| | 15 | 53 | 50 | 55 | 52 |
| Mat | -15 | 41 | 47 | 41 | 49 |
| | 0 | 204 | 213 | 213 | 220 |
| | 15 | 38 | 38 | 38 | 40 |
| Terrasensa | -15 | 58 | 71 | 63 | 74 |
| | 0 | 234 | 241 | 239 | 250 |
| | 15 | 56 | 64 | 58 | 66 |
| Total | | 1300 | 1392 | 1340 | 1441 |

Table 4-7: Number of instants for each terrain condition with the third method – Parkinson patients.

| Terrain | Inclination [deg] | EC | IC |
|----------------|------------------------------|-----------|-----------|
| Flat | -15 | 0 | 0 |
| | 0 | 72 | 77 |
| | 15 | 0 | 0 |
| M | -15 | 0 | 0 |
| | 0 | 69 | 74 |
| | 15 | 0 | 0 |
| Mat | -15 | 0 | 0 |
| | 0 | 78 | 84 |
| | 15 | 0 | 0 |
| Terrasensa | -15 | 0 | 0 |
| | 0 | 79 | 90 |
| | 15 | 0 | 0 |
| Total | | 298 | 325 |

4.2 Detection analysis

The percentage values of the correct, missed and extra events in all the three methods (4.2.1, 4.2.2, 4.2.3) used are presented. The correct events are the method events that are confrontable with the gold standard. The missed events are the gold standard events that not have a correspondent value detected by the method and the extra events are the method events in the threshold that have a bigger temporal distance to the gold standard events than the identified correct events.

4.2.1 Method 1: Zijlstra

This method, that uses the IMU on the pelvis, has 90% of correct events detected. So the percentage of missed events is 10%, but where these events were missed? We can see it in the Figure 4.1.

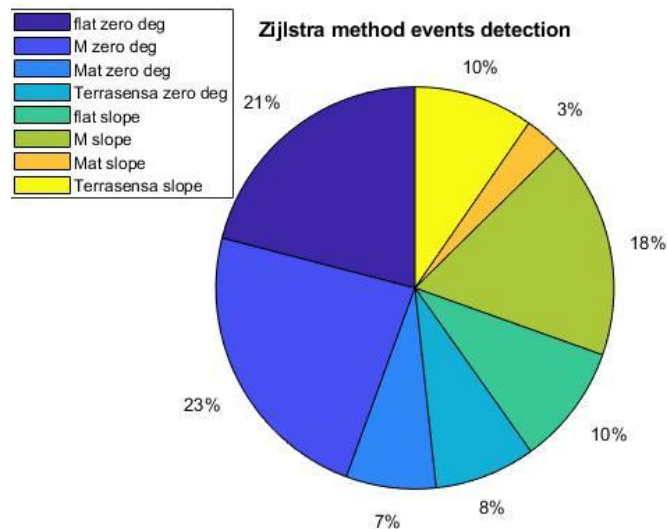


Figure 4.1: Missed events areogram – Zijlstra method.

In particular:

- In the flat terrain trials in slope:
 - the 23.1% at 15 degrees;
 - the 76.9% at -15 degrees.
- In the M terrain trials in slope:
 - the 21% at 15 degrees;
 - the 79% at -15 degrees.
- In the Mat terrain trials in slope:
 - all of them at 15 degrees.
- In the Terrasensa trials in slope:
 - the 46% at 15 degrees;
 - the 54% at -15 degrees.

Furthermore, it has only a 4.7% of extra events, events detected by the code that do not exist in the reality.

These events are divided as follows in the Figure 4.2:

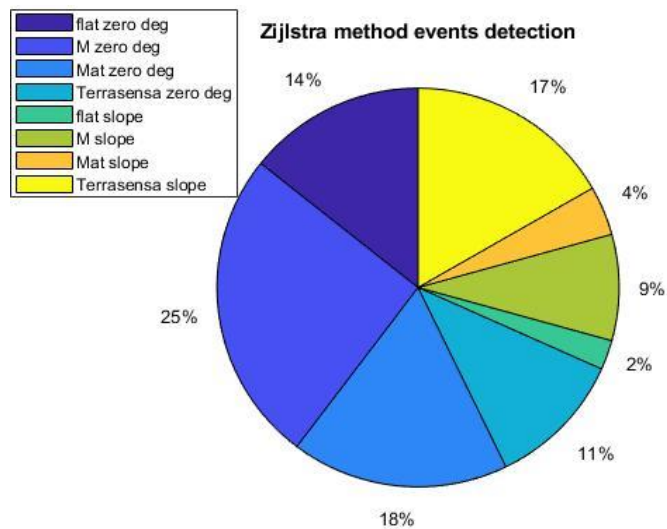


Figure 4.2: Extra events areogram – Zijlstra method.

In particular:

- In the flat terrain trials in slope:
 - all of them at -15 degrees.
- In the M terrain trials in slope:
 - the 36.4% at 15 degrees;
 - the 63.6% at -15 degrees.
- In the Mat terrain trials in slope:
 - the 80% at 15 degrees;
 - the 20% at -15 degrees.
- In the Terrasensa trials in slope:
 - the 48% at 15 degrees;
 - the 52% at -15 degrees.

4.2.2 Method 2: IMU on the foot

For the left foot and the EC instants, we have the 33.8% of correct events, the 66.2% of missed events and the 28.4% of extra events.

For what concerns the missed events, they are divided as follows in the Figure 4.3:

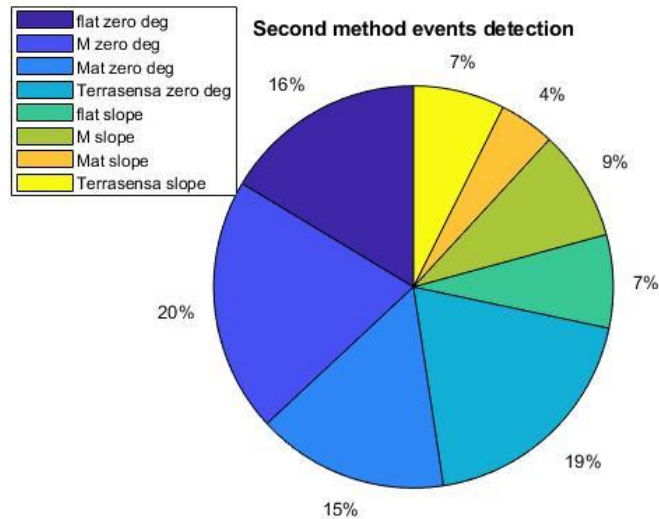


Figure 4.3: Missed EC events areogram – method of the IMU on the left foot.

In particular:

- In the flat terrain trials in slope:
 - the 49.3% at 15 degrees;
 - the 50.7% at -15 degrees.
- In the M terrain trials in slope:
 - the 50.6% at 15 degrees;
 - the 49.4% at -15 degrees.
- In the Mat terrain trials in slope:
 - the 50% at 15 degrees;
 - the 50% at -15 degrees.
- In the Terrasensa trials in slope:

- the 54.5% at 15 degrees;
- the 45.5% at -15 degrees.

Instead, for the extra events in the Figure 4.4:

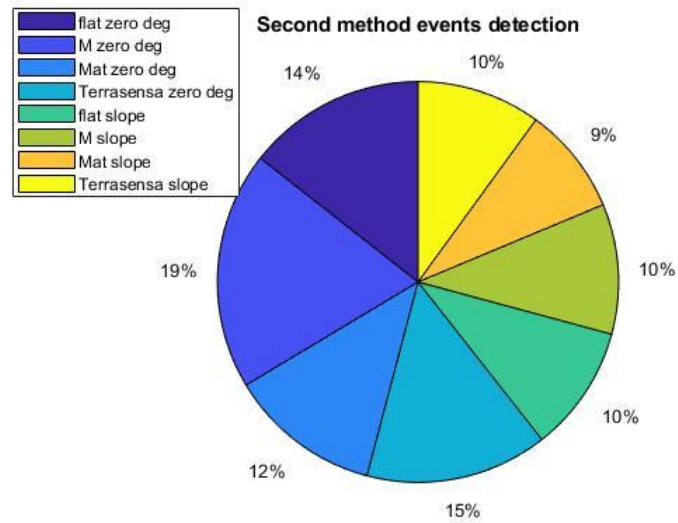


Figure 4.4: Extra EC events areogram – method of the IMU on the left foot.

In particular:

- In the flat terrain trials in slope:
 - the 49% at 15 degrees;
 - the 51% at -15 degrees.
- In the M terrain trials in slope:
 - the 40% at 15 degrees;
 - the 60% at -15 degrees.
- In the Mat terrain trials in slope:
 - the 39.4% at 15 degrees;
 - the 60.6% at -15 degrees.

- In the Terrasensa trials in slope:
 - the 47.4% at 15 degrees;
 - the 52.6% at -15 degrees.

Now always for the left foot, but IC instants. The 92.6% is the value for the correct events detected. The percentage of extra events is 63.3% and for the missed events the 7.4%.

For the missed events we have these percentage values in the Figure 4.5:

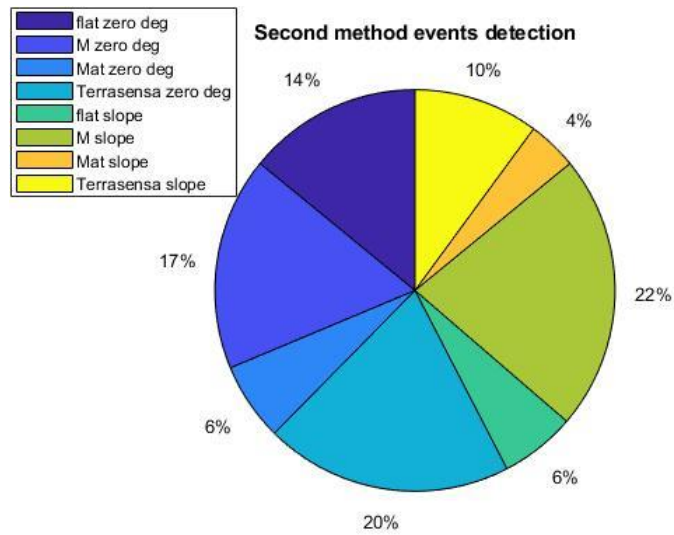


Figure 4.5: Missed IC events areogram – method of the IMU on the left foot.

In particular:

- In the flat terrain trials in slope:
 - the 50% at 15 degrees;
 - the 50% at -15 degrees.
- In the M terrain trials in slope:

- the 50% at 15 degrees;
- the 50% at -15 degrees.
- In the Mat terrain trials in slope:
 - the 25% at 15 degrees;
 - the 75% at -15 degrees.
- In the Terrasensa trials in slope:
 - the 50% at 15 degrees;
 - the 50% at -15 degrees.

For the extra events in the Figure 4.6:

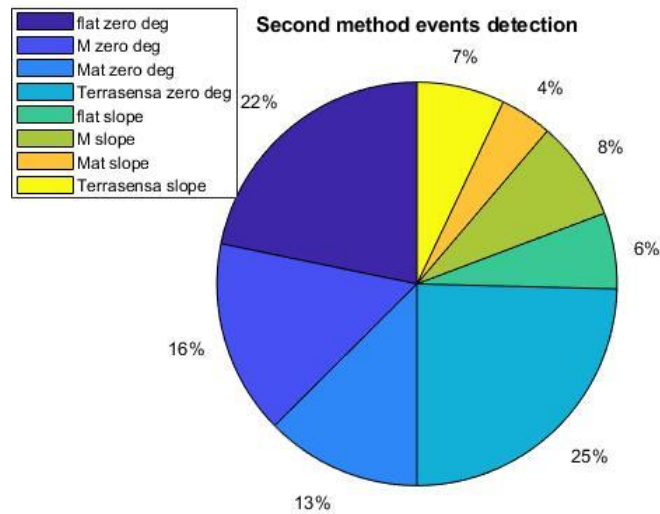


Figure 4.6: Extra IC events areogram - method of the IMU on the left foot.

In particular:

- In the flat terrain trials in slope:
 - the 45% at 15 degrees;
 - the 55% at -15 degrees.

- In the M terrain trials in slope:
 - the 35.7% at 15 degrees;
 - the 64.3% at -15 degrees.
- In the Mat terrain trials in slope:
 - the 51.7% at 15 degrees;
 - the 48.3% at -15 degrees.
- In the Terrasensa trials in slope:
 - the 43.4% at 15 degrees;
 - the 56.6% at -15 degrees.

We miss to analyze the right foot. For the EC instants the percentages are these: correct events 31.6%, missed events 68.4% and extra events 26.2%.

For the missed events in particular, they are divided on the terrains as follows in the Figure 4.7:

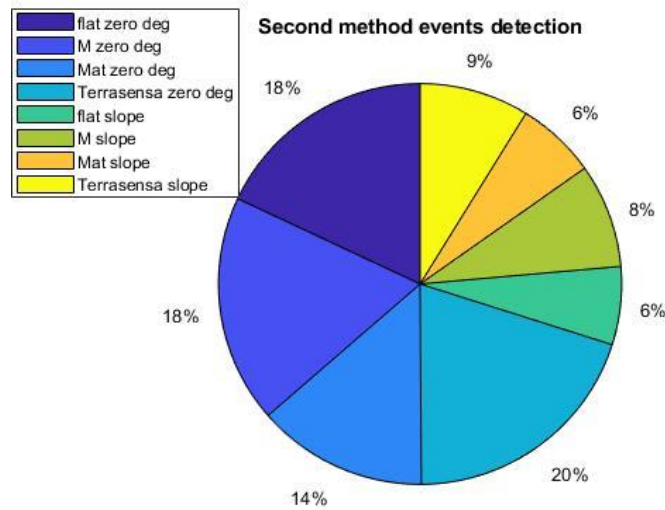


Figure 4.7: Missed EC events areogram – method of the IMU on the right foot.

In particular:

- In the flat terrain trials in slope:
 - the 51.7% at 15 degrees;
 - the 48.3% at -15 degrees.
- In the M terrain trials in slope:
 - the 40.3% at 15 degrees;
 - the 59.7% at -15 degrees.
- In the Mat terrain trials in slope:
 - the 39.7% at 15 degrees;
 - the 60.3% at -15 degrees.
- In the Terrasensa trials in slope:
 - the 45.6% at 15 degrees;
 - the 54.4% at -15 degrees.

For the extra events, they are divided on the terrains as follows in the Figure 4.8:

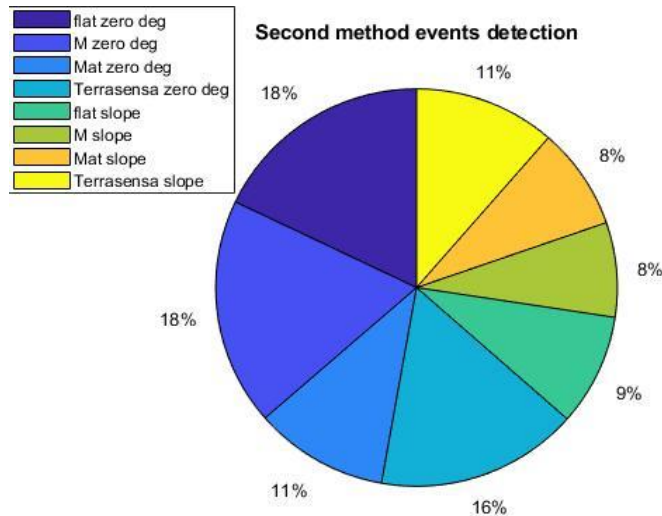


Figure 4.8: Extra EC events areogram – method of the IMU on the right foot.

In particular:

- In the flat terrain trials in slope:
 - the 46.8% at 15 degrees;
 - the 53.2% at -15 degrees.
- In the M terrain trials in slope:
 - the 18.5% at 15 degrees;
 - the 81.5% at -15 degrees.
- In the Mat terrain trials in slope:
 - the 44.8% at 15 degrees;
 - the 55.2% at -15 degrees.
- In the Terrasensa trials in slope:
 - the 45% at 15 degrees;
 - the 55% at -15 degrees.

Now, we analyze the IC instants detection of the right foot of this method. We have the 92.3% of correct events, the 7.7% of missed events and the 63.3% of extra events.

We start to see how the missed events are divided on each terrain in the Figure 4.9:

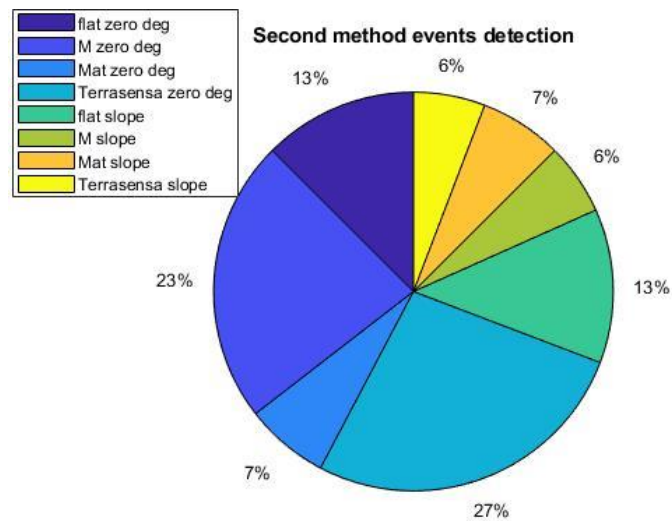


Figure 4.9: Missed IC events areogram – method of the IMU on the right foot.

In particular:

- In the flat terrain trials in slope:
 - the 61.5% at 15 degrees;
 - the 38.5% at -15 degrees.
- In the M terrain trials in slope:
 - the 16.7% at 15 degrees;
 - the 83.3% at -15 degrees.
- In the Mat terrain trials in slope:

- all of them at -15 degrees.
- In the Terrasensa trials in slope:
 - the 66.7% at 15 degrees;
 - the 33.3% at -15 degrees.

Now for the extra events in the Figure 4.10:

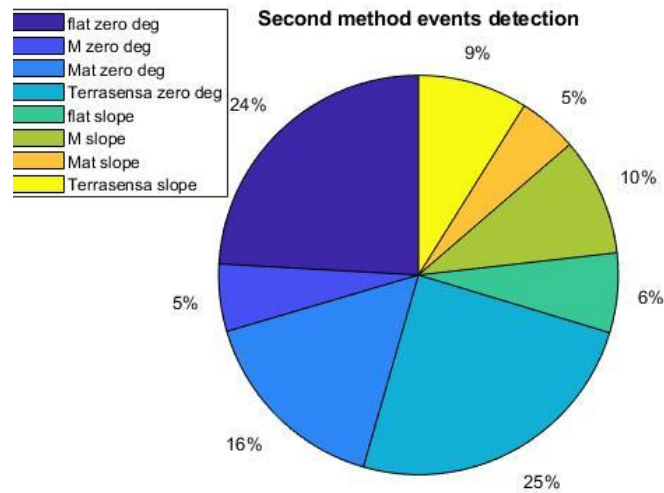


Figure 4.10: Extra IC events areogram – method of the IMU on the right foot.

In particular:

- In the flat terrain trials in slope:
 - the 33% at 15 degrees;
 - the 67% at -15 degrees.
- In the M terrain trials in slope:
 - the 41.8% at 15 degrees;
 - the 58.2% at -15 degrees.
- In the Mat terrain trials in slope:

- the 52.2% at 15 degrees;
- the 47.8% at -15 degrees.
- In the Terrasensa trials in slope:
 - the 45.3% at 15 degrees;
 - the 54.7% at -15 degrees.

4.2.3 Method 3: IMU on the shank

The third and last method used to segment the gait cycle in this work is the algorithm that uses the IMU positioned on the shank of the subjects. As before, let's see the percentage values, starting with the left shank and the EC instants. The correct events are the 83.5%, the missed events the 16.5% and the extra events the 13.3%. First the missed events are divided on each terrain as follows in the Figure 4.11:

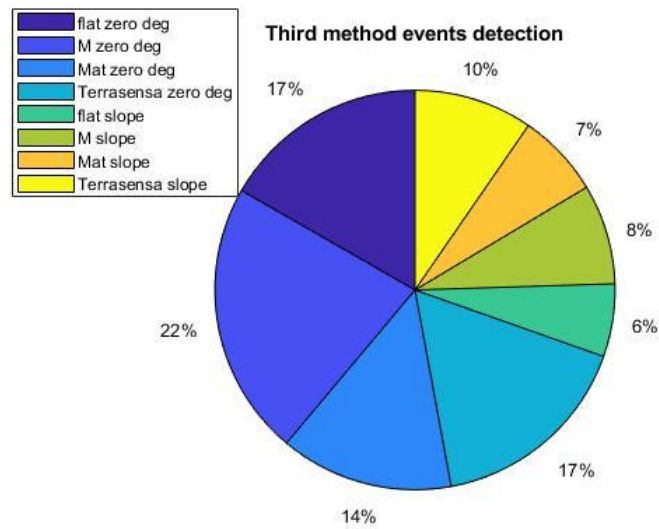


Figure 4.11: Missed EC events areogram – method of the IMU on the left shank.

In particular:

- In the flat terrain trials in slope:
 - all of them at 15 degrees.
- In the M terrain trials in slope:
 - the 83.3% at 15 degrees;
 - the 16.7% at -15 degrees.

- In the Mat terrain trials in slope:
 - the 93.3% at 15 degrees;
 - the 6.7% at -15 degrees.
- In the Terrasensa trials in slope:
 - the 71.4% at 15 degrees;
 - the 28.6% at -15 degrees.

For the extra events in the Figure 4.12:

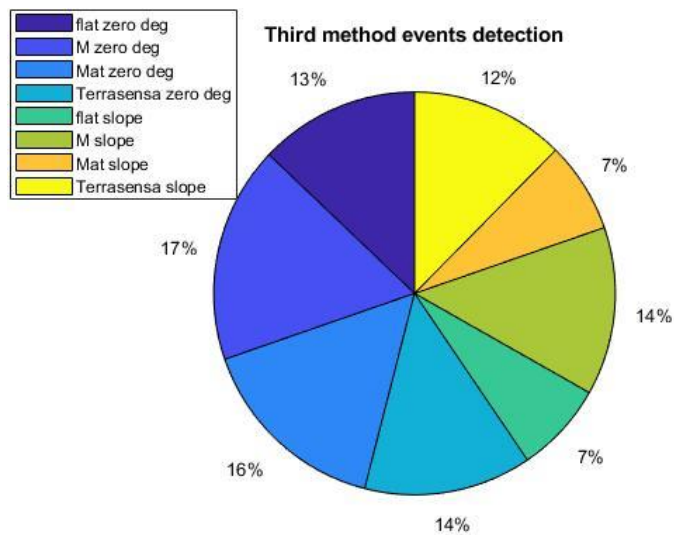


Figure 4.12: Extra EC events areogram – method of the IMU on the left shank.

In particular:

- In the flat terrain trials in slope:
 - the 76.9% at 15 degrees;
 - the 23.1% at -15 degrees.
- In the M terrain trials in slope:
 - the 66.7% at 15 degrees;
 - the 33.3% at -15 degrees.

- In the Mat terrain trials in slope:
 - all of them at 15 degrees.
- In the Terrasensa trials in slope:
 - the 68.2% at 15 degrees;
 - the 31.8% at -15 degrees.

Now, for the same shank, but the IC instants. The correct events are the 87.4%, the missed events the 12.6% and the extra events the 12.5%.

Let's see how the missed events are divided on each terrain in the Figure 4.13:

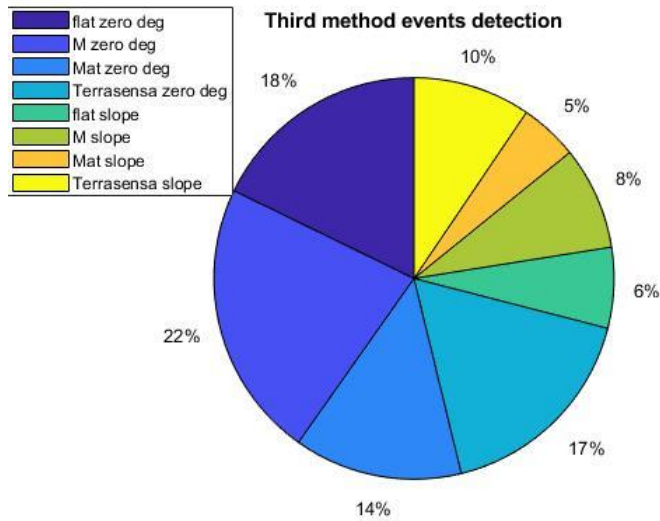


Figure 4.13: Missed IC events areogram – method of the IMU on the left shank.

In particular:

- In the flat terrain trials in slope:
 - all of them at 15 degrees.
- In the M terrain trials in slope:
 - the 85.7% at 15 degrees;
 - the 14.3% at -15 degrees.
- In the Mat terrain trials in slope:
 - the 87.5% at 15 degrees;
 - the 12.5% at -15 degrees.
- In the Terrasensa trials in slope:
 - the 75% at 15 degrees;
 - the 25% at -15 degrees.

Instead, for what concerns the extra events in the Figure 4.14:

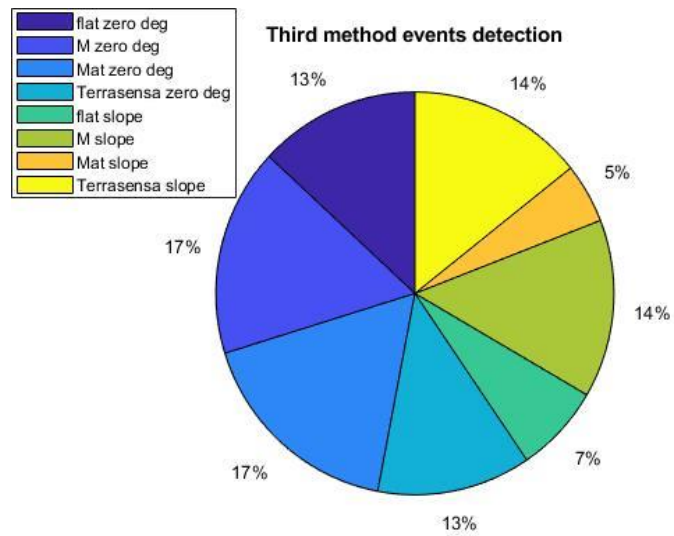


Figure 4.14: Extra IC events areogram – method of the IMU on the left shank.

In particular:

- In the flat terrain trials in slope:
 - the 75% at 15 degrees;
 - the 25% at -15 degrees.
- In the M terrain trials in slope:
 - the 62.5% at 15 degrees;
 - the 37.5% at -15 degrees.
- In the Mat terrain trials in slope:
 - all of them at 15 degrees.
- In the Terrasensa trials in slope:
 - the 58.3% at 15 degrees;
 - the 41.7% at -15 degrees.

Now, the right shank. The EC instants has the 82.4% of correct events, the 17.6% of missed events and the 21.4% of extra events. And for the missed events are divided as follows in the Figure 4.15:

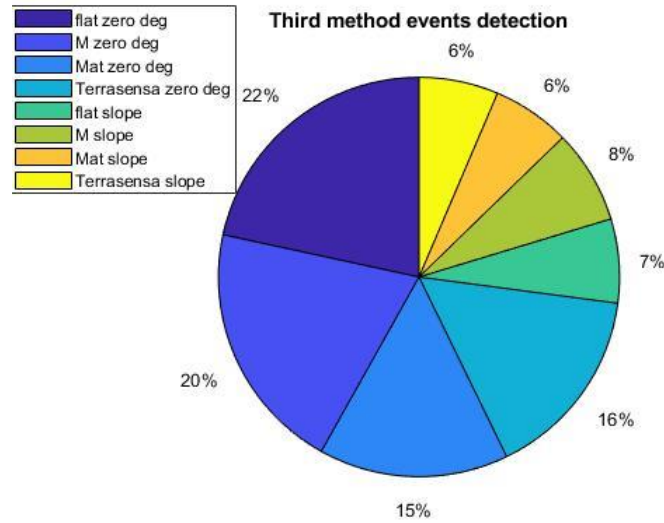


Figure 4.15: Missed EC events areogram – method of the IMU on the right shank.

In particular:

- In the flat terrain trials in slope:
 - the 68.8% at 15 degrees;
- In the M terrain trials in slope:
 - the 77.8% at 15 degrees;
 - the 22.2% at -15 degrees.
- In the Mat terrain trials in slope:
 - the 80% at 15 degrees;
 - the 20% at -15 degrees.
- In the Terrasensa trials in slope:
 - the 93.3% at 15 degrees;

- the 6.7% at -15 degrees.

For the extra events in the Figure 4.16:

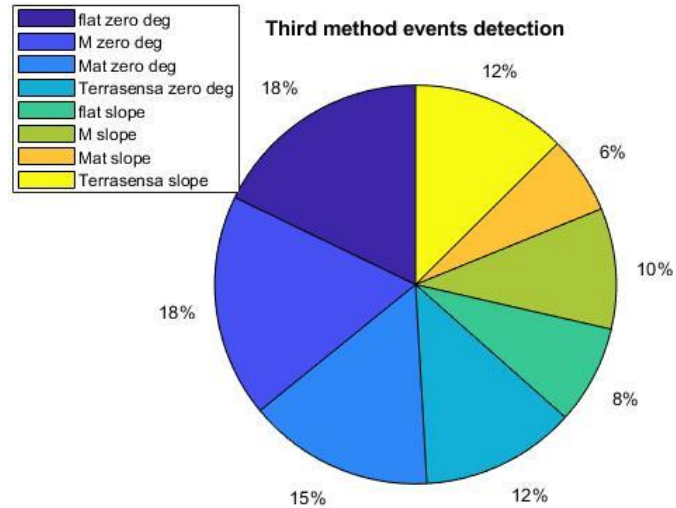


Figure 4.16: Extra EC events areogram – method of the IMU on the right shank.

In particular:

- In the flat terrain trials in slope:
 - the 69.6% at 15 degrees;
 - the 30.4% at -15 degrees.
- In the M terrain trials in slope:
 - the 53.6% at 15 degrees;
 - the 46.4% at -15 degrees.
- In the Mat terrain trials in slope:
 - the 61.1% at 15 degrees;
 - the 38.9% at -15 degrees.
- In the Terrasensa trials in slope:

- the 66.7% at 15 degrees;
- the 33.3% at -15 degrees.

For the IC instants of the right shank, the correct events are the 84.2%, the missed events the 15.8% and the extra events the 23.2%.

The instants of the missed events are divided as follows in the Figure 4.17:

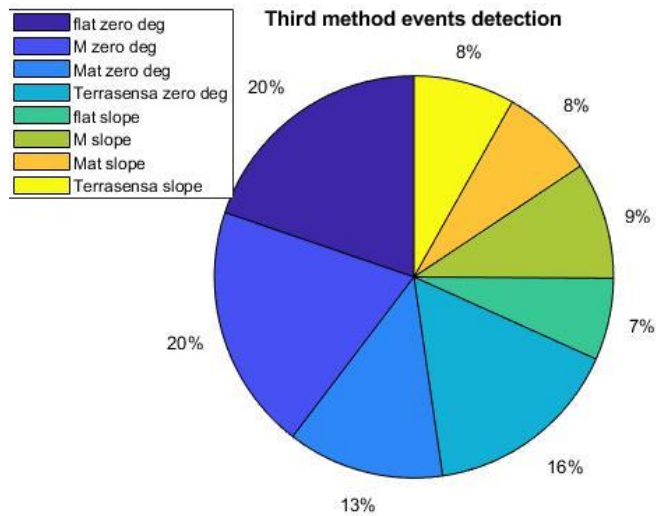


Figure 4.17: Missed IC events areogram – method of the IMU on the right shank.

In particular:

- In the flat terrain trials in slope:
 - the 71.4% at 15 degrees;
 - the 28.6% at -15 degrees.
- In the M terrain trials in slope:
 - the 65% at 15 degrees;
 - the 35% at -15 degrees.

- In the Mat terrain trials in slope:
 - the 81.3% at 15 degrees;
 - the 18.7% at -15 degrees.
- In the Terrasensa trials in slope:
 - the 94% at 15 degrees;
 - the 6% at -15 degrees.

For the extra events, instead, are divided as follows in the Figure 4.18:

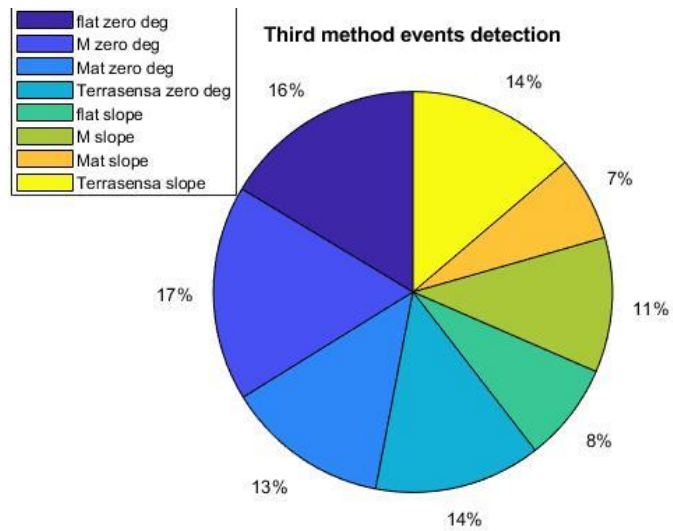


Figure 4.18: Extra IC events areogram – method of the IMU on the right shank.

In particular:

- In the flat terrain trials in slope:
 - the 68% at 15 degrees;
 - the 32% at -15 degrees.
- In the M terrain trials in slope:
 - the 47% at 15 degrees;

- the 53% at -15 degrees.
- In the Mat terrain trials in slope:
 - the 57% at 15 degrees;
 - the 43% at -15 degrees.
- In the Terrasensa trials in slope:
 - the 67% at 15 degrees;
 - the 33% at -15 degrees.

4.3 Statistical analysis on the errors

The statistical analysis results are presented as follows for all the methods (4.3.1, 4.3.2, 4.3.3).

4.3.1 Method 1: Zijlstra

A Boxplot to see how the Parkinson disease patients affect the errors on the different terrains is shown in the Figure 4.19.

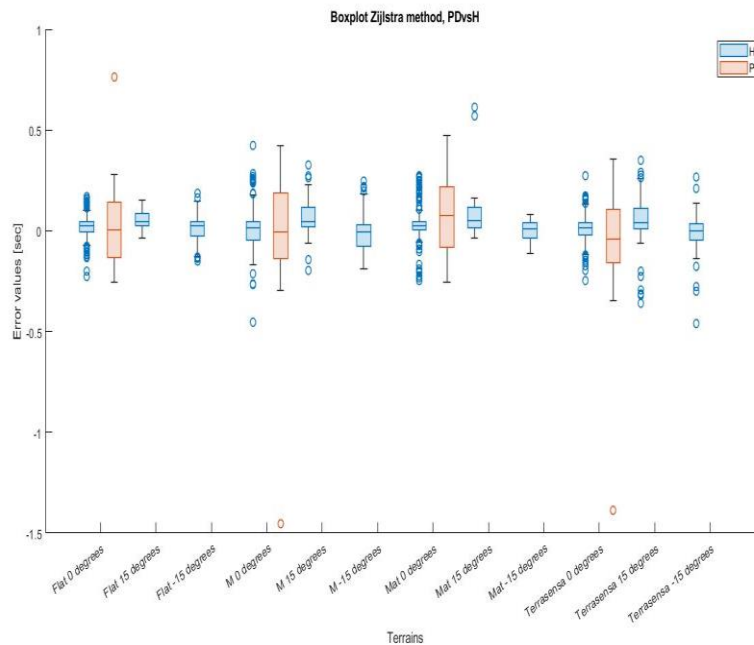


Figure 4.19: Zijlstra method boxplot, errors on different terrains. Healthy subjects vs Parkinson disease patients.

Another boxplot of the errors in each healthy subject is shown in the Figure 4.20.

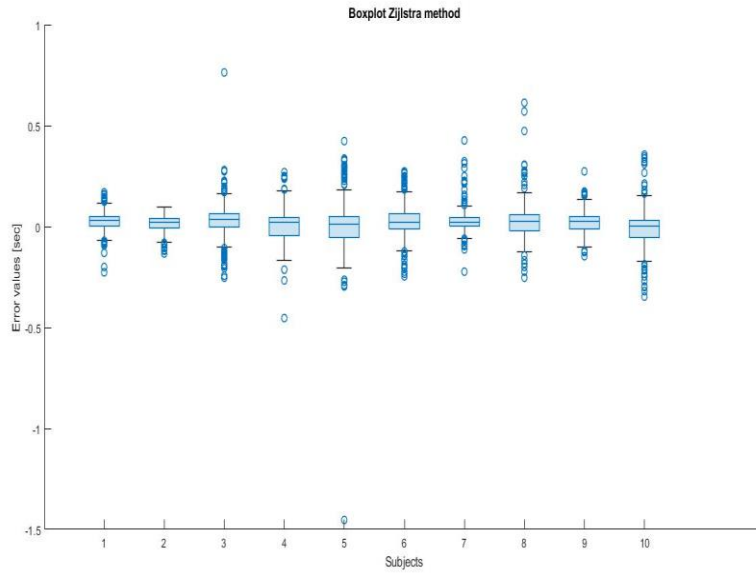


Figure 4.20: Zijlstra method boxplot, errors of each healthy subject.

We can see the Anova performed in Matlab shown in the Figure 4.21.

| Analysis of Variance | | | | | |
|----------------------|---------|-------|----------|------|--------|
| Source | Sum Sq. | d. f. | Mean Sq. | F | Prob>F |
| bmi | 0.01876 | 2 | 0.00938 | 2.09 | 0.1239 |
| Error | 9.14345 | 2038 | 0.00449 | | |
| Total | 9.16221 | 2040 | | | |

Sequential (Type I) sums of squares.

Figure 4.21: Anova on the BMI group – Zijlstra method.

Now, we can see the results on the analysis of variance of the terrain inclinations and terrain groups in the Figure 4.22.

| Analysis of Variance | | | | | |
|----------------------|---------|-------|----------|-------|--------|
| Source | Sum Sq. | d. f. | Mean Sq. | F | Prob>F |
| terrain | 0.06061 | 3 | 0.0202 | 4.85 | 0.0023 |
| inclination | 0.63272 | 2 | 0.31636 | 76.02 | 0 |
| Error | 8.46887 | 2035 | 0.00416 | | |
| Total | 9.16221 | 2040 | | | |

Sequential (Type I) sums of squares.

Figure 4.22: Anova on the terrain and inclination groups – Zijlstra method.

So, a boxplot of the errors on the three different inclinations can be visualized in the Figure 4.23.

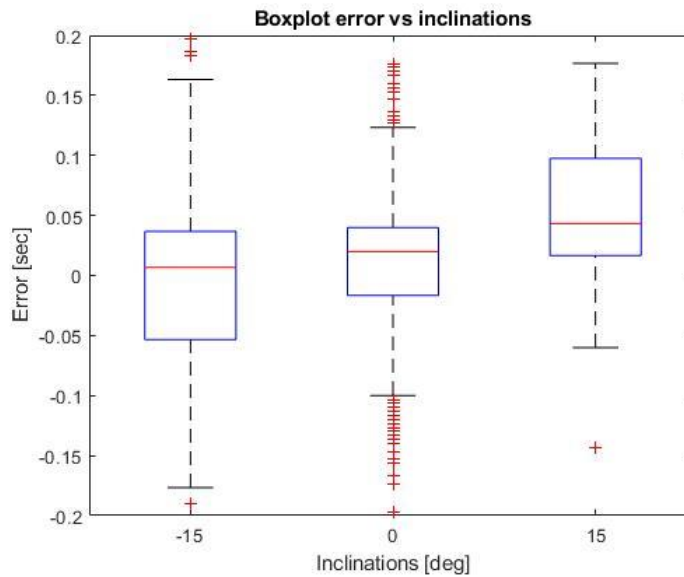


Figure 4.23: Boxplot of the errors on the different terrain inclinations - Zijlstra method.

With the error plot in the Figure 4.24 with the mean and the standard deviation of the errors on each terrain and inclination, we can see if there is a regularity.

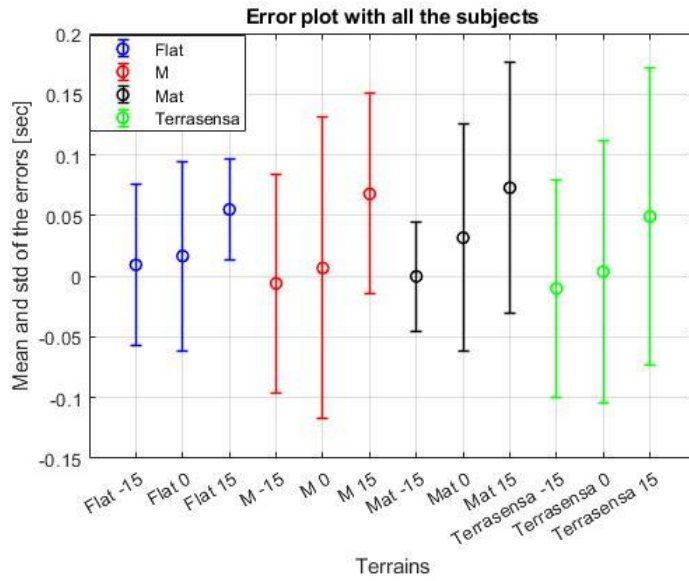


Figure 4.24: error plot of all the subjects - Zijlstra method.

4.3.2 Method 2: IMU on the foot

We consider only the IC instants. First the IMU on the left foot. We see the boxplot in the Figure 4.25 with all the subjects, dividing the Parkinson patients and the healthy subjects. And then another boxplot in Figure 4.26 with the healthy subjects only.

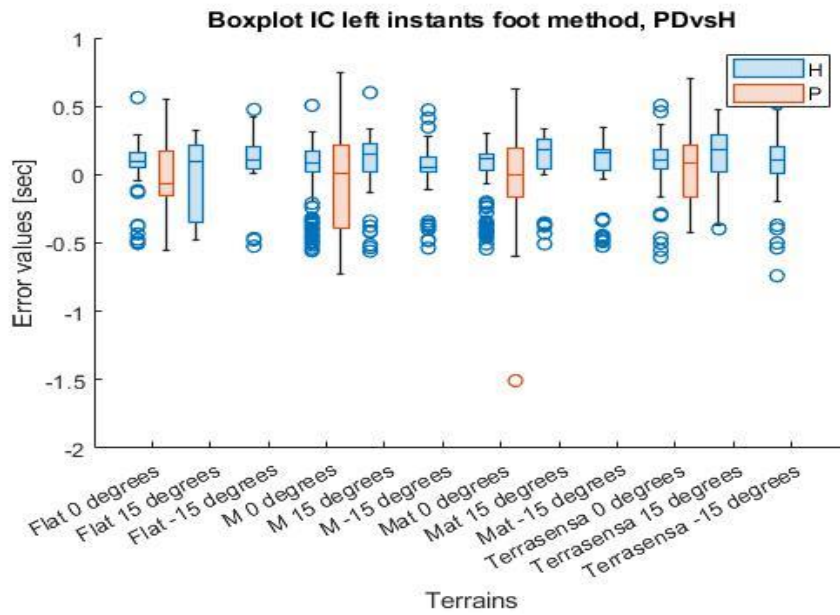


Figure 4.25: foot method boxplot, errors on different terrains. Healthy subjects vs Parkinson disease patients. IC left instants.

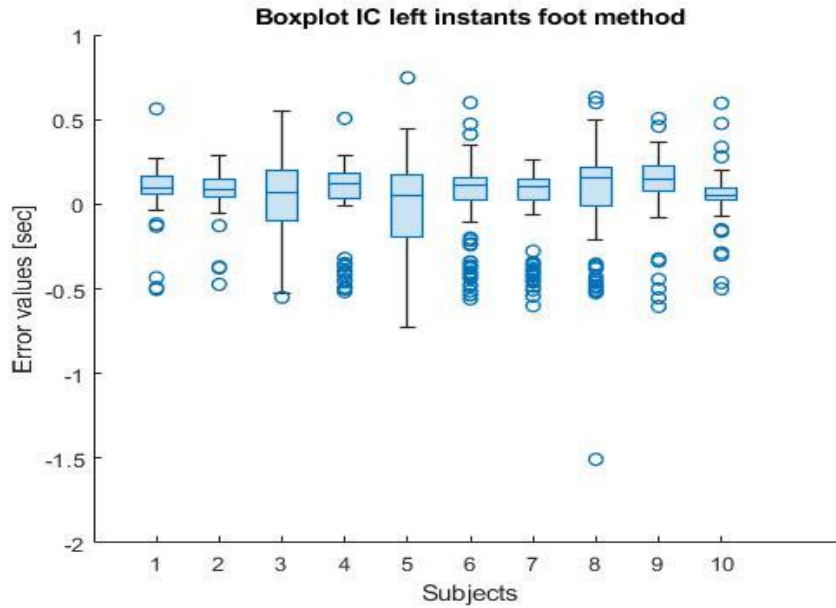


Figure 4.26: foot method boxplot, errors of each healthy subject. IC left instants.

Then, the Anova we performed on the height group, shown in the Figure 4.27.

| Analysis of Variance | | | | | |
|----------------------|---------|-------|----------|------|--------|
| Source | Sum Sq. | d. f. | Mean Sq. | F | Prob>F |
| height | 0.2861 | 2 | 0.14303 | 2.98 | 0.051 |
| Error | 59.4168 | 1239 | 0.04796 | | |
| Total | 59.7029 | 1241 | | | |

Sequential (Type I) sums of squares.

Figure 4.27: Anova from MATLAB on the height group of the IC instants – left foot method.

Another different Anova is presented in the Figure 4.28.

| Analysis of Variance | | | | | |
|----------------------|---------|-------|----------|-------|------------|
| Source | Sum Sq. | d. f. | Mean Sq. | F | Prob>F |
| bmi | 1.0572 | 2 | 0.52862 | 11.17 | 1.5593e-05 |
| Error | 58.6456 | 1239 | 0.04733 | | |
| Total | 59.7029 | 1241 | | | |

Sequential (Type I) sums of squares.

Figure 4.28: Anova from MATLAB on the BMI group of the IC instants – left foot method.

Now, always the IC instants, but we analyze the IMU on the right foot. First with two boxplots shown in the Figure 4.29 and 4.30.

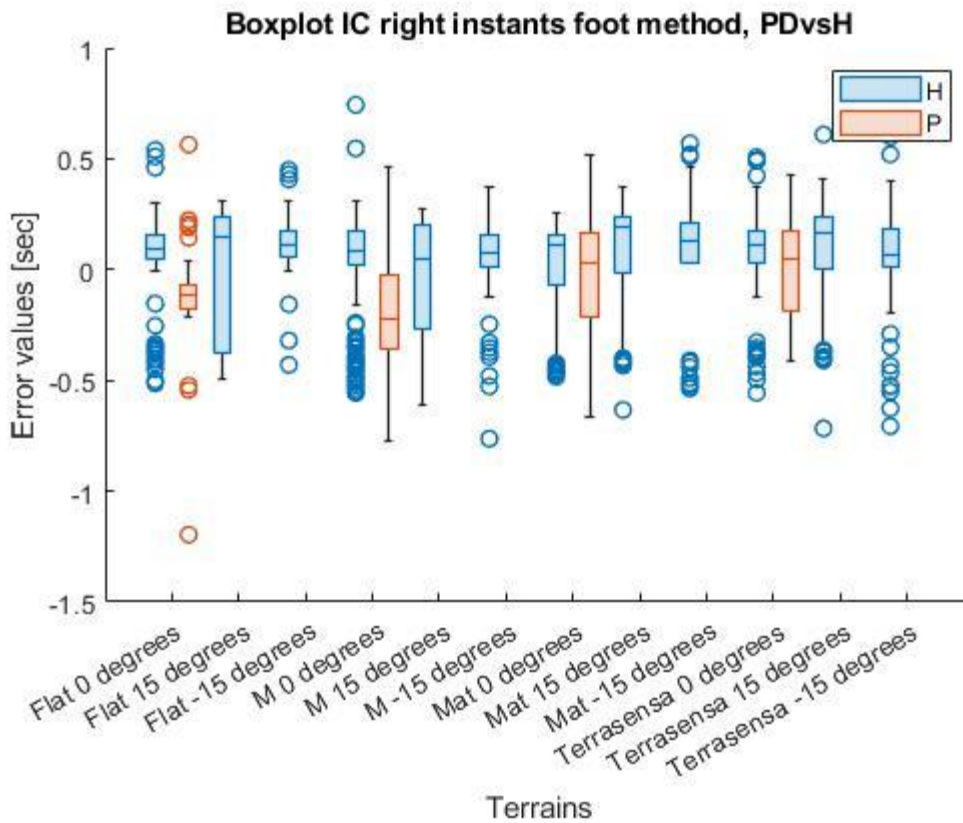


Figure 4.29: foot method boxplot, errors on different terrains. Healthy subjects vs Parkinson disease patients. IC right instants.

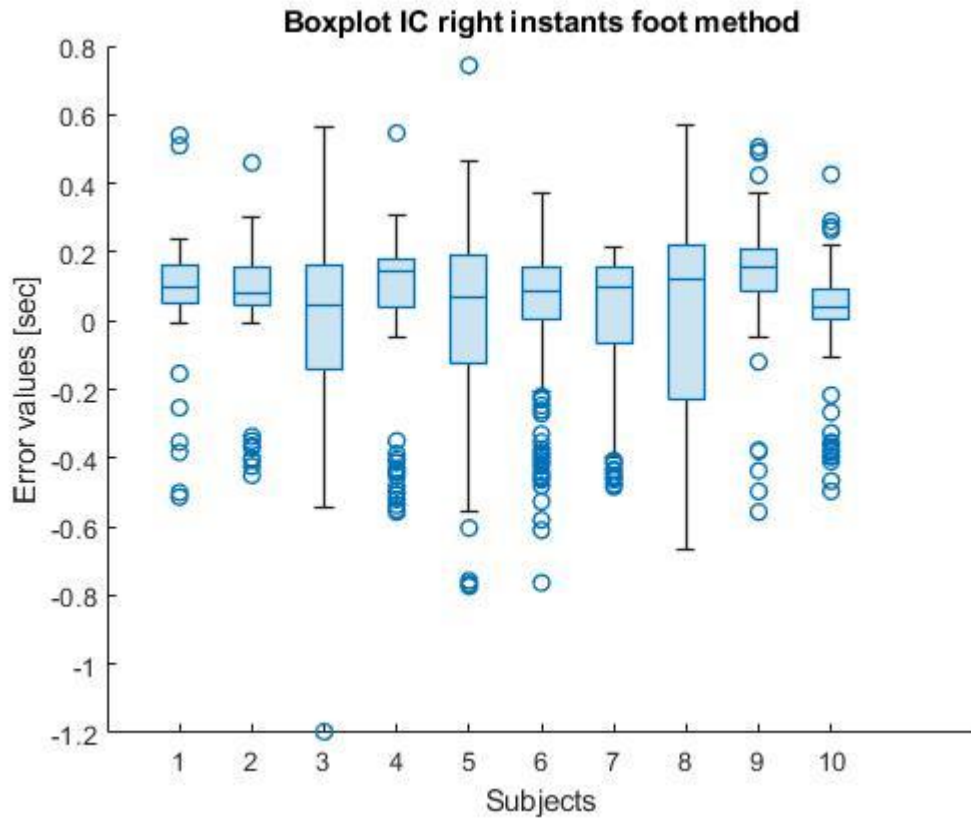


Figure 4.30: foot method boxplot, errors of each healthy subject. IC right instants.

The analysis of variance is shown in the Figure 4.31.

| Analysis of Variance | | | | | |
|----------------------|---------|-------|----------|-------|-------------|
| Source | Sum Sq. | d. f. | Mean Sq. | F | Prob>F |
| bmi | 1.3991 | 2 | 0.69954 | 13.31 | 1.91796e-06 |
| Error | 64.9298 | 1235 | 0.05257 | | |
| Total | 66.3288 | 1237 | | | |

Sequential (Type I) sums of squares.

Figure 4.31: Anova from MATLAB on the BMI group of the IC instants – right foot method.

4.3.3 Method 3: IMU on the shank

We first consider the left shank and the EC instants. We see the two boxplots shown in the Figure 4.32 and 4.33.

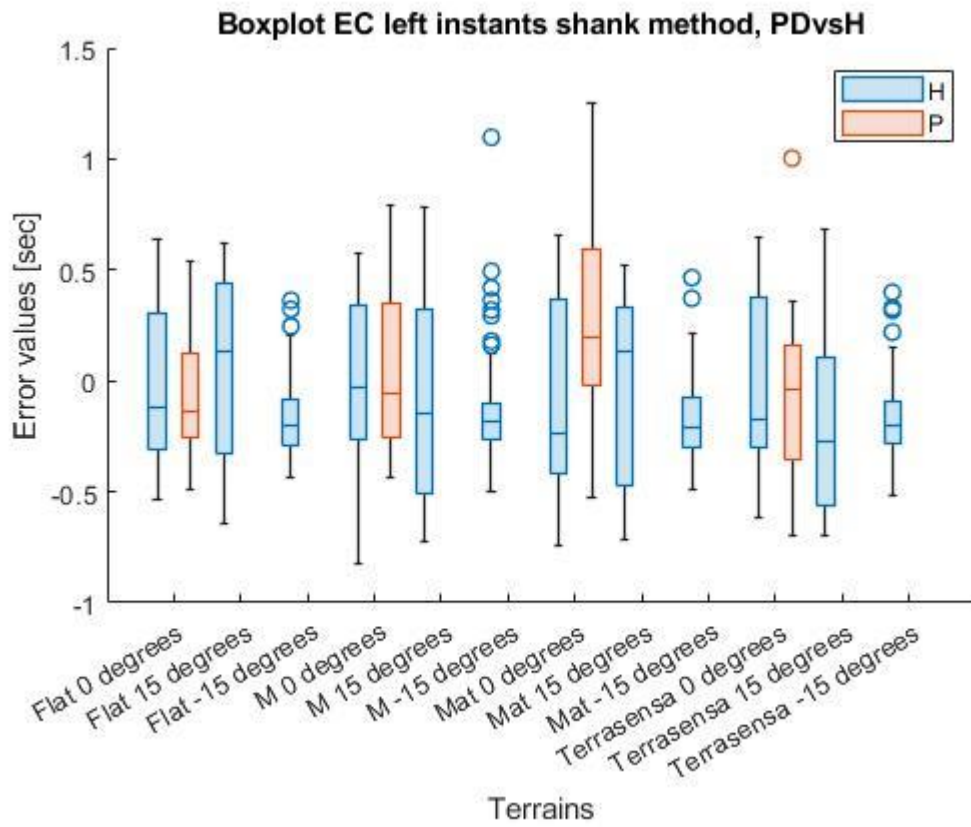


Figure 4.32: shank method boxplot, errors on different terrains. Healthy subjects vs Parkinson disease patients. EC left instants.

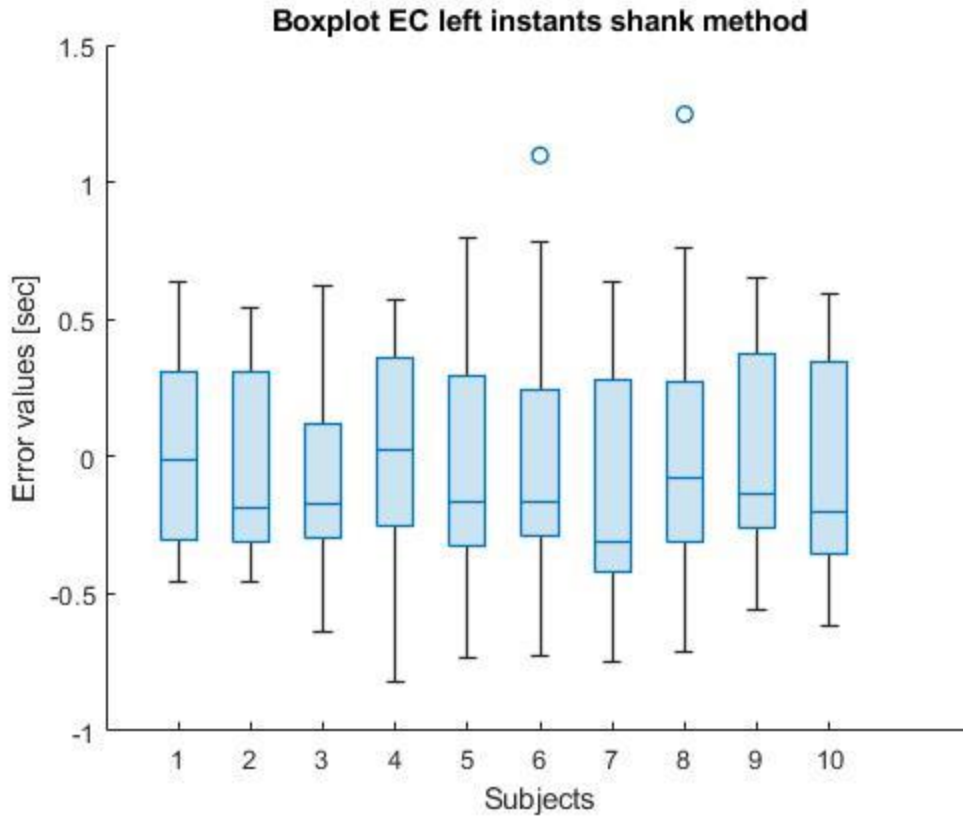


Figure 4.33: shank method boxplot, errors of the healthy subjects. EC left instants.

The Anova in the Figure 4.34 was performed on the BMI group with the categories for each subject.

| Analysis of Variance | | | | | |
|----------------------|---------|-------|----------|-----|--------|
| Source | Sum Sq. | d. f. | Mean Sq. | F | Prob>F |
| bmi | 0.075 | 2 | 0.03773 | 0.3 | 0.7429 |
| Error | 142.049 | 1119 | 0.12694 | | |
| Total | 142.124 | 1121 | | | |

Sequential (Type I) sums of squares.

Figure 4.34: Anova from MATLAB on the height group of the EC instants – left shank method..

Another Anova to see how much the error is influenced by the terrains and the inclinations is shown in the Figure 4.35.

| Analysis of Variance | | | | | |
|----------------------|---------|-------|----------|-------|--------|
| Source | Sum Sq. | d. f. | Mean Sq. | F | Prob>F |
| terrain | 0.335 | 3 | 0.11172 | 0.9 | 0.4408 |
| inclination | 3.184 | 2 | 1.59193 | 12.82 | 0 |
| Error | 138.605 | 1116 | 0.1242 | | |
| Total | 142.124 | 1121 | | | |

Sequential (Type I) sums of squares.

Figure 4.35: Anova from MATLAB on the terrain and inclination groups of the EC instants – left shank method.

The boxplot of the errors on the various inclinations is shown in the Figure 4.36.

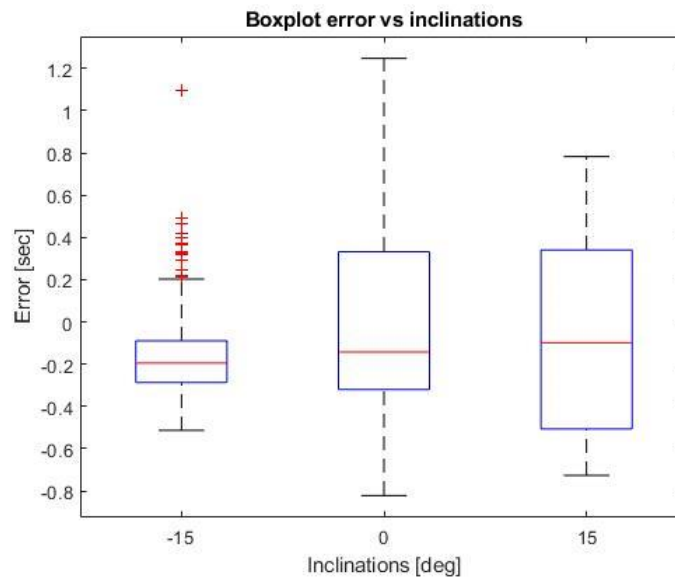


Figure 4.36: Boxplot of the errors on the different terrain inclinations of the EC instants - left shank method.

Instead, the error plot of all the subjects is shown in the Figure 4.37.

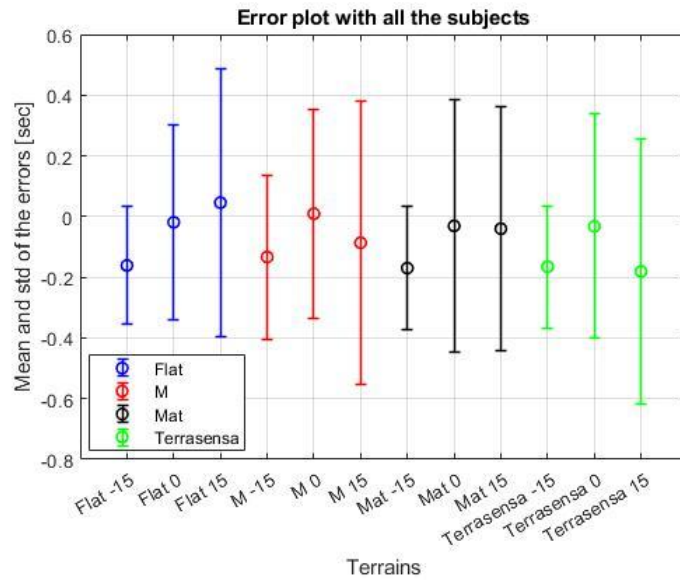


Figure 4.37: error plot of all the subjects of the EC instants - left shank method.

Now the IC instants on the left shank. The boxplots are shown in the Figure 4.38 and 4.39.

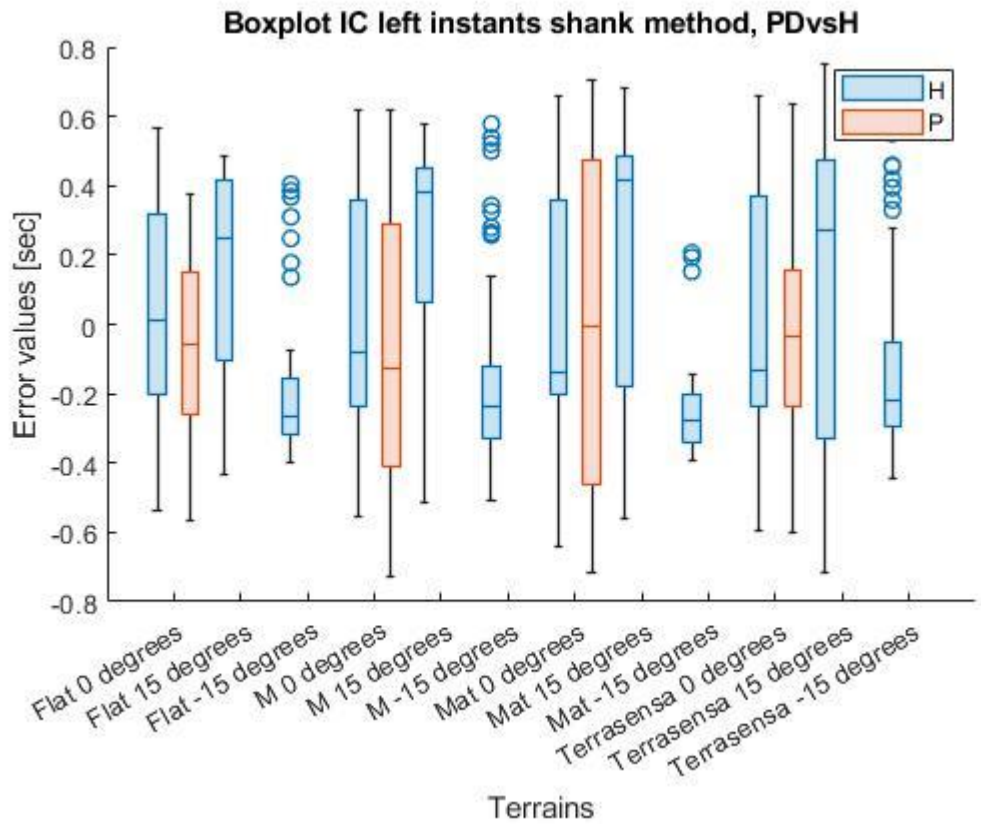


Figure 4.38: shank method boxplot, errors on different terrains. Healthy subjects vs Parkinson disease patients. IC left instants.

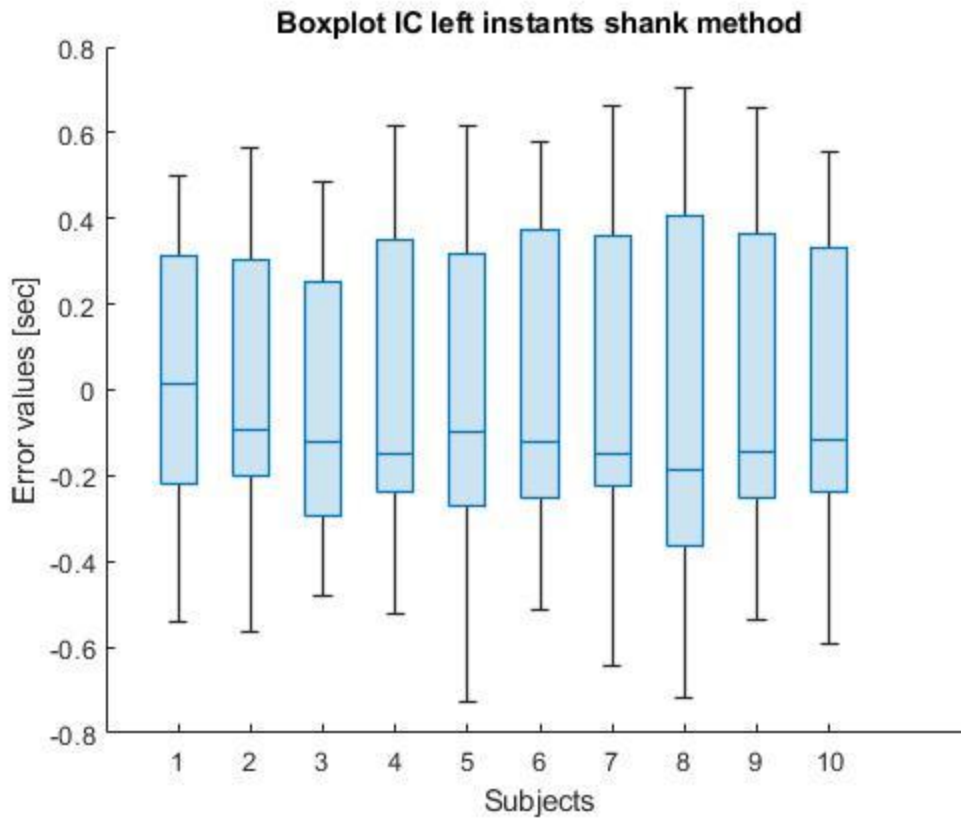


Figure 4.39: shank method boxplot, errors of each healthy subject. IC left instants.

The Anova on the BMI group is shown in the Figure 4.40.

| Analysis of Variance | | | | | |
|----------------------|---------|-------|----------|------|--------|
| Source | Sum Sq. | d. f. | Mean Sq. | F | Prob>F |
| bmi | 0.623 | 2 | 0.31156 | 2.89 | 0.0559 |
| Error | 125.938 | 1169 | 0.10773 | | |
| Total | 126.562 | 1171 | | | |

Sequential (Type I) sums of squares.

Figure 4.40: Anova from MATLAB on the BMI group of the IC instants – left shank method..

The Anova on the inclination and terrain groups can be performed and it is shown in the Figure 4.41.

| Analysis of Variance | | | | | |
|----------------------|---------|-------|----------|-------|--------|
| Source | Sum Sq. | d. f. | Mean Sq. | F | Prob>F |
| terrain | 0.039 | 3 | 0.01294 | 0.13 | 0.9422 |
| inclination | 10.631 | 2 | 5.31531 | 53.48 | 0 |
| Error | 115.892 | 1166 | 0.09939 | | |
| Total | 126.562 | 1171 | | | |

Sequential (Type I) sums of squares.

Figure 4.41: Anova from MATLAB on the terrain and inclination groups of the IC instants – left shank method.

The boxplot of the errors on the different inclinations is presented in the Figure 4.42.

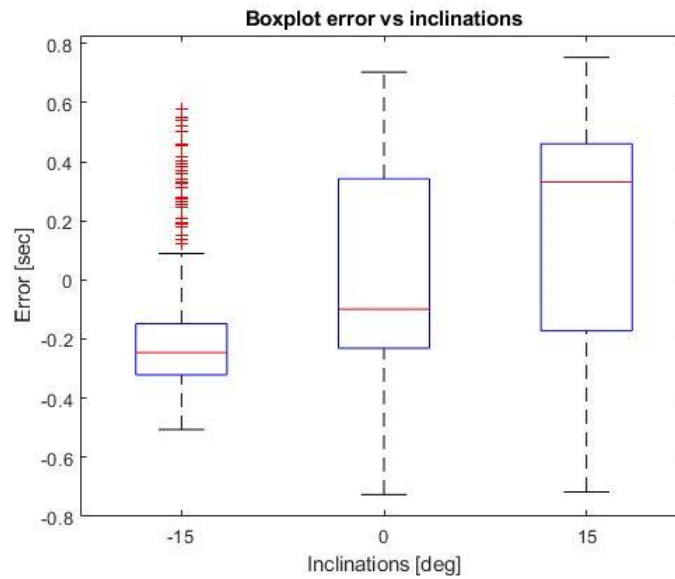


Figure 4.42: boxplot of the errors on the various inclinations of the IC instants – left shank method.

So, an error plot of all the subjects mean and standard deviation on every terrain is shown in the Figure 4.43.

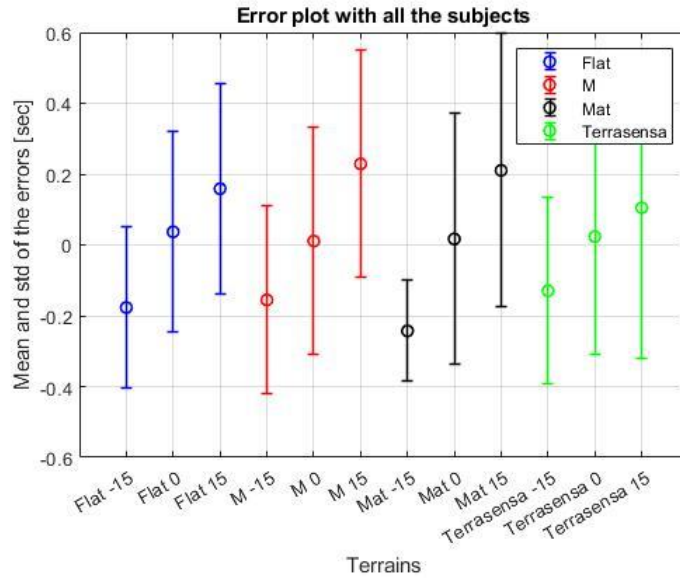


Figure 4.43: error plot of all subjects of the IC instants – left shank method.

Now we see the results for the right shank. We first see the results for the EC instants.

The boxplots are shown in the Figure 4.44 and 4.45.

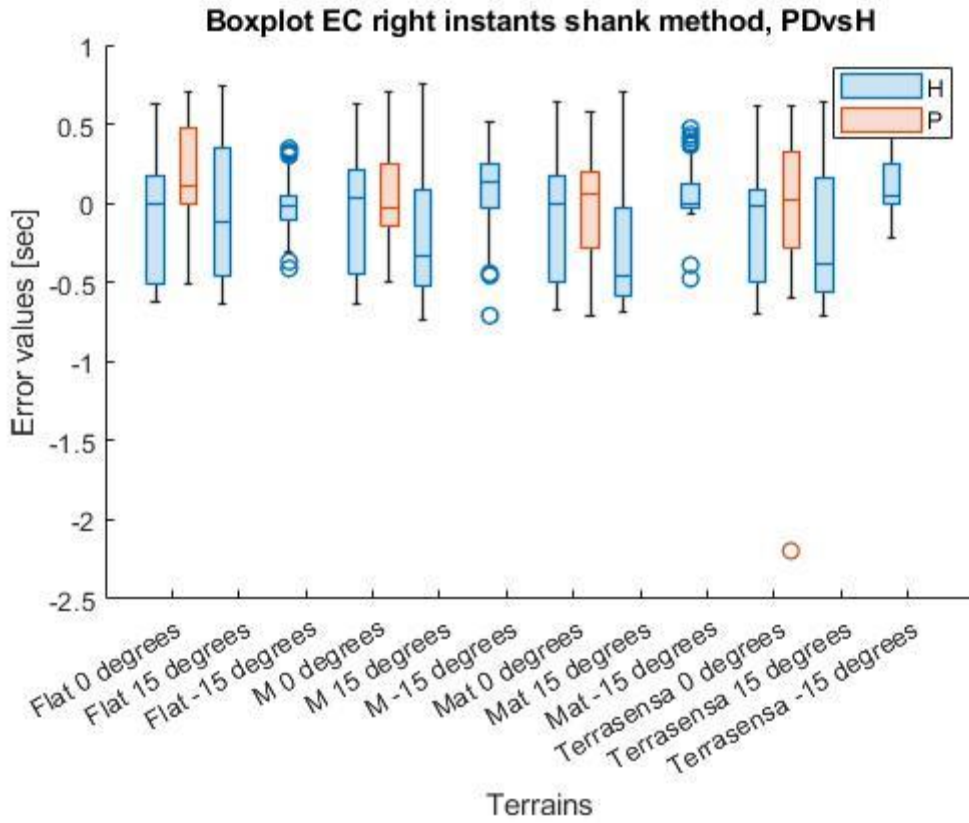


Figure 4.44: shank method boxplot, errors on different terrains. Healthy subjects vs Parkinson disease patients. EC right instants.

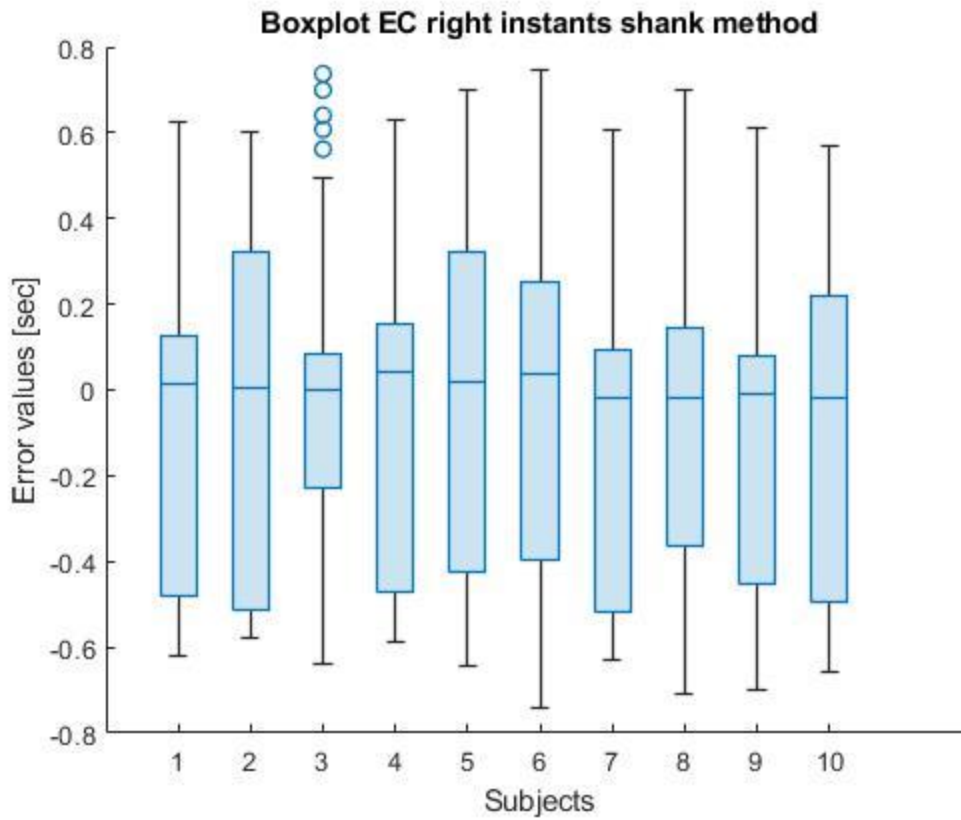


Figure 4.45: shank method boxplot, errors of each healthy subject. EC right instants.

The Anova on the BMI group is shown in the Figure 4.46.

| Analysis of Variance | | | | | |
|----------------------|---------|-------|----------|------|--------|
| Source | Sum Sq. | d. f. | Mean Sq. | F | Prob>F |
| bmi | 0.444 | 2 | 0.22199 | 1.66 | 0.1903 |
| Error | 147.211 | 1102 | 0.13359 | | |
| Total | 147.655 | 1104 | | | |

Sequential (Type I) sums of squares.

Figure 4.46: Anova from MATLAB on the BMI group of the EC instants – right shank method.

The Anova on the terrain and inclination groups is shown in the Figure 4.47.

| Analysis of Variance | | | | | |
|----------------------|---------|-------|----------|-------|--------|
| Source | Sum Sq. | d. f. | Mean Sq. | F | Prob>F |
| terrain | 0.759 | 3 | 0.25299 | 1.96 | 0.1189 |
| inclination | 4.739 | 2 | 2.36954 | 18.32 | 0 |
| Error | 142.157 | 1099 | 0.12935 | | |
| Total | 147.655 | 1104 | | | |

Sequential (Type I) sums of squares.

Figure 4.47: Anova from MATLAB on the terrain and inclination groups of the EC instants – right shank method.

The boxplot on the various inclinations is shown in the Figure 4.48.

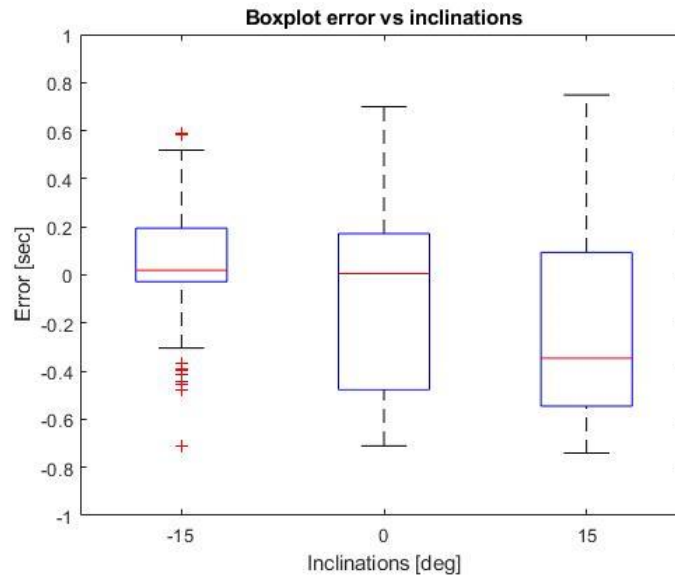


Figure 4.48: boxplot of the errors on the various inclinations of the EC instants – right shank method.

The error plot for all the subjects is shown in the Figure 4.49.

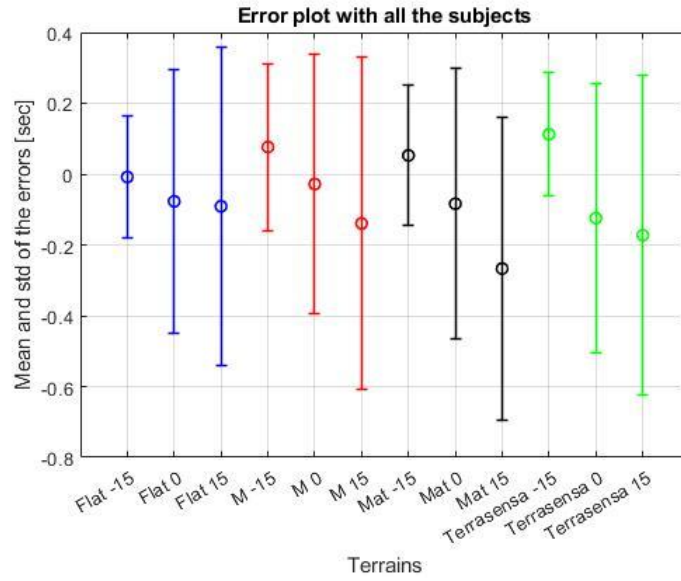


Figure 4.49: error plot of all subjects of the EC instants – right shank method.

To conclude, now we see the results for the IC instants, always for the IMU positioned on the right shank. We can see two boxplots in the Figure 4.50 and 4.51.

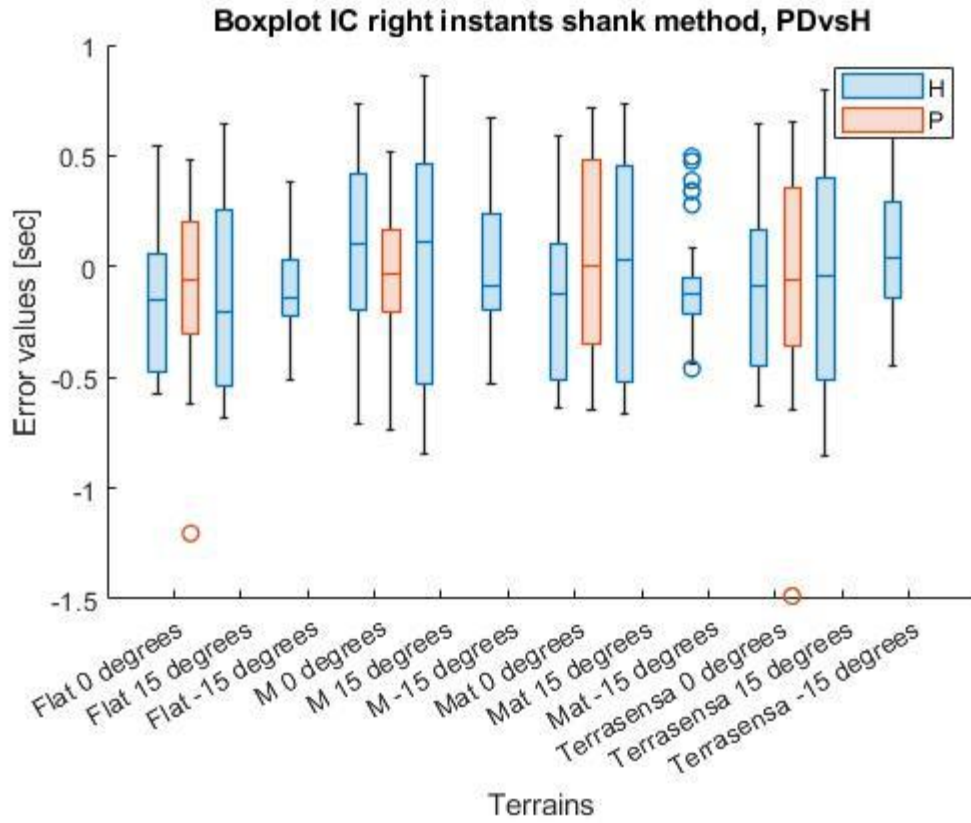


Figure 4.50: shank method boxplot, errors on different terrains. Healthy subjects vs Parkinson disease patients. IC right instants.

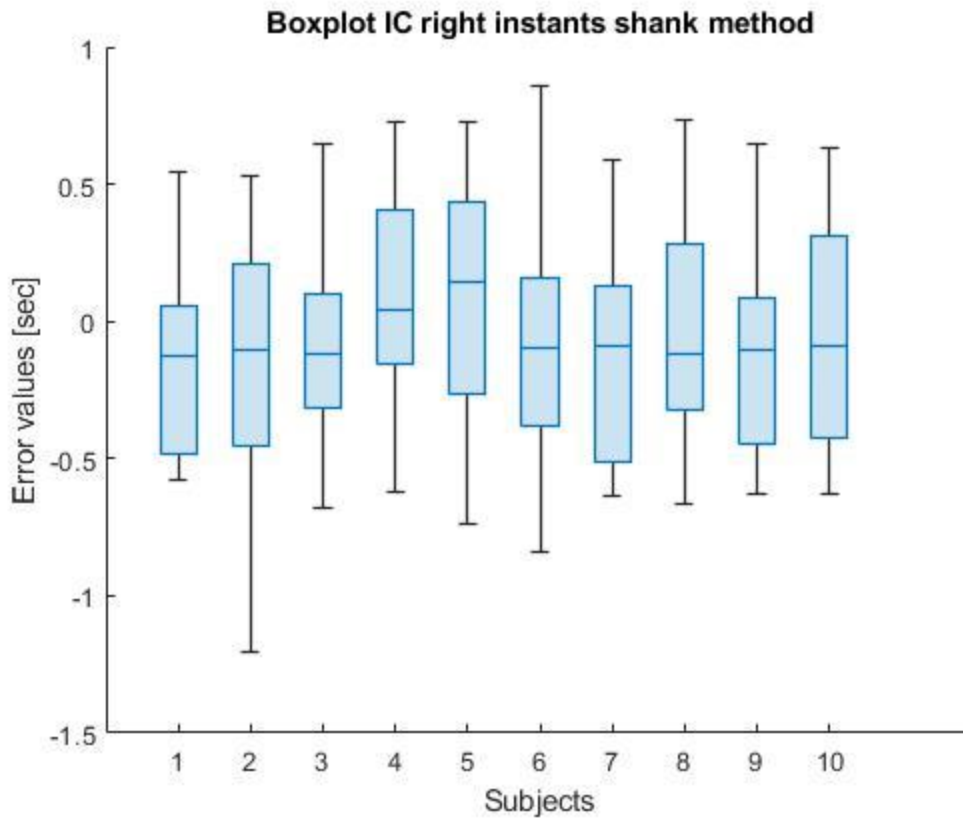


Figure 4.51: shank method boxplot, errors of each healthy subject. IC right instants.

And the Anova of the BMI group is shown in the Figure 4.52.

| Analysis of Variance | | | | | |
|----------------------|---------|-------|----------|-------|-------------|
| Source | Sum Sq. | d. f. | Mean Sq. | F | Prob>F |
| bmi | 2.881 | 2 | 1.44036 | 10.95 | 1.94934e-05 |
| Error | 148.239 | 1127 | 0.13153 | | |
| Total | 151.12 | 1129 | | | |

Sequential (Type I) sums of squares.

Figure 4.52: Anova from MATLAB on the BMI group of the IC instants – right shank method.

Chapter 5 - Discussion

We start the discussion, considering the areogram plots from the chapter 4 'Results', in the 'Detection analysis' section. The foot method for the IC events seems to be the best detector method if we see the percentage value of the correct events. But, we can see that the method detects many more instants than the gold standard, so only the threshold helps the method to work better. This fact is confirmed by the percentage value of the extra events, the events detected by the method but not interesting for the error analysis. These extra events are more present in trials at zero degrees, but this fact can be caused by the large amount of data that we have for these trials comparing them to the trials in slope, as we can see in the tables 4-4 of the method and 4-1 of the gold standard in the 'Experimental database' section in the chapter 4 'Results'. The irregular terrain that has more extra events, as we could expected, is the Terrasensa terrain. So, seeing all the percentage values, the best detector method is the first one, the method that uses the IMU on the pelvis. It has an high percentage value of correct events, therefore a low value for the missed events, but also the lowest value for what concerns the extra events. In addition, the values of the missed events and the extra events are almost evenly distributed on the inclined and level walking conditions. And, to conclude, for both the terrain that has most not correct events is an irregular terrain, in particular the M terrain. Therefore, considering the IC instants, also the method that uses the IMU on the shank provides good percentage values of correct, missed and extra events, so it can be considered for further analysis.

As for the EC events, the shank method is better than the foot one, considering all the percentage values calculated. For this reason and for the too low correct percentage values, it was decided to not continue the analysis of the foot method for the detection of the EC instants. The shank method provides quite good

percentage values and for both right and left shank, the terrains that provide more missed and extra events are the irregular ones, with an exception regarding the IMU on the right shank at the level walking configuration on the flat terrain that present more missed events than any other terrain. The reason why the IMU on the foot has negative performances lies in the fact that this sensor is characterized by other movements that condition the performance of the sensor and consequently they make the signal noisier. So, we can say that the other three IMUs on the shanks and on the pelvis function like low pass filters that delete small right and left swing in the movement and the signal is affected in the positive way.

As mentioned earlier, only the methods that presented acceptable detection percentage values were subjected to a more in-depth analysis. The procedure was the same for all the selected and appropriate methods. A first look was given to the boxplots of the errors on the different terrains and inclinations, dividing the healthy subjects from the Parkinson patients to evaluate if the method works in the same way for both subjects categories. For the first method, it is possible to see in the Figure 4.19 that the variabilities of the errors on the different conditions for the Parkinson patients is higher than the ones for the healthy subjects. Also for the second method this happens. Instead, for the third method the Parkinson patients present similar error variabilities.

Another boxplot with all the healthy subjects was performed for all the methods, because as said previously in this work, the first subject of the study performed a bit different set of trials, but for this reason, it is interesting to see which method performs in a comparable way with the other kind of trials, the majority in this study. All the methods had acceptable and comparable errors for the first subject.

The last analysis is that of the variance. This analysis has two steps in this work. With the first step we want to see if the method depends on the anthropometric

parameters of the subjects. If not, we can further investigate on the different variables that influence the errors variability, in particular if the terrain or the inclination conditions the accuracy of the method. The analysis of the variance on the BMI group of the method (Figure 4.28 and 4.31) that uses the IMU on the foot says to us that this method depends on the anthropometric parameters of the subjects. All the other methods do not depend on the anthropometric values of the subjects, only the IC detection method that uses the IMU positioned on the right shank depends on these, as we can see in the Figure 4.52, so it cannot be further investigated.

For the remaining methods, the inclination is most significative parameter that affects the variability of the error, but also the kind of terrain has an impact. Some indications can be given as to which terrain to use which method. Seeing the Figure 4.23, the method that uses the IMU on the pelvis has performances that are comparable on the terrains with inclinations at 15 and -15 degrees, instead on the terrains inclined at zero degrees has a better performance, but presents some outliers. Therefore, seeing the Figure 4.24 the average error increases on every terrain from the -15 to 15 degrees inclination. The highest average error is on the Mat terrain inclined at 15 degrees, the standard deviations are higher in the irregular terrains like the M terrain and the Terrasensa terrain. So, this method can be used on flat terrains, also inclined at -15 degrees.

For what concerns the method that uses the sagittal angular velocity from the IMU positioned on the shank, seeing all the boxplots on the Figure 4.36, 4.42 and 4.48, the lowest error variability occurs with the terrain inclination at -15 degrees. In particular, analyzing the EC events detection, the method anticipates the correct instants identified by the gold standard. For what concerns the IC instants, the method anticipates the gold standard on the configurations at -15 degrees and has more positive errors with the inclination of the terrains at 15 degrees, so it is late in comparison with the gold standard. Analyzing now the error plot in the Figure

4.37 of the EC left events detection method, the lowest average errors are in the configurations at zero degrees of all the terrains, in general the method presents a good performance in all the configurations of the flat terrain. Seeing the error plot shown in the Figure 4.43, the fact that the method on the configurations at -15 degrees tends to anticipate the gold standard is confirmed by all the average errors at these configurations are negative. All the average errors at zero degrees configurations are near to the zero, so the method works well with this inclination. The highest average error is present on the M terrain 15 degrees inclined. To conclude, analyzing the error plot shown in the Figure 4.49, the best performances are performed on the flat terrain at all configurations. The worst terrain and inclination is the Mat terrain at 15 degrees.

In the 'Statistical analysis' section in the chapter 2, it was said that to be Anova applicable, two hypotheses had to be verified before the analysis. This work presents a complex situation with a large amount of degrees of freedom so the verification of the hypotheses of the analysis of variance should be conducted on every different condition that these experimental trials present. Therefore, the database should be improved to have the same number of instants detected in each condition and for each kind of subjects, healthy and Parkinson patients, to have a statistical analysis of a better quality. Having said that in some situations, the hypothesis of a normality distribution was verified, as we can see from the histogram plot of the errors of the first method of Zijlstra shown in the Figure 5.1 below.

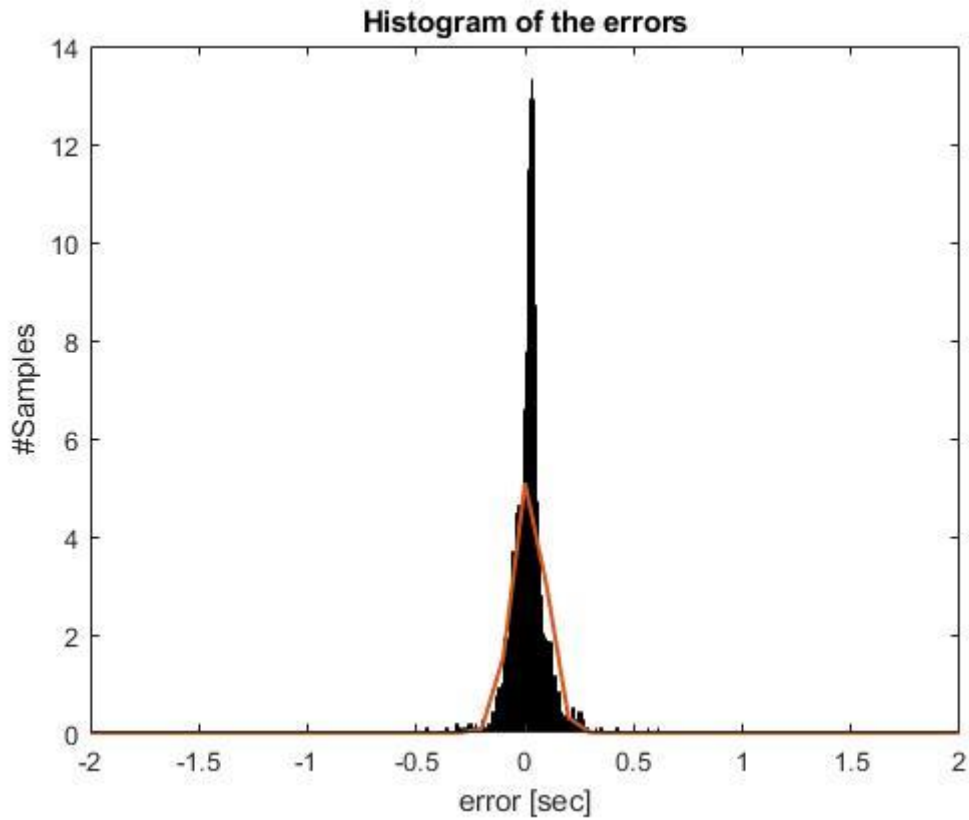


Figure 5.1: histogram of the errors – Zijlstra method.

On the plot was graphed also the Gaussian Bell (in orange) following the [eq. 3.1] with the mean and the standard deviation of the errors.

An histogram that does not respect the normal distribution of the errors is the following one in the Figure 5.2, that belongs to the method that uses the IMU positioned on the right foot.

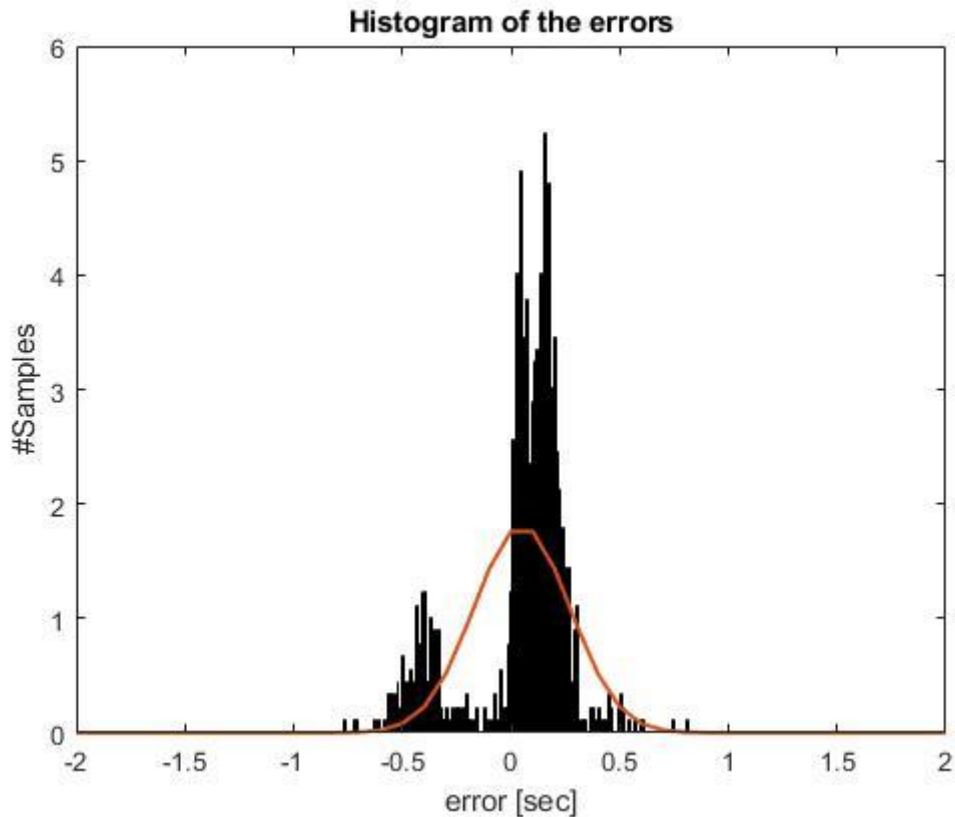


Figure 5.2: histogram of the errors – right foot method, IC instants.

When the histogram seemed to suggest that the hypothesis of normal distribution had not to be accepted, a verification with Shapiro-Wilk W test was always performed with a significance level of 0.05. Every time the tests executed confirmed the impressions from the histograms.

For what concerns the second hypothesis of the Anova, the equality of variances was never perfectly accepted for the groups used. In fact, the Barlett's test was performed on every group (subjects, categories of mass, height and BMI, terrains and inclinations), but none presents a p-value > 0.05 . These results have to be analyzed better with an analysis that goes more in depth of the data, maybe it has to be analyzed every different condition of terrain as said before.

Chapter 6 – Conclusion

The aim of this thesis was to understand if gait events could be efficiently identified by using algorithms based on IMU sensors in comparison with a stereophotogrammetry system, usually considered as a gold standard in gait analysis. Last but not least such methods have been applied to gait on challenging terrains viable for its inclination, for irregularity characteristics and for stiffness. The experimental campaign produced a large quantity of gait events data which constitute the data set to check four IMU methods performances. The four methods require inertial sensors on the pelvis, or on the shank or on the foot. We validated them for their detection capability, having considered the gold standard as reference, including correct events, 'missed events' when events detected by the gold standard are not detected by IMU methods, called 'missed events', and 'extra events' when the events detected by IMU methods do not correspond to those obtained by the gold standard. Moreover for the correct events, we considered the temporal error between the comparable events of the method and the gold standard and we analyzed it. The results suggest that a unique best method suitable for all the tested conditions does not exist, but some useful indication can be read from this study. It is shown in fact that, indicatively for all the methods, there is an increase in time error for each event, moving from negative to positive inclination in all terrains. Beside that for each terrain the most performant method, among the four considered, can be identified, giving useful indications to the experimenter, for the specific conditions. In general, the IMU on the foot is not the perfect solution on irregular terrains and/or when considering Parkinson patients, while the IMU positioned on the pelvis and the shank are the best choices for gait event detection on irregular terrains, probably for the low pass filtering effect of the subject body when moving from the distal part to a more proximal one.

Bibliography

- [Prasanth, 2021] Hari Prasanth, Miroslav Caban, Urs Keller, Grégoire Courtine, Auke Ijspeert, Heike Vallery and Joachim von Zitzewitz. *Wearable Sensor-Based Real-Time Gait Detection: A Systematic Review*. Sensors, 2021.
- [A.L. Benabid, 2009] J. Mitrofanis P. Pollak A.L. Benabid, S. Chabardes. *Deep brain stimulation of the subthalamic nucleus for the treatment of Parkinson's disease*. Lancet Neurol., 2009.
- [Ferrari, 2010] Pietro Garofalo Michele Raggi Monique Heijboer Angelo Cappello Angelo Davalli Alberto Ferrari, Andrea Giovanni Cutti. *First in vivo assessment of "Outwalk": a novel protocol for clinical gait analysis based on inertial and magnetic sensors*. Med Biol Eng Comput, 2010.
- [Kleiner and Pandis, 2015] Maria Gaglione Daniela Hildebrand Patrizio Sale Giorgio Albertini Fabrizio Stocchi Ana Kleiner, Manuela Galli and Maria Francesca De Pandis. *The Parkinsonian Gait Spatiotemporal Parameters Quantified by a Single Inertial Sensor before and after Automated Mechanical Peripheral Stimulation Treatment*. Parkinson's Disease, 2015.
- [Karatsidis, 2019] H. Martin Schepers Giovanni Bellusci Mark de Zee Peter H. Veltink Michael Skipper Andersen Angelos Karatsidis, Moonki Jung. *Musculoskeletal model-based inverse dynamic analysis under ambulatory conditions using inertial motion capture*. Medical Engineering and Physics, 2019.

- [A.R. De Asha, 2012] G.J. Barton A.R. De Asha, M.A. Robinson. *A marker based kinematic method of identifying initial contact during gait suitable for use in real-time visual feedback applications*. Gait Posture, 2012.
- [Cappozzo, 2005] Alberto Leardini Lorenzo Chiari Aurelio Cappozzo, Ugo Della Croce. *Human movement analysis using stereophotogrammetry Part 1: theoretical background*. Gait Posture, 2005.
- [Benjaminse and Otten, 2020] Ruben; Gokeler Alli; Benjaminse, Anne; Bolt and Bert Otten. *A validity study comparing Xsens with Vicon*. ISBS Proceedings Archive: Vol. 38: Iss. 1, Article 190, 2020.
- [Bloem BR, 2004] Visser JE Giladi N Bloem BR, Hausdorff JM. *Falls and freezing of gait in Parkinson's disease: a review of two interconnected, episodic phenomena*. Mov Disord., 2004.
- [C.H. Adler, 2014] J.G. Hentz H.A. Shill J.N. Caviness E. Driver-Dunckley M.N. Sabbagh L.I. Sue S.A. Jacobson C.M. Belden et al. C.H. Adler, T.G. Beach. *Low clinical diagnostic accuracy of early vs advanced Parkinson disease: clinicopathologic study*. Neurology, 2014.
- [Trojaniello and Croce, 2014] Elisa Pelosin Laura Avanzino Anat Mirelman Jeffrey M Hausdorff Diana Trojaniello, Andrea Cereatti and Ugo Della Croce. *Estimation of step-by-step spatio-temporal parameters of normal and impaired gait using shank-mounted magneto-inertial sensors application to elderly hemiparetic parkinsonian and choreic gait*. Journal of Neuroengineering and Rehabilitation, 2014.

- [A. Garcia and Siqueira, 2022] Marco H. Terra Francisco A. Garcia, Juan C. Pérez-Ibarra and Adriano A. G. Siqueira. *Adaptive Algorithm for Gait Segmentation Using a Single IMU in the Thigh Pocket*. IEEE SENSORS JOURNAL, 2022.
- [G. V. Prateek and Nehorai, 2020] Gammon M. Earhart G. V. Prateek, Pietro Mazzoni and Arye Nehorai. *Gait Cycle Validation and Segmentation Using Inertial Sensors*. Life Fellow, IEEE, 2020.
- [Giladi N, 2013] Hausdorff JM Giladi N, Horak FB. *Classification of gait disturbances: distinguishing between continuous and episodic changes*. Mov Disord., 2013.
- [J. C. Perez-Ibarra and Krebs, 2020] A. A. G. Siqueira J. C. Perez-Ibarra and H. I. Krebs. *Real-time identification of gait events in impaired subjects using a single-IMU foot-mounted device*. IEEE Sensors J., 2020.
- [J. D. Farah and Lemaire, 2019] N. Baddour J. D. Farah and E. D. Lemaire. *Design, development, and evaluation of a local sensor-based gait phase recognition system using a logistic model decision tree for orthosis-control*. J. Neuroeng. Rehabil., 2019.
- [M. Jasiewicz, 2006] James W. Middleton Andrew Barriskill PeterCondie Brendan Purcell Raymond Che Tin Li Jan M. Jasiewicz, John
- [H.J. Allum, 2006] H.J. Allum. *Gait event detection using linear accelerometers or angular velocity transducers in able-bodied and spinal-cord injured individuals*. GaitPosture, 2006.

- [K. Gruber, 1998] J. Denoth K. Schneider K. Gruber, H. Ruder. *A comparative study of impact dynamics: wobbling mass model versus rigid body models*. Journal of Biomechanics, 1998.
- [Chiari, 2005] Alberto Leardini Aurelio Cappozzo Lorenzo Chiari, Ugo Della Croce. *Human movement analysis using stereophotogrammetry: Part 2: Instrumental errors*. Gait Posture, 2005.
- [Messa and Rossi, 2019] Davide Momi Lucia Monti Carla Battisti David Cioncoloni Barbara Pucci Emiliano Santarnecchi Luca Valerio Messa, Federica Ginanneschi and Alessandro Rossi. *Functional and Brain Activation Changes Following Specialized Upper-Limb Exercise in Parkinson's Disease*. Frontiers in Human Neuroscience, 2019.
- [Schepers] Giovanni Bellusci Martin Schepers, Matteo Giuberti. *Xsens MVN: Consistent Tracking of Human Motion Using Inertial Sensing*. XSENS TECHNOLOGIES B.V.
- [P. Mavor and Graham, 2020] Allison L. Clouthier Thomas Karakolis Matthew P. Mavor, Gwyneth B. Ross and Ryan B. Graham. *Validation of an IMU Suit for Military-Based Tasks*. Sensors, 2020.
- [Milad Nazarahari, 2022] Atif Khan Hossein Rouhani Milad Nazarahari, Aminreza Khandan. *Foot angular kinematics measured with inertial measurement units: A reliable criterion for real-time gait event detection*. Journal of Biomechanics, 2022.
- [Mirelman A, 2019] Camicioli R Ellis TD Giladi N Hamilton JL et al. Mirelman A, Bonato P. *Gait impairments in Parkinson's disease*. Lancet Neurol., 2019.

- [Nutt JG, 2000] Giladi N Hallett M Horak FB Nieuwboer A Nutt JG, Bloem BR. *Freezing of gait: moving forward on a mysterious clinical phenomenon*. Lancet Neurol, 2000.
- [Plotnik M, 2011] Dagan Y Hausdorff JM Plotnik M, Giladi N. *Postural instability and fall risk in Parkinson's disease: impaired dual tasking, pacing, and bilateral coordination of gait during the 'ON' medication state*. Exp Brain Res, 2011.
- [Reijne, 2018] Eline Van Der Kruk Marco M. Reijne. *Accuracy of human motion capture systems for sport applications;state-of-the-art review*. European Journal of Sport Science, 2018.
- [Roemmich and Hass, 2014] Fregly B.J. Roemmich, R.T. and C.J. Hass. *Neuromuscular complexity during gait is not responsive to medication in persons with Parkinson's disease*. Ann. Biomed. Eng., 2014.
- [S.B. Thies, 2007] L. Kenney D. Howard J.Y. Goulermas C. Smith J. Rigby S.B. Thies, P. Tresadern. *Comparison of linear accelerations from three measurement systems during "reach grasp"*. Medical Engineering Physics, 2007.
- [Shubham Sharma, 2019] Mohit Kumar Lavanya Sharma Shubham Sharma, ShubhankarVerma. *Use of Motion Capture in 3D Animation: Motion Capture Systems, Challenges, and Recent Trends*. International Conference on Machine Learning, Big Data, Cloud and Parallel Computing, 2019.
- [Shuo Jiang, 2017] Maria Kyrarini Axel Gräser Shuo Jiang, Xingchen Wang. *A Robust Algorithm for Gait Cycle Segmentation*. 25th European Signal Processing Conference (EUSIPCO), 2017.

- [Springer S, 2006] Peretz C Yogev G Simon ES Hausdorff JM Springer S, Giladi N. *Dual-tasking effects on gait variability: the role of aging, falls, and executive function*. *Mov Disord.*, 2006.
- [Wei Fu and Chen, 2022] Qiwen Yu Jiajia Fang Guohua Zhao Yi Li Chenying Pan Hao Dong Di Wang Haiyan Ren Yi Guo Qingjun Liu Jun Liu Wei Fu, Linxin Xu and Xing Chen. *Artificial Intelligent Olfactory System for the Diagnosis of Parkinson's Disease*. ACS Omega, 2022.
- [W.H.K. de Vries, 2009] C.T.M. Baten F.C.T. van der Helm W.H.K. de Vries, H.E.J. Veeger. *Magnetic distortion in motion labs, implications for validating inertial magnetic sensors*. *Gait Posture*, 2009.
- [Wiebren Zijlstra, 2003] At L. Hof Wiebren Zijlstra. *Assessment of spatio-temporal gait parameters from trunk accelerations during human walking*. *Gait Posture*, 2003.
- [Robert-Lachaine, 2017] Christian Larue André Plamondon Xavier Robert-Lachaine, Hakim Mecheri. *Validation of inertial measurement units with an optoelectronic system for whole-body motion analysis*. *Med Biol Eng Comput*, 2017.
- [Thenaisie and Moraud, 2022] Charlotte Moerman Stefano Scafa Andrea Gálvez Elvira Pirondini Morgane Burri Jimmy Ravier Alessandro Puiatti Ettore Accolla Benoit Wicki André Zacharia Mayte Castro Jiménez Julien F. Bally Grégoire Courtine Jocelyne Bloch Yohann Thenaisie, Kyuhwa Lee and Eduardo Martin Moraud. *Principles of gait encoding in the subthalamic nucleus of people with Parkinson's disease*. *Science Translational Medicine*, 2022.

- [Yuzhe Yang and Katabi, 2022] Guo Zhang Hao Wang Ying-Cong Chen Yingcheng Liu Christopher G. Tarolli Daniel Crepeau Jan BukartykMithri R. Junna Aleksandar Videnovic Terry D. Ellis Melissa C. Lip- ford Ray Dorsey Yuzhe Yang, Yuan Yuan and Dina Katabi. *Artificial intelligence-enabled detection and assessment of Parkinson's disease using nocturnal breathing signals*. Nature Medicine, 2022.
- [Stucki G, 2007] Stucki G, Cieza A, Melvin J. *The International Classification of Functioning, Disability and Health (ICF): a unifying model for the conceptual description of the rehabilitation strategy*. J Rehabil Med, 2007.
- [Bensoussan L, 2008] Bensoussan L, Viton JM, Barotsis N, Delarque A. *evaluation of patients with gait abnormalities in physical and rehabilitation medicine settings*. J Rehabil Med, 2008.
- [Mayich DJ, 2014] Mayich DJ, Novak A, Vena D, Daniels TR, Brodsky JW. *Gait analysis in orthopedic foot and ankle surgery-topical review, part 1: principles and uses of gait analysis*. Foot Ankle Int, 2014.
- [Kempen JC, 2016] Kempen JC, Doorenbosch CA, Knol DL, de Groot V, Beckerman H. *Newly identified gait patterns in patients with multiple sclerosis may be related to push-off quality*. Phys Ther, 2016.
- [Mirek E, 2016] Mirek E, Kubica JL, Szymura J, Pasiut S, Rudzinska M, Chwala W. *Assessment of gait therapy effectiveness in patients with Parkinson's disease on the basis of three dimensional movement analysis*. Front Neurol, 2016.
- [Geroïn C, 2013] Geroïn C, Mazzoleni S, Smania N, et al., Italian Robotic Neurorehabilitation Research Group. *Systematic review of outcome measures of walking training using electromechanical and robotic devices in patients with stroke*. J Rehabil Med, 2013.

- [M. D. J. Perry, 1992] M. D. J. Perry. *Gait Analysis: Normal and Pathological Function*. 1st ed. Thorofare, NJ, USA: SLACK Incorporated, 1992.
- [J. Taborri, 2016] J. Taborri, E. Palermo, S. Rossi, and P. Cappa. *Gait partitioning methods: A systematic review*. *Sensors*, 2016.
- [R. Caldas, 2017] R. Caldas, M. Mundt, W. Potthast, F. B. de Lima Neto, and B. Markert. *A systematic review of gait analysis methods based on inertial sensors and adaptive algorithms*. *Gait Posture*, 2017.
- [Torres-Pardo A., 2022] Adriana Torres-Pardo, David Pinto-Fernández, Manolo Garabini, Franco Angelini, David Rodriguez-Clanca, Stefano Massardi, Jesús Tornero, Juan C Moreno, Diego Torricelli. *Legged locomotion over irregular terrains: state of the art of human and robot performance*. *Bioinspir. Biomim.*, 2022.
- [Thies, S.B., 2005] Thies, S.B., Richardson, J.K., Ashton-Miller, J.A. *Effects of surface irregularity and lighting on step variability during gait: A study in healthy young and older women*. *Gait & Posture*, 2005.
- [F. Dijkstra and P. J. Slycke, 2010] F. Dijkstra and P. J. Slycke. *Method and System for Enabling a Wireless Communication Between a Master Unit and a Sensor Unit*. 2010. US Patent: US8947206 B2.
- [F. Dijkstra and P. J. Slycke, 2009] F. Dijkstra and P. J. Slycke. *A Method and a System for Enabling a Wireless Communication Between a Master Unit and a Sensor Unit*. 2009. EU Patent: EP2320288 B1.
- [G. Bellusci, 2014] G. Bellusci, R. Zandbergen, and P. J. Slycke. *Reduced Processor Load for Wireless Communication Between Master Unit and Sensor Unit*. 2014. US Patent: US9526028 B2.

- [G. Bellusci, 2015] G. Bellusci, R. Zandbergen, and P. J. Slycke. *Reduced Processor Load for Wireless Communication Between Master Unit and Sensor Unit*. 2015. EU Patent: EP2958337 B1.
- [Emily J. Miller, 2022] Emily J. Miller, Riley C. Sheehan, Kenton R. Kaufman. *IMU filter settings for high intensity activities*. *Gait & Posture*, 2022.
- [Daniel W.T. Wundersitz, 2014] Daniel W.T. Wundersitz, Paul B. Gastin, Chris Richter, Samuel J. Robertson and Kevin J. Netto. *Validity of a trunk-mounted accelerometer to assess peak accelerations during walking, jogging and running*. *BIOMECHANICS AND MOTOR CONTROL*, 2014.
- [H.W. Lilliefors, 1969] H.W. Lilliefors. *On the KolmogorovSmirnov test for the exponential distribution with mean unknown*. *J. Am. Stat. Assoc.* , 1969.
- [H. Levene, 1960] H. Levene. *Robust tests for equality of variances, in Contribution to Probability and Statistics: Essays in Honor of Harold Hotelling*. ed. by I. Olkin, H. Hotelling, et al. (Stanford University Press), 1960.
- [M. S. Barlett, 1937] M.S. Bartlett. *Properties of sufficiency and statistical tests*. *Proc. R. Stat Soc*, 1937.